

**GENETICALLY ENCODED CALCIUM INDICATORS
BASED ON TROPONIN C AND FLUORESCENT
PROTEINS**

Dissertation zur Erlangung des Doktorgrades der Naturwissenschaften

an der Fakultät für Biologie
der Ludwig-Maximilians-Universität
München

vorgelegt von
Nicola Heim

München, 2005

Erstgutachter: Prof. Dr. Alexander Borst

Zweitgutachter: Prof. Dr. Rainer Uhl

Tag der mündlichen Prüfung: 24. Oktober 2005

TABLE OF CONTENTS

TABLE OF CONTENTS.....	V
1. ABSTRACT.....	1
2. INTRODUCTION	3
2.1 Fluorescence Techniques	3
2.1.1 Fluorescence and FRET.....	3
2.1.2 The Green Fluorescent Protein	8
2.1.3 Fluorescent Calcium Probes	11
2.2 Calcium-Binding Proteins	15
2.2.1 EF-Hands.....	15
2.2.2 The Troponin Family.....	16
3. ABBREVIATIONS.....	21
4. MATERIALS AND METHODS.....	23
4.1 Working with DNA	23
4.1.1 Spectrometric Determination of DNA Concentration.....	23
4.1.2 Gene Amplification by PCR	23
4.1.3 Site-directed Mutagenesis by PCR	24
4.1.4 Restriction of DNA.....	25
4.1.5 Ligation of DNA Fragments	25
4.1.6 Preparation of Competent <i>E. Coli</i>	25
4.1.7 Quick Transformation of Chemically Competent <i>E. Coli</i>	26
4.2 Working with Proteins.....	26
4.2.1 Recombinant Protein Expression in Bacteria.....	26
4.2.2 Purification of Recombinantly Expressed Proteins.....	26
4.3 Cell Culture.....	27
4.3.1 Preparation of Dissociated Rat Neurons	27
4.3.2 Transfection of Dissociated Rat Neurons	28
4.3.3 Transfection of HEK293 Cells.....	28
4.4 Histology and Immunohistochemistry.....	29
4.4.1 Cryosections of PFA-fixed Mouse Brains	29
4.4.2 Acute Slice Preparation of Mouse Brains	29
4.4.3 Antibody Staining of Cultured Cells.....	29

4.4.4	Antibody Staining of Fixed Brain Sections	30
4.5	Transgenic Animals.....	30
4.5.1	DNA Preparation for Mouse Oocyte Injections.....	30
4.5.2	Creation and Breeding of Transgenic mice	31
4.5.3	Genotyping of Transgenic Mice	31
4.6	Microscopy and Imaging	32
4.6.1	FRET-Setup.....	32
4.6.2	Determining the Ratio Change of Ratiometric Indicator Proteins	33
4.6.3	Measuring Kd Values	33
4.6.4	Measuring Dissociation Kinetics.....	34
4.7	Materials.....	35
4.7.1	Instruments.....	35
4.7.2	Consumables	35
4.7.3	Buffers, Solutions, and Media	35
4.7.4	Chemicals and Products	37
4.7.5	DNA Plasmids and <i>E. coli</i> Strains.....	39
4.7.6	Primer Sequences	39
5.	RESULTS	43
5.1	Construction of New Fluorescent Indicator proteins	43
5.1.1	On the Design of Troponin Linker Domains	43
5.1.2	Construction of CFP/YFP Constructs with csTnC, humTnC, and TPC1....	46
5.1.3	Construction of Non- <i>Aequoria</i> Constructs	50
5.1.4	Tuning Promising Constructs (I): Truncating and Multiplying the EF-hands of csTnC 55	
5.1.5	Tuning Promising Constructs (II): Mutating EF-hands of TN-L15	57
5.1.6	<i>In vitro</i> Kinetics.....	59
5.2	Functionality of TnC-Indicators in Cell Culture: TN-L15, TN-humTC and their derivatives.....	61
5.2.1	Cytosolic Expression in HEK293	61
5.2.2	Cytosolic Expression in Dissociated Neurons	63
5.2.3	Subcellular Targeting of TnC-based Indicators and Their Functionality in HEK293 Cells	64
5.2.4	Subcellular Targeting in Neurons: TN-L15 D107A-Ras and Others.....	68
5.3	Transgenic Mice Expressing TN-L15 in the Cytosol of Neurons	71

5.3.1	Choosing an Adequate Promoter and Indicator Construct	71
5.3.2	Expression Patterns and Expression Levels	73
5.3.3	Imaging of Live Brain Tissue	78
6.	DISCUSSION.....	81
6.1	New Ratiometric Calcium Indicator Probes and Their Physical Properties.....	81
6.1.1	Generating New Functional Constructs	81
6.1.2	<i>In Vitro</i> Characterization of Selected Constructs	84
6.2	Tests in Live Cells	86
6.2.1	Cell Culture Experiments.....	86
6.2.2	Transgenic Mouse Lines.....	88
6.3	Further Outlook.....	91
7.	REFERENCES	93
	THANKS AND ACKNOWLEDGEMENTS	105
	CURRICULUM VITAE.....	106

1. ABSTRACT

Genetically encoded calcium probes allow the visualization and quantification of intracellular calcium dynamics with great specificity and sensitivity. Until now, all genetically encoded calcium indicators have shared a common design that consists of mutants of the green fluorescent protein (GFP) as fluorophores and calmodulin as the calcium binding moiety, in several configurations. However, most of these calmodulin-based probe types show deficiencies such as reduced dynamic ranges when expressed within transgenic organisms and a lack of calcium sensitivity in certain subcellular targetings. A likely reason for this reduced sensitivity is that calmodulin is an ubiquitous signal protein in cell metabolism and thus stringently regulated. Thus, we chose to develop novel types of calcium probes based on the muscle calcium sensor troponin C, a protein that is not a constituent of non-muscle cells and therefore less likely to interact with cytosolic activities. By going through a series of cloning optimization steps, a set of new ratiometric calcium indicators was created using domains of skeletal and cardiac muscle troponin C variants as calcium binding moieties. These constructs showed *in vitro* FRET ratio changes of up to 140 %, had calcium dissociation constants ranging from 470 nM to 29 μ M, and were functional in intracellular targetings in which previous indicators had failed. The new indicators expressed homogeneously with no signs of aggregation in HEK293 cells as well as in rat hippocampal neurons, and large and dynamic ratio changes could be quantified after drug stimulation in cell culture. Membrane labeling experiments with the indicator construct TN-L15 were successful in HEK293 cells and hippocampal neurons. When targeted to the plasma membrane, the indicator readily responded to agonist-induced increases in cytosolic calcium and kept its full dynamic range. In the last part of this work, transgenic mouse lines were created expressing one of the new calcium indicators in the cytosol of neurons. Imaging experiments in live tissue cultures and brain slices revealed responses to rises in calcium that were superior to previously published indicator performance in mouse lines expressing other calcium probes.

The novel troponin C-based probes of intracellular calcium developed in this work have the potential for monitoring calcium dynamics in applications in which previous calmodulin-containing calcium indicators failed, possibly because they interact less with the cellular biochemical machinery and are thus more compatible with transgenic expression in tissue and whole organisms.

2. INTRODUCTION

2.1 *Fluorescence Techniques*

Fluorescence microscopy is a very sensitive form of dark-field microscopy which allows the detection of even low levels of emitted light against an - ideally - black background. The high contrast of the images is achieved by the use of fluorescent probes, either in the form of small fluorescent synthetic dye molecules or fluorescent proteins. Fluorescent dyes can be applied to living specimen and are therefore immensely useful tools to visualize, track, and quantify particular components of complex biomolecular assemblies, including live cells and tissue. Technical progress in chemical and biological engineering has led to an increasing number of fluorescent probes that can be localized to specific regions of a biological specimen, a feature that greatly enhances the spatial resolution of fluorescence microscopy. Apart from their use as visible markers, fluorescent dyes can also be turned into very sensitive and selective reporters of responses to a specific stimulus, enabling researchers to probe the dynamics, conformational changes and interactions of single molecules in real-time imaging experiments.

2.1.1 **Fluorescence and FRET**

Fluorescence is the result of a three-stage process that occurs in certain molecules (generally polyaromatic hydrocarbons or heterocycles) called fluorophores or fluorescent dyes. A Jablonski diagram illustrates the electronic-states that are responsible for the fluorescence of a fluorophore (Figure 1). The first stage is called the excitation process. Here, a photon of energy $h\nu_A$ is supplied by an external source such as a lamp or a laser and absorbed by the fluorophore, creating an excited electronic singlet state (S1). This excited-state lasts considerably longer than the excitation process: the excited-state lifetime, that is, the average time between its excitation and the return to the ground state, of an organic fluorophore typically has a duration of 1–10 nanoseconds. In this stage, the fluorophore undergoes conformational changes and can interact in many ways with its molecular environment. These interactions have two important consequences: First, the energy of S1 is partially dissipated, and the fluorophore generally relaxes to the lowest energy level of the excited state from which the subsequent fluorescence emission originates. Second, not all the molecules that were initially excited to the excited state

return to the ground state S_0 by fluorescence emission. Non-radiative decay can also depopulate the excited state S_1 ; such processes include collisional quenching, fluorescence resonance energy transfer (FRET) and intersystem crossing. The amounts of radiative and non-radiative decay are expressed in the fluorescence quantum yield, which is the ratio of the number of fluorescence photons emitted to the number of photons absorbed in the excitation process. In a last stage, fluorescence emission returns a fluorophore to its ground state S_0 by emission of a photon of energy $h\nu_F$. Due to energy dissipation during the excited-state lifetime mentioned above, the energy of the emitted photon is lower than the one of the excitation photon $h\nu_A$. Emission therefore occurs at a longer wavelength than excitation, and the difference in energy or wavelength represented by $(h\nu_A - h\nu_F)$ is called "Stokes' shift". The Stokes' shift is one of the reasons for the high sensitivity of fluorescence microscopy because it allows emitted photons to be detected at another wavelength than excitation photons, leaving visible only the emission sources. This makes for a low background in imaging experiments, in contrast to bright-field transmitted light microscopy techniques.

Another reason for the high sensitivity of fluorescence microscopy is the fact that the entire fluorescence process is cyclical. Unless the fluorophore is irreversibly destroyed in the excited state, for example by photobleaching (see below), the same single fluorophore can be excited repeatedly and thus generate many thousands of detectable photons. For general background reading on fluorescence, see Lakowicz (1999).

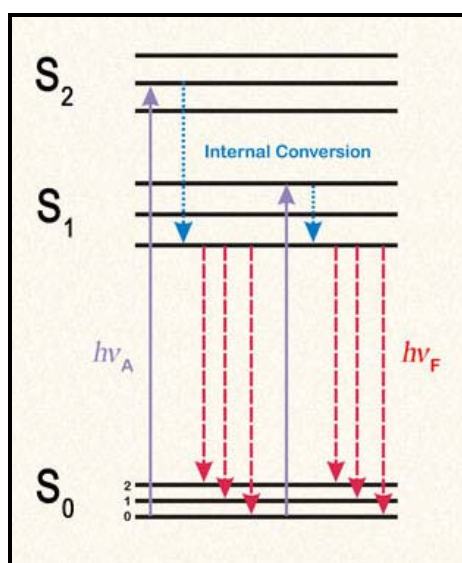


Figure 1: Jablonski diagram of the three main stages of fluorescence. S_0 , fluorescence ground state. S_1 , excited state. $h\nu_A$, excitation by a photon of energy $h\nu_A$. $h\nu_F$, emission of a photon of energy $h\nu_F$. From <http://amanda.berkeley.edu/~bramall/>

There are however certain drawbacks in fluorescence microscopy that compromise detection sensitivity. One limitation is background fluorescence, that is the signals emitted from the sample itself (referred to as autofluorescence) or from nonspecifically bound probes (referred to as reagent background). The phenomenon of background fluorescence can be minimized for example by mathematical background subtraction from data images or by selecting fluorescent probes that absorb and emit at longer wavelengths. One advantage of such red-shifted probes is the fact that biological samples show minimal autofluorescence when they are excited at >500 nm. Furthermore, light scattering in tissues is reduced at longer wavelengths, thus allowing excitation light to penetrate further.

A second problem encountered in fluorescence microscopy is photobleaching, the irreversible destruction of the excited fluorophore under high-intensity illumination conditions. Apart from the illumination intensity, the rate of bleaching depends on the photolability of the fluorophore and is enhanced by the presence of reactive molecules like oxygen.

The general environmental sensitivity of fluorescence is a third problem one has to be aware of. Fluorescence intensity can be decreased by a variety of quenching processes caused by either fluorophore–fluorophore interactions between two adjacent fluorophores or between a fluorophore and other species in the surrounding environment. Examples are processes like collisional quenching, in which the excited state fluorophore is deactivated by contact with another molecule in solution, or self-quenching in which one fluorophore is quenched by another. The latter is especially prominent whenever high dye concentrations or labeling densities are used. Generally, fluorescence emission spectra and quantum yields are more dependent on the environment than absorption spectra and extinction coefficients. However, the environmental sensitivity of fluorescent dyes can be a useful trait in cases where dyes are used as reporter probes of environmental changes such as pH, intermolecular proximity, or ion concentration.

One way to decrease the problem of environmental sensitivity of fluorescence is conducting so-called ratiometric measurements such as FRET experiments (see below). Some fluorescent probes used to respond to a stimulus or to report environmental changes undergo shifts in the excitation or emission spectra upon stimulation, and the excitation or emission intensities of the probe can therefore be monitored at different wavelengths. In these cases, the response signal is made up by the ratio R of the fluorescence intensities, as

opposed to a simple increase in fluorescence intensity in single wavelength measurements (Figure 2). The most common ratiometric measurements are dual-wavelength experiments employing a fluorescent probe which emits light at two different wavelengths. Ratiometric measurements have the advantage of reducing the data distortions caused by sample motion artefacts, by variations in probe loading and retention, as well as by instrumental factors such as illumination stability. The ratioing therefore helps correct for occurrences such as sample movements, variations in indicator concentration, cell shape, lamp and detector fluctuations and photobleaching, and leads to a more stable signal output (Helmchen, 2000), (Molecular Probes, 2004).

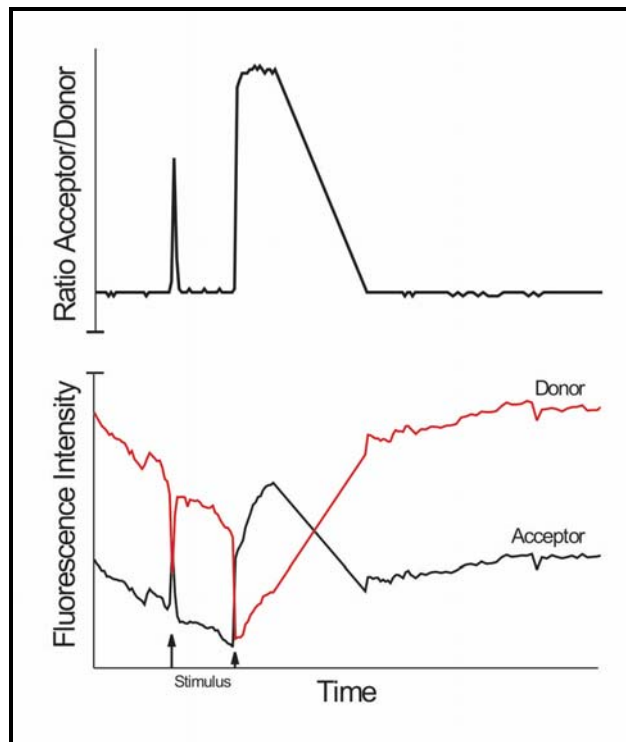


Figure 2: Benefits of dual-wavelength ratiometric measurements of a fluorescent probe. The two emission intensity traces of the donor and the acceptor fluorophore are unstable and noisy due to internal and external factors such as motion of the sample, uneven illumination, bleaching and quenching (lower part of the figure). However, the ratioed signal of acceptor intensity/donor intensity in the upper part of the figure shows a clearer and more stable signal before and after stimuli (arrows).

One type of fluorescent dye used for ratiometric imaging make use of a phenomenon referred to as fluorescence resonance energy transfer (FRET). FRET is a quantum-mechanical transfer of energy from the excited state of a donor fluorophore to the ground state of a neighboring (fluorescent or non-fluorescent) acceptor molecule, without emission of a photon. FRET occurs under the condition that the absorption spectrum of the

acceptor and the fluorescence emission spectrum of the donor overlap. Second, donor and acceptor molecules must be in close proximity to each other (typically 10-60 Å) since FRET is an extremely distance-dependent interaction between the electronic excited states of the two dye molecules. The efficiency of FRET is dependent on the inverse sixth power of the intermolecular separation, making it useful over distances comparable with the dimensions of biological macromolecules. Third, the mutual orientation of the donor and acceptor chromophores also affect FRET efficiency and must be favorable for the occurrence of FRET. Thus, FRET is an important technique for investigating biological phenomena that produce changes in molecular proximity and orientation, such as colocalization of proteins and other molecules. It is difficult, though, to convert FRET measurements into absolute distance between fluorophores because both distance and mutual orientation affect FRET. Another application that is at the very heart of the work presented here is the technique of engineering pairs of macromolecules to serve as biosensors that change their FRET in response to biochemical and physiological signals. One example of such a biosensor is shown in Figure 3. The schematic drawing shows a donor and an acceptor fluorescent protein attached to each other by a ligand-binding linker unit. During FRET, the donor transfers some of its energy onto the acceptor, and the fluorescent acceptor in turn re-emits the transferred energy as its own fluorescence at longer wavelengths. In probes of this design, the linker is capable of binding a specific ligand and responds by a conformational change. If this conformational change sufficiently alters the distance and orientation of the two fluorophores, then a change in FRET will be observable by intensity changes in the fluorescence emissions of donor and acceptor.

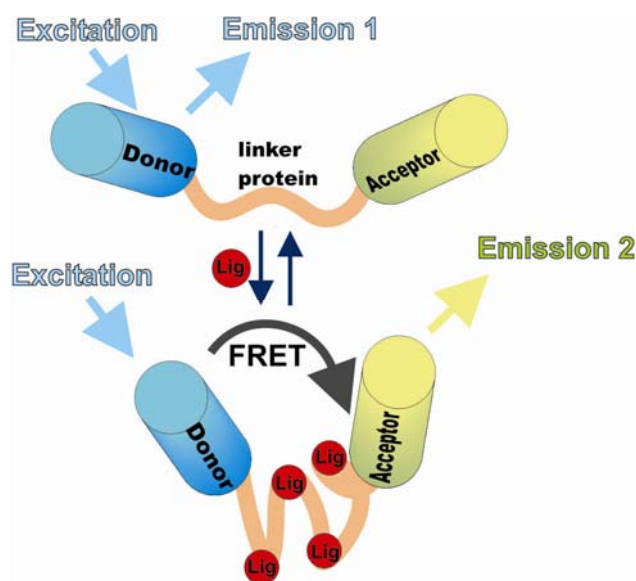


Figure 3: Schematic representation of FRET occurring in a ratiometric indicator consisting of two fluorescent proteins with a ligand binding linker protein in between. Ligand (Lig) binding to the linker leads to a conformational change in the whole macromolecule, thereby enhancing the fluorescence resonance energy transfer (FRET) from the donor to the acceptor moiety. The illumination wavelength is chosen so as to excite only the donor, and the ensuing donor and acceptor emissions are monitored separately at their respective wavelengths.

Monitoring signal changes at two different wavelengths in such FRET-based indicators allows emission ratioing. As mentioned above, this offers the advantage of fewer artefacts in the measurement because variations in sample position, excitation intensity, collection efficiency, and number of donor-acceptor pairs are cancelled out.

2.1.2 The Green Fluorescent Protein

The first and most well-known of all fluorescent proteins is the green fluorescent protein (GFP) from the Pacific Northwest jellyfish *Aequoria victoria*. Shimomura and coworkers discovered it in the 1960's when they were characterizing a luminescent protein from the same jellyfish, aequorin (Shimomura et al., 1962). The structure of GFP was solved in 1996 (Yang et al., 1996), (Ormo et al., 1996) and it was found to have a novel three-dimensional structure: the β -barrel (or β -can). The protein has the overall shape of a cylinder, with a diameter of 30Å and a length of 40Å. Eleven tightly-fitted staves of β -sheets form the body of the barrel (hence its name) and an α -helix runs up the axis (Figure 4). This α -helix on the inside of the barrel forms a scaffolding onto which the fluorophore of the protein is held. Because of this location inside the cylinder, the fluorophore is protected against photochemical damage or the passage of interfering diffusible ligands.

The chromophore itself is a conjugated π -electron system made up by two aromatic rings; it derives from a modified Ser-Tyr-Gly sequence (residues 65-67) in wildtype GFP. This tripeptide condenses spontaneously into the cyclic conformation of a 4-(p-hydroxybenzylidene) imidazolid-5-one without any cofactors or enzymatic components, and only molecular oxygen is needed in the last step for the dehydrogenation of the tyrosine α - β bond to a conjugated double bond (Cody et al., 1993), (Reid and Flynn, 1997). This ability to perform an autocatalytical cyclization in its own peptide backbone without the help of external cofactors is rarely observed in other protein species and makes GFP ideal for intracellular applications.

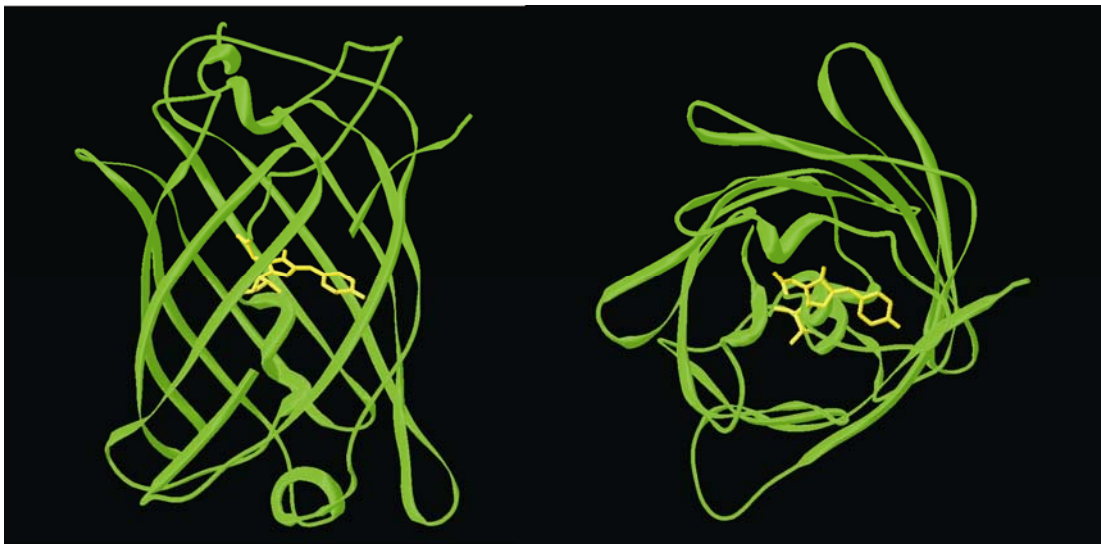


Figure 4: Crystal structure of GFP with a Thr-Tyr-Gly sequence forming the chromophore. Side view (left) and top view (right) of the β -barrel. Some amino acids were deleted in the right picture to allow a better view of the fluorophore (yellow). Modified from pdb-entry 1Q4A (Jain and Ranganathan, 2004).

The wildtype GFP sequence has been mutated extensively to alter and improve the physical properties of the protein; a good review of this work can be found in (Tsien, 1998). Mutations in and around the chromophore region lead to shifts in the excitation and emission spectra and therefore to differently colored GFP variants such as "cyan fluorescent protein" (CFP) with an indole ring (Y66W) and "blue fluorescent protein" (BFP) with an imidazole (Y66H) in the chromophore, "Sapphire" with the mutation T203I adjacent to the chromophore, and "yellow fluorescent protein" (YFP) with the mutations S65G and T203F in the chromophore region. Other mutations in the wildtype sequence were made to address known problems with early GFP variants such as low mammalian expression levels, pH and Cl^- sensitivity, low photostability, and slow folding kinetics. The

two *Aequoria victoria*-derived fluorescent proteins used most widely in the work presented here are the ECFP variant containing the mutations F64L, S65T, Y66W, N146I, M153T, and V163A (Heim and Tsien, 1996). The second fluorescent protein mainly used here is the Citrine variant of YFP containing the mutations S65G, V68L, Q69M, S72A, T203Y, and V163A (Griesbeck et al., 2001).

Ongoing work on fluorescent proteins deals not only with the protein family derived from *Aequoria victoria* GFP. Other marine organisms are also continually being screened for new fluorescent proteins, and a whole set of fluorescent proteins that are structurally homologous to *Aequoria victoria* GFP have been described. Many of these were found in various Anthozoan species, the most prominent being the DsRed protein from a *Discosoma* coral which, as its name indicates, emits light in the red region of the visible spectrum and is therefore an important complement to the blue and green emitting *Aequoria* proteins (Matz et al., 1999). Other new proteins that also emit in the blue and green range include zoanGFP from *Zoanthus* sp. (Matz et al., 1999), Cop-Green (or ppluGFP2) from *Copepoda*, and Phi-Yellow (or Phialidium-YFP) from *Hydrozoa* (Shagin et al., 2004). However, most of these new discoveries suffer from the same shortcomings as early GFP variants, that is, low brightness, poor folding at 37°C (as most of these organisms evolved in cold seawater), and a persistent tendency to form dimers and tetramers which makes them unsuitable for applications where protein-protein interactions and trafficking are to be observed. Profound protein engineering similar to the work done on GFP will be necessary to get rid of all these unwanted effects. Promising results were recently published on DsRed which was turned into a variety of monomeric forms with improved color spectrum, brightness and stability (Shaner et al., 2004).

Such optimized fluorescent proteins, first and foremost *Aequoria* GFP and its derivatives, have been expressed with great success as functional transgenes in bacteria, *C. elegans*, yeast, slime mold, plants, *Drosophila*, zebrafish and mammalian cells, making them invaluable tools in cell, developmental and molecular biology (Chalfie et al., 1994), (Yeh et al., 1995), (Amsterdam et al., 1995), (Prasher, 1995). One important application of fluorescent proteins is their use as noninvasive, passive visible markers in living cells. It has been shown that fusions of GFP to a protein rarely affect the investigated protein's activity or mobility, and GFP also turned out to be nontoxic in most cases. Therefore, GFP and its derivatives constitute good fluorescent fusion tags for applications such as

monitoring protein localizations, tracing cell lineages, reporting gene expression, or measuring protein-protein interactions (Lippincott-Schwartz and Patterson, 2003).

2.1.3 Fluorescent Calcium Probes

A second application of fluorescent proteins is their use as active indicators of biochemical processes such as metabolite concentrations or enzyme activity. Many of these biochemical events can also be monitored by small fluorescent organic molecules engineered to report changes in, for example, ion concentration, pH, membrane potential, and other cellular processes (for an overview, see *Molecular Probes* (2004) and Tsien (1989)). However, most of these organic dyes have a number of disadvantages. For one thing, they have to be loaded into cells either through external bath application or by direct injection. Both methods make it hard to label specific subsets of tissues or cellular structures, and imaging experiments can only be performed for a limited amount of time due to leaking of the dye. Another drawback of organic molecules is that it is difficult to design probes for larger and more complex ligands such as peptides, small proteins, carbohydrates, nucleotides, and others. Indicators based on proteins on the other hand can be modified to respond to even very complex biological signals such as phosphorylation events or enzyme activation, and they can be targeted and restricted with great precision to subcellular compartments by means of the cellular protein trafficking machinery. Furthermore, they can be introduced into tissues and whole animals by means of gene transfer, and their expression can be regulated spatially and temporally by the choice of promoter for gene expression (Zhang et al., 2002), (Rudolf et al., 2003), (Griesbeck, 2004).

Some of the first probes based on fluorescent proteins for measuring dynamic processes were indicators responding to changes in intracellular calcium concentration. In 1997, both Miyawaki et al. and Romoser et al. reported the construction of FRET indicators that consisted of two GFP proteins of different color fused to a calcium-sensitive linker molecule (Miyawaki et al., 1997), (Romoser et al., 1997). The general design of the probes by Miyawaki – a class of indicators that became known as „Cameleons“ – consisted of two GFP molecules with overlapping spectra; a first pair were BFP and GFP which were later changed to the combination CFP and YFP for reasons of better resistance to bleaching, less autofluorescence, and enhanced brightness. In between the two fluorescent proteins, a calmodulin protein was fused in its full length as a calcium binding moiety. As it turned out, calmodulin by itself did not induce a large enough conformational change to

achieve a good FRET response, and in addition it seemed problematic to introduce a large amount of exogenous calmodulin into a cell as this might have disturbing effects. Therefore a calmodulin binding peptide (the 26-residue calmodulin binding peptide M13 of myosin light chain kinase) was fused C-terminally to the calmodulin domain to convert this calcium indicator into a functional, more self-contained system. The two proteins were separated by a short glycine linker to enhance the flexibility of the ensemble. Figure 3 shows the schematic configuration of such a probe; in the case of a Cameleon, the linker peptide consists of the succession calmodulin-Gly-Gly-M13. This indicator design, a protein unit responsive to a biochemical signal sandwiched between the two fluorophores CFP and YFP, has become very popular ever since for the construction of a whole variety of other fluorescent probes. Examples include indicators of phosphorylation events mediated by protein kinases such as PKB (Kunkel et al., 2005), PKA (Zhang et al., 2001), PKC (Violin et al., 2003), and cdc42 (Itoh et al., 2002), (Seth et al., 2003). Other examples are fluorescent reporter constructs that report binding of second messengers like cAMP (Zaccolo et al., 2000), cGMP (Honda et al., 2001), inositol-3,4,5-trisphosphate (Hirose et al., 1999), and many more.

The most common techniques used for real-time imaging of cellular events monitored by CFP/YFP based FRET indicators is wide-field fluorescence microscopy or laser scanning confocal microscopy. Confocal imaging gives less out-of-focus signals but has the disadvantage of depending on commercially available laser lines of which only few allow specific excitation of CFP at 430 nm or less. Both imaging techniques suffer from the problem that CFP emission and YFP excitation spectra overlap (Figure 5) and are therefore hard to separate completely, even with narrow bandpass filters. CFP emission is very likely to show up in the YFP emission channel, thereby continually contributing to a substantial amount of background FRET. These defects could be overcome by FRET probes with a larger Stokes' shift allowing a better separation of excitation and emission wavelengths. Good candidates for this could be for example the high Stokes' shift-GFP variant Sapphire together with some red-shifted form of fluorescent protein.

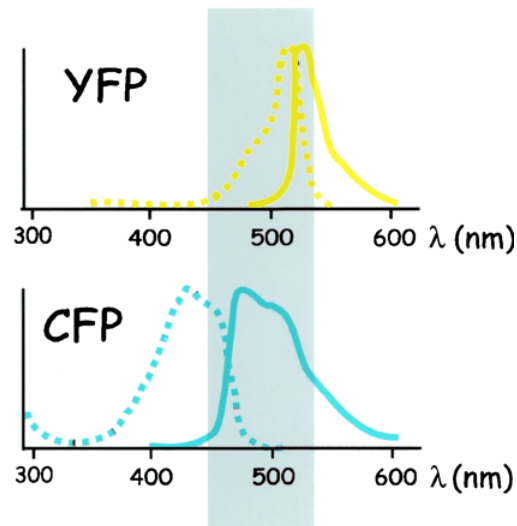


Figure 5: Excitation and emission spectra of CFP and YFP. Dotted lines are the excitation, straight lines the emission spectra of the two proteins. The gray box shows to which degree CFP emission and YFP excitation overlap. From (Zaccolo, 2004).

The construction design used in the creation of Calmodulin-type calcium indicators - that is, a calmodulin protein fused to fluorescent proteins - was later imitated in another variety of calcium indicators consisting of only a single fluorescent protein. After studies had suggested that a GFP protein could tolerate the insertion of large proteins at a few specific sites in its sequence, researchers began fuse calmodulin into these sites and thereby managed to create probes responding to calcium with fluorescence intensity changes. Calmodulin was inserted at amino acid residue 145 first in the YFP and later the Citrine protein sequence, these calcium probes became known as Camgaroo-1 and Camgaroo-2 (Baird et al., 1999), (Griesbeck et al., 2001). Another single-GFP indicator variety was created by fusing calmodulin and its binding partner M13 to a so-called circularly permuted GFP; these cp proteins consist of two halves of a GFP that were cut open at position 145 and reattached to each other in inverse order by a short linker peptide (Nakai et al., 2001), (Nagai et al., 2001). Many single fluorescent protein probes have brighter and faster signals than the FRET based ones of the Cameleon type. However, most of them can only be used in non-ratiometric measurements which makes their response signals more vulnerable to artefacts. Some suffer from additional drawbacks such as increased pH sensitivity and insufficient folding at 37°C (Nakai et al., 2001).

FRET-based and single-GFP calcium indicators have been expressed and put to use extensively in live applications like cell and tissue culture and transgenic animals. Even the earliest published Cameleon indicators could already be successfully expressed in cell

culture, and calcium imaging was possible in the cytosol as well as in the ER and the nucleus (Miyawaki et al., 1997). During the following years, calcium indicators were targeted to various other cellular sites and organelles, and expression attempts were undertaken in live animals. As it turned out, not all of these efforts were successful. In some targeting studies, the early versions of Cameleon indicators lost their functionality, for example at the cell membrane and in certain fusion constructs like synaptic proteins and receptor domains. The same is true for expression of functional calcium indicators in transgenic animals. First successful calcium imaging experiments with protein-based calcium indicators in transgenic organisms were done in *C. elegans* (Kerr et al., 2000), *Drosophila* (Fiala et al., 2002), (Reiff et al., 2002), zebrafish (Higashijima et al., 2003), and mice (Ji et al., 2004), (Hasan et al., 2004). One has to note though that the signals obtained in living organisms were in almost all cases considerably lower than could be expected from the *in vitro* and cell culture performance of the respective indicator (an overview is listed in (Griesbeck, 2004)). Ratiometric Cameleon indicators seem to perform especially bad in mammals. Experiments in a transgenic mouse line expressing Yellow Cameleon 3.60 in neurons under control of the β -actin promoter showed that even tetanic stimulation in hippocampal brain slices led to only as little as a 3 % ratio change (Nagai et al., 2004). Other research groups did not manage to get functional responses from Cameleon indicators in transgenic mice at all (Hasan et al., 2004). Because all calcium indicators to date use the combination calmodulin-M13 as calcium binding domain, it was suspected that the calmodulin unit could be responsible for the inactivation or modification of probes encountered in certain expression systems. Calmodulin has numerous functions as a signaling molecule in the cell; it is bound by a multitude of proteins, has a large number of phosphorylation sites, and is altogether heavily regulated (Jurado et al., 1999), (Erickson et al., 2001). If calmodulin was indeed the reason for the indicators' loss of function, then replacing it by a different calcium binding linker that interferes less with cell metabolism might be a solution to that problem. The task of this thesis project was therefore to provide a new calcium binding linker protein that could be introduced into a fluorescent protein indicator, keeping the functionality and dynamic range as favorable as possible while at the same time being less sensitive to interaction with cellular components. In order to find protein candidates that had the potential to fulfill these requirements, a closer look was taken at the best known families of calcium binding proteins.

2.2 Calcium-Binding Proteins

2.2.1 EF-Hands

Calcium is one of the most important metals in living organisms, controlling vital processes from bone mineralization and muscle contraction to enzyme activation, cell signaling and many types of secretory responses (Berridge et al., 2000). Although calcium ions interact with a very large number of proteins, the variety of configurations of protein calcium-binding sites is rather limited. The most common type of a calcium-binding domain is the so-called "EF-hand" motif, found in numerous protein families with quite diverse biological functions ranging from the regulation of cellular activities to calcium transport and buffering (Kawasaki et al., 1998). The name "EF-hand" originates from two helix domains of the muscle protein parvalbumin labeled "E" and "F" in which such a calcium-binding loop motif was first discovered. A typical representative of an EF-hand has an affinity for calcium as well as magnesium and induces a conformational change upon ion binding. This conformational change in turn transmits the calcium signal to other components of the signaling cascade.

Generally, an EF-hand domain consists of a helix-loop-helix motif in which the twelve-residue loop is flanked on both sides by a twelve residue α -helical domain. A calcium ion is coordinated in a pentagonal-bipyramidal configuration by six amino acid residues as shown in Figure 6. The amino acids involved in the calcium binding are located in positions 1, 3, 5, 7, 9 and 12 of the twelve-residue loop and are designated X, Y, Z, -X, -Y, and -Z. A rather conserved set of amino acids is found in these positions: X and Y are usually made up of the side chains of Asp or Asn, the Z position contains Asp, Asn, or Ser side chains, and a carbonyl oxygen lies at -Y. The -X position is usually a water molecule, and -Z is an almost invariant Glu or Asp residue which works as a bidentate ligand in the coordination of Ca^{2+} by providing two oxygens (Lewit-Bentley and Rety, 2000).

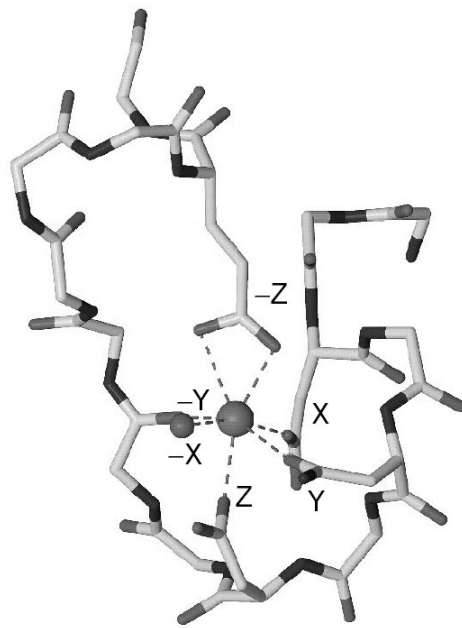


Figure 6: Schematic drawing of an EF-hand motif showing the positions of the amino acid residues coordinating a calcium ion. From (Lewit-Bentley and Rety, 2000).

Since EF-hand motifs often occur in adjacent pairs, a protein containing four EF-hands usually has two domains, each formed by a pair of EF-hands separated by a flexible linker. Good examples for this are the dumbbell structures of calmodulin and troponin C, the two calcium binding proteins studied in this work (Sundaralingam et al., 1985), (Houdusse et al., 1997). The EF-hands within one protein usually differ in their binding affinities for Ca^{2+} and Mg^{2+} , and studies suggest that those EF-hands involved in regulation of cellular activities display a lower Ca^{2+} and Mg^{2+} affinity than do nonregulatory EF-hand domains that have only structure-stabilizing functions (Szczesna et al., 1996), (Davis et al., 2002). The technique of exchanging one or more of the six amino acid residues in the EF-hand loop crucial to ion complexing has been used extensively as a tool to investigate the effects on Ca^{2+} and Mg^{2+} binding properties (Tikunova et al., 2002), (Davis et al., 2002), (Tikunova and Davis, 2004).

2.2.2 The Troponin Family

As presented above, the motivation underlying the present work was to find a calcium binding protein that could act as replacement for calmodulin in fluorescent calcium indicator proteins. Among all the possible candidates for such a linker protein, one of the first choices was the troponin protein family.

Troponin proteins are part of a regulatory complex involved in contraction and relaxation of striated skeletal and cardiac muscle. The thin filament of a muscle consists of polymerized F-actin filaments to which the dimeric coiled-coil α -helices of tropomyosin (Tm) and the troponin complex (Tn) attach. Each tropomyosin is associated with one troponin complex and covers the surface of an actin helix strand with a ratio of one tropomyosin per seven actin monomers. The troponin complex contains three different subunits: troponin T (TnT), which binds to tropomyosin; troponin I (TnI), which binds to actin and inhibits the actomyosin ATPase; and troponin C (TnC), which relieves the TnI inhibition when calcium binds to its N-terminal regulatory domain. Thus, the troponin complex as a whole acts as a Ca^{2+} -sensitive molecular switch (Farah and Reinach, 1995).

A cycle of muscle contraction-relaxation begins with the binding of Ca^{2+} to the troponin C regulatory sites. Since TnC does not interact directly with actin or tropomyosin, the Ca^{2+} -binding signal must be transmitted to the thin filament via the other two troponin subunits. This series of protein-protein interactions in turn results in a strong interaction between myosin crossbridges of the thick filament and actin, removing TnI inhibition of the ATPase. As ATP is hydrolyzed, the two filaments slide past one another and generate muscle force (Gordon et al., 2000).

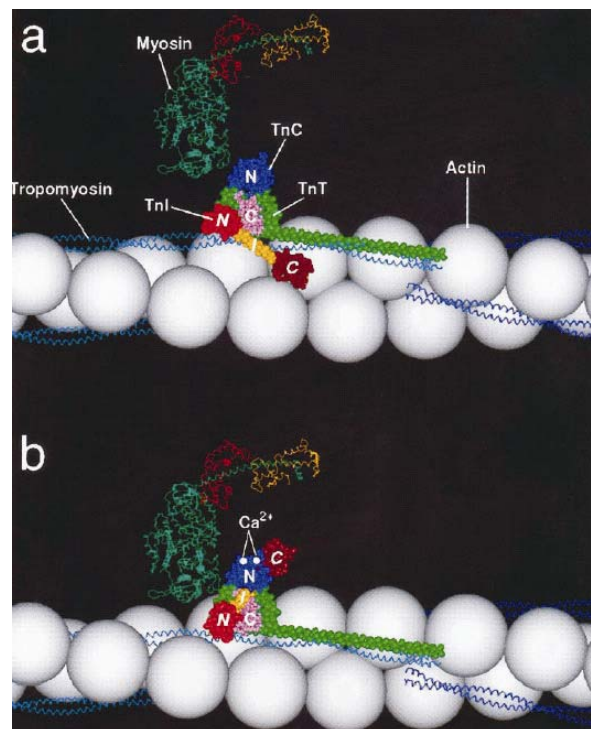


Figure 7: Model of the troponin-tropomyosin-actin organization. The N- and C-terminal domains of TnC are shown in blue and pink. From (Berchtold et al., 2000).

Whereas a great deal is known so far about the structural details of the actin-myosin interface, the mechanisms of how the initial Ca^{2+} -binding signal is passed on to TnI, TnT, Tm and actin are still under investigation. Since the signal transduction among these proteins has been found to be the consequence of a cascade of conformational changes, a variety of studies have focused on resolving the structural details of the individual components of the Tn-Tm complexes in order to understand their function in the whole contractile machinery. A first crystal structure of the entire Tn complex of human cardiac muscle was accomplished in 2003 (Takeda et al., 2003), but troponin C remains the one subunit of the Tn complex whose structure has been investigated most extensively up to date (Vassilyev et al., 1998), (Houdusse et al., 1997), (Mercier et al., 2001), (Strynadka et al., 1997).

Troponin C (TnC or TNC) is a dumbbell-shaped, ~160 residue, highly α -helical calcium binding protein consisting of two similarly sized globular domains connected by a central linker helix. Each of these domains contains two potential metal binding sites with a helix-loop-helix pattern that is typical of the EF-hand motifs found in many calcium binding proteins. The four metal binding sites are numbered I-IV starting from the N-terminus of the protein and have different affinities for calcium and magnesium (Mercier et al., 2000).

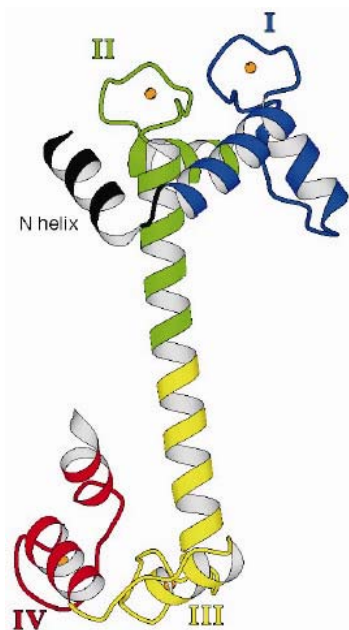


Figure 8: Ribbon diagram of a rabbit TnC crystal structure in the 4 Ca^{2+} -bound state. The four metal binding EF-hand loop regions are numbered I-IV. From (Houdusse et al., 1997).

Two isoforms of TnC exist in vertebrates, one is found in fast skeletal muscle (sTnC) and the other in slow skeletal and cardiac muscle (cTnC). They vary in their number of functional metal binding sites as well as their affinities for Ca^{2+} and Mg^{2+} ions. The skeletal versions of vertebrate TnC contain two binding sites in the N-terminal domain capable of binding two Ca^{2+} ions in a fast reaction with moderate affinities (Kd values of $\sim 3 \mu\text{M}$), whereas the two C-terminal binding sites were found to bind Ca^{2+} ions with slow kinetics but much higher affinities (Kd values of $\sim 50 \text{ nM}$) (Johnson et al., 1994). Both domains of sTnC are also able to bind magnesium, the C-terminal binding sites again with higher affinities than the N-terminal sites. Because of their high Ca^{2+} and Mg^{2+} affinities and slow exchange rates, the C-domain sites are occupied by either Ca^{2+} or Mg^{2+} even under resting physiological conditions and are therefore considered to play a structural role by anchoring sTnC into the sTn complex. On the other hand, the N-domain sites of sTnC are believed to play a role in the regulation of muscle contraction and relaxation, which is why the N-terminal part of TnC is also called the regulatory domain (for review, see (Berchtold et al., 2000)). However, magnesium binding is not solely restricted to the C-domain sites of sTnC since the second EF-hand of TnC has also been shown to bind Mg^{2+} competitively under physiological Mg^{2+} concentrations (Davis et al., 2002).

The vertebrate cardiac troponin C variants differ from the skeletal versions in several respects. Whereas the Ca^{2+} and Mg^{2+} -binding properties of their structural C-domain sites are similar to those of skeletal TnC, their regulatory N-domains are capable of binding only one Ca^{2+} ion at the second EF-hand. The first EF-hand of cTnC is unable to bind Ca^{2+} because of a single residue insertion (Val28) and two Ca^{2+} -coordinating ligand substitutions Asp29Leu and Asp31Ala (Spyracopoulos et al., 1998).

Troponin C in the fruit fly *Drosophila melanogaster* comes in 3 isoforms; isoform 1 is present only in adult fly muscles, isoform 2 is found almost exclusively in larval muscles, and isoform 3 is present in both larval and adult muscles. *Drosophila* troponin C isoform 1 (also called TPC1_DROME) is a polypeptide 154 amino acids long and originates from the gene called TpnC41C or TnC41C. The structure of *Drosophila* troponin C isoform 1 also comprises four EF-hand domains; here, the second and the fourth loop regions of the EF-hands (amino acids 57 to 68 and 133 to 144) are responsible for calcium binding whereas loop regions 1 and 3 (amino acids 24 to 35 and 97 to 108, respectively) form ancestral calcium sites that have lost their calcium binding capabilities similar to cTnC with its one defunct EF-hand (Herranz et al., 2004).

3. ABBREVIATIONS

A	adenine
ACSF	artificial cerebrospinal fluid
AM	acetoxymethyl
AMPA	α -amino-3-hydroxy-5-methyl-4-isoxazole propionic acid
APV	2-amino-5-phosphonovalerate
BAPTA	1,2-bis-[2-aminophenoxy]ethane-N,N,N',N'-tetraacetic acid
BBS	BES-buffered saline
BES	N,N-bis[2-hydroxyethyl]-2-aminoethanesulfonic acid
BFP	blue mutant of GFP
C	cytosine
CCD	charge-coupled device
CFP	cyan fluorescent protein
CMV	cytomegalovirus
CNS	central nervous system
csTnC	chicken skeletal muscle troponin C
DMEM	Dulbecco's Modified Eagle Medium
DMSO	dimethyl sulfoxide
DNA	deoxyribonucleic acid
DsRed	red fluorescent protein from <i>Discosoma</i> sp.
EDTA	ethylenediamine tetraacetic acid
EGFP	"enhanced" version of GFP
EGTA	ethylene glycol-bis[β -amino-ethyl ether] N,N,N',N'-tetraacetic acid
ER	endoplasmic reticulum
F	fluorescence light intensity
FAD	flavin adenine dinucleotide
FCS	fetal calf serum
FRET	fluorescence resonance energy transfer
G	guanine
GFP	green fluorescent protein
HBSS	Hanks' balanced salt solution
HEK	human embryonic kidney
HEPES	N-(2-hydroxyethyl)piperazine-N'-(2-ethanesulfonic acid)
humTnC	human cardiac muscle troponin C
IP ₃	inositol-1,4,5-trisphosphate
IPTG	isopropyl- β -D-thiogalactopyranoside
kD	kilodalton
Kd	dissociation constant
k_{off}	dissociation rate constant
k_{on}	association rate constant

M	marker protein
MOPS	3-(N-morpholino)propanesulfonic acid
NADH	nicotinamide adenine dinucleotide (reduced form)
NB	newborn
NMDA	N-methyl-D-aspartate
NTA	nitriloacetic acid
OD	optical density
P	postnatal day
PBS	phosphate-buffered saline
PBT	phosphate-buffered saline with Triton X-100
PCR	polymerase chain reaction
PFA	polyformaldehyde
PIPES	piperazine-1,4-bis(2-ethanesulfonic acid)
PMSF	phenylmethylsulfonylfluoride
R	ratio; fluorescence intensity of acceptor emission over donor emission
R _{max}	ratio R at highest ligand concentration
R _{min}	ratio R in ligand-free conditions
SDS	sodium dodecyl sulfate
T	thymine
TAE	tris-acetate-EDTA electrophoresis buffer
TE	tris-EDTA buffer
TnC	troponin C
TRITC	tetramethylrhodamine isothiocyanate
WT	wildtype
YFP	yellow fluorescent protein
$\Delta F/F$	fractional change in fluorescent light intensity
ΔR	difference of ratio R under Ca-saturated and Ca-free conditions

4. MATERIALS AND METHODS

4.1 Working with DNA

4.1.1 Spectrometric Determination of DNA Concentration

Double-stranded DNA has an absorption maximum at 260 nm; by measuring the absorption of an aqueous DNA dilution in a 1 cm quartz cuvette, the DNA concentration of the sample could be calculated using the following formula:

$$\text{conc. DNA } [\mu\text{g/ml}] = \text{OD}_{260} * 50 * \text{dilution factor}$$

4.1.2 Gene Amplification by PCR

Primer annealing temperatures varied in different reactions and were chosen according to the predicted primer melting temperature which is influenced by the GC content of the primers' overlapping regions.

PCR reaction mix:

50-60 ng plasmid DNA as reaction template

1 μl dNTP solution (12.5 mM)

2 μl primer No. 1 (50 μM)

2 μl primer No. 2 (50 μM)

5 μl polymerase buffer (10x, provided by manufacturer)

38 μl H₂O

1 μl (2 U) Vent polymerase.

Reaction cycles:

5 min heating to 95°C;

30 amplification cycles:

30 sec 95°C: melting of double-stranded DNA

30 sec annealing of primers; temperatures varying from 52-62°C

2 min 72°C: DNA synthesis

After cycle completion: 3 min 72°C; reaction termination by cooling to 15°C

4.1.3 Site-directed Mutagenesis by PCR

In order to achieve a single amino acid exchange in a protein, oligonucleotide primers were designed that introduced a point mutation in the desired DNA codon. A mutagenic primer pair contains the same DNA sequence in opposite directions, while the mutated base is located in the middle with about 10-15 additional bases of the original DNA sequence on both sides. The primer length was chosen so as to reach a melting temperature of about 78°C after the following formula: $T_m = (2^\circ\text{C})(A+T) + (4^\circ\text{C})(G+C)$. Care was taken that the primers' GC content amounted to at least 40% and that both primer ends contained GC bases when possible. In the PCR reaction, primer extension times were set to 2 minutes per 1000 base pairs of template DNA.

PCR reaction mix:

5-50 ng plasmid-DNA as reaction template

0.8 µl dNTP solution (12.5 mM)

2.5 µl primer No. 1 (50 ng/µl)

2.5 µl primer No. 2 (50 ng/µl)

5 µl Pfu polymerase buffer (10x, provided by manufacturer)

37.5 µl H₂O

1 µl (2.5 U) Pfu polymerase.

Reaction cycles:

30 sec heating to 95°C;

16 amplification cycles:

30 sec 95°C: melting of double-stranded DNA

1 min 55°C: annealing of primers

2 min per 1kb template at 68°C: DNA extension

Reaction termination by cooling to 15°C.

In order to get rid of unmutated template DNA, 20 µl of the reaction mix were incubated at 37°C for 2 hours with 1 µl (20 U) Dpn1 restriction enzyme which cuts the unwanted methylated plasmid DNA. 2 µl of this restriction assay were used for transformation in bacteria.

4.1.4 Restriction of DNA

DNA restriction was used to generate vector or insert fragments necessary for DNA cloning. Insert and vector were cut with either one or two restriction enzymes at a time. 0.5 - 1 μg DNA for analytical purposes or about 10 μg DNA for larger preparations were cut with 1 - 5 U restriction enzyme per μg DNA. Buffers were used according to the manufacturer's protocols; to avoid unspecific cutting, the volume of each reaction was raised to a minimum of 10x the amount of restriction enzymes used. Incubation times were at least 3 hours, larger amounts of DNA overnight at the temperature suitable for the respective enzymes. The efficiency of the restriction was controlled by running a test sample on an agarose gel.

4.1.5 Ligation of DNA Fragments

In DNA ligations, the ratio of insert to vector should be at least 3:1; DNA concentrations were determined by agarose gel electrophoresis. The ligation reaction mix was incubated overnight at 16°C; about 1.5 μl of the solution were later used for transformation in bacteria.

Ligation assay:

0.5 μl vector DNA

3 μl insert DNA

1.5 μl ligase buffer (10x; provided by manufacturer)

9 μl H₂O

1 μl (400 U) T4 DNA Ligase

4.1.6 Preparation of Competent *E. Coli*

4 ml LB medium were inoculated with the desired strain of *E. coli* and grown at 37°C overnight. The following morning, the culture was transferred into 300 ml LB medium and grown to a OD₆₀₀ of 0.55, the flask then placed in ice for 20 minutes, and the cells harvested by centrifugation at 2500 g and 4°C for 20 minutes. The medium was completely poured off and remaining drops of medium were removed by putting the open bottles on paper towels for a short time. The cells were resuspended in about 60-80 ml of refrigerated Inoue transformation buffer and harvested by centrifugation at 2500 g and 4°C for 15 minutes. The medium was once again poured off, the cell pellet resuspended in about 20 ml of refrigerated Inoue transformation buffer, and 1.5 ml DMSO added to the

suspension. After 10 minutes incubation on ice, the cells were transferred in small aliquots of 50 μ l into pre-cooled tubes, frozen in liquid nitrogen, and stored at -80°C until usage.

4.1.7 Quick Transformation of Chemically Competent *E. Coli*

Chemically competent *E. coli* cells kept in 50 μ l aliquots at -80°C were thawed on ice, mixed with a small amount of the desired DNA plasmid (1-3 μ l), and incubated on ice for about 20 minutes. A heat shock was applied to the cells by transferring them into a 42°C water bath for 2 minutes, and afterwards they were again incubated on ice for about 10 minutes. The cells were then diluted in about 150 μ l of water or LB medium, and immediately plated onto LB agarose plates containing the appropriate antibiotic substance for selection.

4.2 Working with Proteins

4.2.1 Recombinant Protein Expression in Bacteria

Proteins can be expressed in suitable *E. coli* strains by transforming the bacteria with an expression plasmid such as the pRSETB vector carrying the gene of interest. Most efficient expression levels were reached when bacteria of the BL21 strain were transformed according to the Quick Transformation Protocol and directly transferred afterwards into a 15 ml tube containing 4 ml LB medium with the appropriate selective antibiotic. The starter culture was grown overnight and used to inoculate a larger (usually 200 - 400 ml) culture the next day. Cells were grown until they reached an optical density of 0.8 to 1.0, usually after 5-6 hours, and protein expression was then induced by adding a final concentration of 0.5 to 1 μM IPTG as well as an extra dose of antibiotic. Expression was allowed to run overnight, and the bacteria containing the protein finally harvested by centrifugation at 6000 g for 15 minutes.

4.2.2 Purification of Recombinantly Expressed Proteins

All proteins described in this work were cloned in a pRSETB vector containing a sequence of 6 histidine codons at the 5' end of its multiple cloning site, thereby furnishing the recombinant protein with a 6x His tag that allows protein purification by affinity chromatography using Ni-NTA chelating resin material.

The bacteria pellet obtained from a 200 to 400 ml expression culture was resuspended in 7-10 ml Resuspension Buffer which was supplemented with 1 mM PMSF, 5 µg/ml Pepstatin, and 1 µg/ml Leupeptin. To facilitate cell lysis, the suspension was put in an -80°C freezer and thawed after about 10 minutes. 1 mg lysozyme powder were added per ml lysate and the mixture incubated for 30 minutes on ice. Next, 0.1% Triton-X-100, 5 µg/ml DNaseI, and 5 µg/ml RNase were added and the cell suspension then lysed 20 minutes in an ultrasound bath containing ice water. The lysate was centrifuged for 30 minutes at 13.000 rpm, the supernatant containing the recombinant protein decanted, and 300 - 500 µl of Ni-NTA agarose slurry added to the supernatant. The solution was gently shaken overnight at 4°C and the Ni-NTA resin with the bound protein decanted into a polypropylene column. The column was first washed with 20 column volumes of Resuspension Buffer containing 10 mM imidazole, and the protein eluted afterwards with Resuspension Buffer containing 150 mM imidazole. Eluted proteins were stored at 4°C.

4.3 Cell Culture

4.3.1 Preparation of Dissociated Rat Neurons

17-19-day pregnant Wistar rats were killed with CO₂ and the uterus containing the embryos removed and put in a petri dish with PBS. In a sterile environment, the embryos were dissected out of their sacs and transferred in another petri dish containing PBS. Under a dissection microscope, each embryos' skull was opened using a sharp forceps, the skullcap pulled away from the cortex, and the brain tissue dissected free. Excised brains were immediately placed into cold HBSS, the meninges removed with a pair of sharp fine-tipped forceps, and the desired brain region dissected free. For dissociating the tissue, the preparations were incubated for 20 minutes at 37°C in a solution of 1mg/ml dispase in HBSS. The dispase solution was removed after incubation and replaced with the same amount of DMEM/10% FCS. After this, the cells were dissociated by trituration with a flame-polished glass pipette. Glass-bottom cell culture dishes (35 mm) were pre-incubated for about two hours in Poly-L-Lysine solution, then rinsed with PBS and filled with 2 ml DMEM/10% FCS. The cell density of the triturated neurons was checked and the neurons plated onto the dishes and incubated overnight in DMEM/10% FCS at 37°C and 5% CO₂.

The medium was changed after 8-24 hours to Neurobasal/B27 medium in which the neurons were kept for up to 6 weeks or longer.

4.3.2 Transfection of Dissociated Rat Neurons

For transfection of one 35 mm dish containing about 2 ml medium, 100 μ l of CaCl_2 solution for phosphate transfections were mixed thoroughly with 3 μ g DNA, then 100 μ l 2x BBS solution added, mixed carefully again, and incubated for 20 minutes. Shortly before transfection, some of the old, conditioned medium (~ 0.5 ml) was removed from the dish and stored at 4°C. All 200 μ l of the transfection mix were put in small droplets onto the cell layers and the dishes were incubated at 37°C for 3-5 hours. In order to remove as much of the CaPO_4 precipitate as possible, the dishes were carefully rinsed 2-3 times with pre-warmed Neurobasal medium, and afterwards supplied with 1.5 ml fresh Neurobasal medium together with the 0.5 ml conditioned medium taken out before the transfection. Depending on the promotor efficiency, protein expression could be detected 24-48 hours after transfection and normally lasted for several days.

4.3.3 Transfection of HEK293 Cells

For imaging experiments, HEK293 cells were grown in plastic cell culture dishes at 37°C and 5% CO_2 until they were sufficiently confluent, and then transferred into glass bottom dishes. Cells were detached by removing the original medium, rinsing the dish once with PBS, and adding 0.5 ml of DMEM/trypsin solution. After the cells had visibly detached, they were triturated 3-4 times with a pipet tip, seeded into 35 mm glass bottom dishes containing DMEM/10% FCS, and transfected either immediately or a day after adhesion. The transfection mix was prepared by diluting 2-3 μ g plasmid DNA per dish in 100 μ l FCS-free DMEM, and separately 6 μ l Lipofectin reagent per dish in another 100 μ l FCS-free DMEM. After 30 - 45 minutes incubation time, the two solutions were combined and kept at room temperature for another 15-20 minutes. Each dish received 200 μ l transfection mix, was incubated for 24 hours, and the medium replaced with fresh DMEM/10% FCS. Imaging was performed 1-3 days after transfection.

4.4 Histology and Immunohistochemistry

4.4.1 Cryosections of PFA-fixed Mouse Brains

Mouse brains were removed from the skulls, washed in PBS, and incubated for 2-3 hours in 4% PFA solution at 4°C. The brains were then transferred into 30% Sucrose-PBS solution and kept overnight at 4°C. For cryosectioning, the tissue was frozen in Tissue-Tek mounting medium on a Microm HM400 freezing microtome and cut into slices of 50 µm thickness. Slices were kept in PBS until needed.

4.4.2 Acute Slice Preparation of Mouse Brains

Organotypic slices for fluorescence imaging were prepared after the protocol published by Stoppini (Stoppini et al., 1991): hippocampi from 4-day old mice were cut with a vibratome into 400 µm thick slices, washed, and placed on culture plate filters (Millipore). The filters with the attached slices were cultured for 2 weeks in 6-well plates containing medium (50% BME, 25% horse serum, 25% HBSS with 1 mM glutamine and 5 mg/mg glucose; GIBCO). For imaging experiments, the filter membrane around a slice was cut with a surgical blade, then the slice placed in a glass bottom dish containing HBSS, and held in place by a platinum ring.

4.4.3 Antibody Staining of Cultured Cells

The medium of a cell culture dish was washed off carefully with PBS, and the cells were fixed by incubation with 4% PFA solution for 15-20 minutes at room temperature. The PFA was washed away with PBS and the dish incubated for 20 minutes at room temperature in Blocking Buffer. The primary antibody was added in Blocking Buffer and the dish gently shaken either for 4 hours at room temperature or overnight at 4°C. To avoid background staining, the primary antibody solution was washed with PBS during a minimum of two hours during which the PBS was exchanged every 30 minutes. Afterwards, the secondary antibody was diluted in Blocking Buffer and again left for either 4 hours at room temperature or overnight at 4°C. The washing procedure was repeated and the cell layer covered with 10 µl Mowiol mounting medium immediately after removal of the last PBS residues. Dishes covered in mounting medium were kept refrigerated until imaging analysis.

4.4.4 Antibody Staining of Fixed Brain Sections

Fluorescent protein expression was visualized in fixed 50 μm cryosections of PFA-immersed, PCR-positive mouse brains. Immunostaining was done by incubating brain sections either 4 hours at room temperature or overnight at 4°C with polyclonal anti-GFP rabbit antibodies diluted in PBT buffer containing 10% goat serum. The primary antibody solution was removed by washing the slices three times in PBT and PBS for 30 minutes, then a TRITC-labelled secondary swine antibody was added in PBT/10% goat serum, again for either 4 hours at room temperature or overnight at 4°C. The first washing procedure was repeated and the immunostained slices were finally mounted on glass slides, covered with Gel/Mount mounting medium and a cover glass, and examined with an upright fluorescence microscope.

4.5 Transgenic Animals

4.5.1 DNA Preparation for Mouse Oocyte Injections

Indicator proteins created in this work were to be expressed in transgenic mouse lines under control of the Thy-1.2 promoter as published by P. Caroni (Caroni, 1997). For that purpose, XhoI restriction sites had to be added to both sides of the desired indicator DNA sequence by PCR amplification using a suitable primer pair, and the indicators were then inserted into the XhoI-site of the mouse Thy-1.2 expression cassette contained in a pUC18 vector. The transgene inserts were stripped of all vector sequences by restriction with EcoRI/PvuI and purified via agarose gel electrophoresis and electroelution of the DNA fragment into a Spectra/Por dialysis membrane bag (Sambrook and Russell, 2001a). In order to further purify the DNA of all contaminants, an ion exchange chromatography was performed using a small disposable Elutip-D Minicolumn. The column was first equilibrated in Low Salt DNA Purification Buffer, then the DNA obtained from the electroelution procedure applied to the column, washed with Low Salt Buffer and then eluted with High Salt DNA Purification Buffer. The purified DNA fragments were checked for purity on an agarose gel and their concentration adjusted to 100 ng/ μl with a suitable injection buffer.

4.5.2 Creation and Breeding of Transgenic mice

Purified linear DNA fragments were used for injections into pronuclei of mouse oocytes by the DNA microinjection method (Nagy et al., 2003). All injection procedures were performed by the Transgenic Service facility at the MPI for Biochemistry in Martinsried, Germany. The mouse strains used for oocyte injections were either FVB or FVB:C57BL/6-crosses as the FVB strain is known for its large oocytes and good injection performance (Taketo et al., 1991).

Founder animals were screened for CFP/YFP gene sequences by PCR of genomic DNA obtained from tail lysates by the method described below, and PCR-positive founders were crossed with wildtype mice. Breeding of the transgenic lines was continued with either FVB, C57BL6 or SV129J mouse strains; all animals used were obtained from the MPI for Biochemistry's animal breeding facilities.

4.5.3 Genotyping of Transgenic Mice

A protocol used for the genotyping of transgenic mice carrying fluorescent indicator insertions was established by modifying the "Fluorescent Protein" genotyping protocol available on The Jackson Laboratory's Internet page (<http://jaxmice.jax.org>). The two IL2 primers are used as an internal control to verify the success of the PCR; the two GFP primers had to be slightly modified from the published JAX version to allow a more efficient priming of the Citrine sequence.

Maus-GFP-for	5'-AAG TTC ATC TGC ACC ACC G-3'
Maus-GFP-rev	5'-GTC GTC CTT GAA GAA GAT GGT-3'
Maus-IL2-Ktr-for	5'-CTA GGC CAC AGA ATT GAA AGA TCT-3'
Maus-IL2-Ktr-rev	5'-GTA GGT GGA AAT TCT AGC ATC ATC C-3'

Table 1: Primer sequences of the four primers used in the mouse genotyping PCR protocol suitable for detection of various GFP variants in mouse chromosomal DNA. Modified from <http://jaxmice.jax.org>

Genomic DNA was obtained from mouse tail tissue using the Proteinase K/isopropanol precipitate method described in (Sambrook and Russell, 2001b). Tail tissue samples of about 5 mm length were dissolved in Mouse Tail Lysis Buffer containing proteinase K for 4 hours or longer at 55°C. The lysates were centrifuged at maximum speed for 5 minutes, the supernatant transferred to fresh tubes, and chromosomal DNA precipitated by adding an equal volume of isopropanol. After gentle shaking, the visible DNA precipitate could be picked up with the point of a pipette tip and transferred to

another tube containing TE buffer. Remains of isopropanol were removed by letting the open tubes sit in a heat block for 30 minutes, then the tubes were closed, vortexed gently, and incubated at 4°C overnight to aid the dissolution of the DNA precipitate. The DNA samples were used in the following PCR protocol:

Ingredients for one reaction:

0.5 µl chromosomal DNA in TE buffer as reaction template

0.2 µl dNTP solution (12.5 mM)

0.6 µl primer Maus-GFP-for (20 µM)

0.6 µl primer Maus-GFP-rev (20 µM)

0.3 µl primer Maus-IL2-Ktr-for (20 µM)

0.3 µl primer Maus-IL2-Ktr-rev (20 µM)

1.2 µl Taq polymerase buffer (10x, provided by manufacturer)

7.3 µl H₂O

0.5 µl of a 1:10 dilution of Taq polymerase in glycerol (~ 5 U/µl) were added after heating the reaction mixes to 95°C for 5-10 minutes.

PCR reaction cycles:

1.5 min heating to 95°C;

36 amplification cycles:

30 sec 95°C: melting of double-stranded DNA

1 min 60°C: annealing of primers

1 min 72°C: DNA extension

After completion of cycles: 2 min 72°C; reaction termination by cooling to 10°C.

4.6 Microscopy and Imaging

4.6.1 FRET-Setup

Imaging of fluorescently labeled cells was performed on a Zeiss Axiovert 35M microscope equipped with a CCD camera. The imaging setup was controlled by Metafluor 4.6 software. For ratio imaging of CFP and YFP, a 440/20 excitation filter, a 455 DCLP dichroic mirror and two emission filters (485/35 for CFP, 535/25 for Citrine) operated in a filter wheel were used.

4.6.2 Determining the Ratio Change of Ratiometric Indicator Proteins

To obtain the ratio change of a ratiometric indicator construct, the proteins were purified and subjected to in vitro fluorescence measurements on the same day or up to a week later if the protein had proven to be stable. Fluorescence emission intensities of the indicator's FRET-donor and the FRET-acceptor domain were measured at their respective emission maxima. These values were determined first at zero calcium levels and afterwards at calcium saturation levels. In the first step, an aliquot of the protein was diluted in MOPS buffer for fluorescence spectroscopy containing 20 μM EGTA to ensure a Ca^{2+} free environment. In the second step, a solution of 1 M CaCl_2 was added to the mix to achieve a final concentration of 10 mM CaCl_2 . After each step, the respective emission maxima of the FRET-donor and the FRET-acceptor were measured and the ratio R calculated as acceptor intensity over donor intensity. The fluorescence ratio change obtained when going from a calcium-free to calcium-saturated environment was calculated using the following equation (Miyawaki et al., 1997):

$$\text{Ratio change} = \frac{\Delta R}{R} = \frac{R_{\text{Ca-saturated}} - R_{\text{Ca-free}}}{R_{\text{Ca-free}}} = \frac{R_{\text{Ca-saturated}}}{R_{\text{Ca-free}}} - 1$$

Equation 1: Ratio change of a ratiometric indicator in zero and saturated calcium concentrations

4.6.3 Measuring Kd Values

Kd-values, that is the affinities of indicator proteins for a ligand molecule (in our case, Ca^{2+} or Mg^{2+} ions) can be determined by titration assays. The investigated proteins were purified following the Ni-NTA protein purification procedure and stored in protein resuspension buffer. Titration assays were performed by exposing the proteins to defined ion concentrations in MOPS buffer. Since it is difficult to produce low defined calcium concentrations, commercially available buffer systems containing Ca^{2+} and its chelator K_2EGTA were used (Calcium Calibration Buffer Kits) to which Mg^{2+} was added when necessary. Aliquots of the investigated proteins were mixed with various ratios of two buffer solutions containing either 10 mM K_2EGTA , 100 mM KCl and 30 mM MOPS pH 7.2 or 10 mM Ca EGTA, 100 mM KCl and 30 mM MOPS pH 7.2. The fluorescence emission intensities of the FRET-donor and the FRET-acceptor were then recorded at various concentrations of free calcium. Likewise, magnesium titrations were done by mixing two stock solutions of MOPS buffer, one Mg^{2+} free and the other containing

50 mM MgCl₂. Combining these two solutions led again to defined concentrations of free Mg²⁺ to which aliquots of the investigated protein were added. After each titration experiment, K_d-values of the ligand binding curves could be calculated by plotting the fractional ratio $\frac{\Delta R}{R}$ of the donor and acceptor fluorophores' emission maximum wavelength against the concentration of free ligand on a logarithmic scale. Indicator K_d values could then be derived from sigmoidal curve fits.

4.6.4 Measuring Dissociation Kinetics

The determination of in vitro Ca²⁺ dissociation kinetics was performed in a Cary Eclipse fluorometer equipped with a stopped flow RX2000 rapid kinetics accessory unit for kinetic measurements. About 6 μM purified protein in Low BAPTA Buffer containing 1 mM free Mg²⁺ and either 1 μM, 10 μM, or 50 μM free Ca²⁺ (for indicators with K_d values higher than 5 μM: 50 μM or 300 μM free Ca²⁺) were mixed with High BAPTA Buffer containing 1 mM free Mg²⁺ (for indicators with K_d values higher than 5 μM, the BAPTA concentration was raised to 35 mM); the mixing dead time was 8 ms according to the instrument manufacturer. Samples were excited at the donor emission wavelength (432 nm for CFP) and the acceptor emission monitored (528 nm for Citrine). Data sets from at least five experiments were averaged and the dissociation rate constants derived from monoexponential curve fittings.

4.7 Materials

4.7.1 Instruments

Autoflow CO ₂ Water-Jacketed Incubator	NuAire, Plymouth (USA)
Cary 100 Scan UV-Visible Spectrophotometer	Varian, Mulgrave (Australia)
Cary Eclipse fluorescence spectrophotometer	Varian, Mulgrave (Australia)
CCD-Camera Cool Snap HQ	Roper Scientific, Tucson (USA)
Dissecting Microscope	Leitz, Stuttgart (Germany)
Dyad DNA Engine Peltier Thermal Cycler	MJ Research Inc., Waltham (USA)
Metafluor 4.6 imaging software	Universal Imaging, Downingtown (USA)
Microscope Axiovert 35M	Zeiss, Oberkochen (Germany)
Shutter Lambda 10-2	Sutter Instruments, Novato (USA)
Stopped Flow RX2000 Rapid Kinetics Accessory Unit	Applied Photophysics, Leatherhead (UK)

4.7.2 Consumables

Domed Cap Strips for 48 Well Plates	AB-Gene, Epsom (UK)
Eartags for mice, Monel Nr. 1005-1	National Band & Tag Company, Newport (USA)
Elutip-D Minicolumns	Schleicher & Schüll, Keene (USA)
Falcon Tissue Culture Plate, 12 Well	Becton Dickinson, Franklin Lakes (USA)
Glass Bottom Culture Dishes 35mm, Nr. P35G-0-14-C	MatTek Corp., Ashland (USA)
Polypropylene Columns	Qiagen, Hilden (Germany)
QIAquick Gel Extraction Kit	Qiagen, Hilden (Germany)
QIAquick PCR Purification Kit	Qiagen, Hilden (Germany)
Spectra/Por Dialysis Membrane, MWCO 3500, Nr. 132111	Spectrum Labs Inc., Rancho Dominguez (USA)
Thermo-Fast 48 Well Plates for PCR	AB-Gene, Epsom (UK)

4.7.3 Buffers, Solutions, and Media

Name	Recipe
ACSF	124 mM NaCl
	3 mM KCl
	1.25 mM KH ₂ PO ₄
	2 mM MgSO ₄
	26 mM NaHCO ₃
	2.5 mM CaCl ₂
	10 mM D-Glucose
	pH 7.4

Name	Recipe
BBS (2x)	50 mM BES (acid), pH 6.96 280 mM NaCl 1.5 mM Na ₂ HPO ₄
Blocking Buffer for antibody stainings	10% serum in 1x PBT
CaCl ₂ solution for phosphate transfections	250 mM CaCl ₂ in H ₂ O
DMEM/10% FCS	500 ml DMEM 50 ml FCS, heat-inactivated
DNA Gel Loading Buffer (10x)	100 mM Tris/HCl, pH 7.5 10 mM EDTA 50% Glycerol 1% Orange G
DNA Purification Buffer: High Salt	20 mM Tris/HCl, pH 7.4 1 M NaCl 1 mM EDTA
DNA Purification Buffer: Low Salt	20 mM Tris/HCl, pH 7.4 200 mM NaCl 1 mM EDTA
HBSS for imaging	25 mM HEPES pH 7.4 140 mM NaCl 5 mM KCl 1 mM CaCl ₂ 1 mM MgCl ₂ 1 mM Glucose 0.25% BSA
HBSS with high KCl for imaging	25 mM HEPES, pH 7.4 40 mM NaCl 100 mM KCl 1 mM CaCl ₂ 1 mM MgCl ₂ 1 mM Glucose 0.25% BSA
High BAPTA Buffer for dissociation kinetics	10 mM MOPS, pH 7.0 200 mM KCl 20 mM BAPTA
Inoue Transformation Buffer for competent cells	10 mM PIPES, pH 6.7 250 mM KCl 15 mM CaCl ₂ 55 mM MnCl ₂
Low BAPTA Buffer for dissociation kinetics	10 mM MOPS, pH 7.0 200 mM KCl 1mM BAPTA
MOPS Buffer for fluorescence spectroscopy	10 mM MOPS, pH 7.0 100 mM KCl

Name	Recipe
Mouse Tail Lysis Buffer	100 mM Tris/HCl, pH 8 250 mM NaCl 1 mM EDTA 0.2% SDS 200 µg/ml Proteinase K added freshly
Neurobasal/B27	500 ml Neurobasal medium 10 ml B27 supplement
PBS (10x)	100 mM Na ₂ HPO ₄ , pH 7.4 20 mM KH ₂ PO ₄ 1.37 M NaCl 27 mM KCl
PBT (1x)	0.05% Triton X-100 in 1x PBS
PFA (4%)	4% (w/v) Polyformaldehyde in 1x PBS, pH 7.4
Poly-L-Lysine	0.01% (w/v) Poly-L-Lysine Hydrobromide in H ₂ O
Protein Resuspension Buffer	20 mM NaPO ₄ , pH 7.8 300 mM NaCl
Sucrose-PBS Solution (30%)	30% (w/v) sucrose in 1X PBS
TAE (10x)	48.4 g Tris base 11.4 ml glacial acetic acid 20 ml of 0.5 M EDTA, pH 8.0 add H ₂ O to 1 liter
TAE (1x)	40 mM Tris-acetate 1 mM EDTA
TE (1x)	10 mM Tris/HCl, pH 8.4 1 mM EDTA

4.7.4 Chemicals and Products

Name	Supplier
Agar	Sigma, St. Louis (USA)
Ampicillin, sodium salt	Roth, Karlsruhe (Germany)
AP5 (D-AP5)	Tocris Cookson, Bristol (UK)
AP5 (DL-AP5)	Tocris Cookson, Bristol (UK)
BAPTA, AM-ester	Molecular Probes, Eugene (USA)
BAPTA, tetrapotassium salt	Molecular Probes, Eugene (USA)
BES	Roth, Karlsruhe (Germany)
Bovine Serum Albumin (BSA)	Sigma, St. Louis (USA)
Calcium Calibration Buffer Kit #1	Molecular Probes, Eugene (USA)
Calcium Calibration Buffer Kit #3	Molecular Probes, Eugene (USA)

Name	Supplier
Calcium Calibration Buffer Kit with Magnesium #1	Molecular Probes, Eugene (USA)
Calcium Chloride, dihydrate	Sigma, St. Louis (USA)
Carbachol	Sigma, St. Louis (USA)
Deoxyribonuclease	Sigma, St. Louis (USA)
Dispase	Gibco, Grand Island (USA)
Dithiothreitol	Sigma, St. Louis (USA)
DMSO (Dimethylsulfoxide)	Sigma, St. Louis (USA)
Dulbecco's modified Eagle's medium (DMEM) w/o Sodium Pyruvate; w/ 4500 mg/ml Glucose; w/ Pyridoxine-HCl	Invitrogen, Carlsbad (USA)
Dulbecco's modified Eagle's medium /F12	Invitrogen, Carlsbad (USA)
EGTA (Ethylene glycol bis(beta-amino ethyl ether tetra- acetic acid)	Sigma, St. Louis (USA)
Foetal Bovine Serum	Gibco, Grand Island (USA)
Gel/Mount mounting medium	Biomedex, Foster City (USA)
Glucose (D-+)-Glucose anhydrous, min 99%)	Sigma, St. Louis (USA)
Glycine	Merck, Darmstadt (Germany)
HEPES free acid	Sigma, St. Louis (USA)
Imidazole	Merck, Darmstadt (Germany)
Ionomycin, calcium salt	Sigma, St. Louis (USA)
Leupeptin hydrochloride	Sigma, St. Louis (USA)
L-Glutamic acid	Roth, Karlsruhe (Germany)
Lipofectin	Invitrogen, Carlsbad (USA)
Lysozyme	Sigma, St. Louis (USA)
Magnesium chloride hexahydrate	Merck, Darmstadt (Germany)
MES monohydrate	Sigma, St. Louis (USA)
MOPS	Merck, Darmstadt (Germany)
NeuroBasal medium	Gibco, Grand Island (USA)
Ni-NTA Agarose	Qiagen, Hilden (Germany)
NMDA (N-Methyl-D-Aspartic Acid)	Sigma, St. Louis (USA)
Penicillin-Streptomycin	Gibco, Grand Island (USA)
Pepstatin A	Sigma, St. Louis (USA)
Pfu polymerase	Stratagene, La Jolla (USA)
Phenylmethylsulfonylfluoride (PMSF)	Sigma, St. Louis (USA)
PIPES	Sigma, St. Louis (USA)
Pluronic F-127 in DMSO	Molecular Probes, Eugene (USA)
Poly-L-lysine hydrobromide	Sigma, St. Louis (USA)
Potassium chloride	Merck, Darmstadt (Germany)
Ribonuclease A	Sigma, St. Louis (USA)
Saccharose	Merck, Darmstadt (Germany)
Sodium bicarbonate	Sigma, St. Louis (USA)
Sodium chloride	Sigma, St. Louis (USA)

Name	Supplier
Sodium phosphate monobasic, anhydrous	Sigma, St. Louis (USA)
T4-Ligase	New England Biolabs, Beverly (USA)
Tissue-Tek	Sakura, Tokyo (Japan)
Triton-X-100	Sigma, St. Louis (USA)
Trizma Base	Sigma, St. Louis (USA)
Trypsin	Sigma, St. Louis (USA)
Trypsin-EDTA	Gibco, Grand Island (USA)
Vent polymerase	New England Biolabs, Beverly (USA)

4.7.5 DNA Plasmids and *E. coli* Strains

Plasmid name	Supplier
pCDNA3	Invitrogen, Carlsbad (USA)
pRSETB	Invitrogen, Carlsbad (USA)
Strain name	Supplier
BL21(DE3)	Invitrogen, Carlsbad (USA)
DH5 α	Invitrogen, Carlsbad (USA)

4.7.6 Primer Sequences

No.	Primer Name	Primer DNA Sequence
1	sTnC-Sacl	5'-GCG AGC TCC TGC ACA CCC TCC ATC ATC TTC-3'
2	SphI-Leu-sTnC	5'-ACA TGC ATG CTA ATG GCG TCA ATG ACG GAC CAG-3'
3	SphI-csTnC-EF2	5'-ACA TGC ATG CTA GGC CAG AAC CCC ACC AAA GAG-3'
4	csTnC-N90-Sacl	5'-GCG AGC TCG GCG TCC TCT TTC ATC TGG CG-3'
5	csTnC-EF1-Sacl	5'-GCG AGC TCG CCC AGC ATC CTC ATC ACC G-3'
6	SphI-TnC-L14	5'-ACA CGC ATG CTC AGC GAG GAG ATG ATT GCT GAG-3'
7	SphI-TnC-E17	5'-ACA CGC ATG CTC GAG GAG ATG ATT GCT GAG TTC-3'
8	SphI-TnC-A21	5'-ACA CGC ATG CTT GCT GAG TTC AAA GCT GCC TTT G-3'
9	humcTnC-Sacl	5'-GCG AGC TCC TCC ACA CCC TTC ATG AAC TCC-3'
10	SphI-humcTnC	5'-ACA TGC ATG CTA ATG GAT GAC ATC TAC AAG GCT GCG-3'
11	SphI-humcTC-L12	5'-ACA CGC ATG CTG ACA GAA GAG CAG AAA AAT G-3'
12	SphI-TPC1 fl	5'-ACA TGC ATG CTG AGC GAT GAA TTG ACT AAG GAG C-3'
13	SphI-TPC1-L5	5'-ACA TGC ATG CTG ACT AAG GAG CAA ACT GCA TTA CTA C-3'
14	Sacl-TPC1-fl	5'-GCG AGC TCG TCG TCG CCA CCG GTC ATT ACT TC-3'
15	Sacl-TnI48-GGSGG	5'-GCG AGC TCG GCG GCA GCG GCG GCT CTG ATG AAG AGA AAA AGC GTC G-3'
16	TnI48-GGSGG-Sacl rev	5'-GCG AGC TCG CCG CCG CTG CCG CCA TGC TCT GCC AGG TAG TTT TGC-3'
17	Sacl-TnI48-GSG	5'-GCG AGC TCG GCA GCG GCT CTG ATG AAG AGA AAA AGC GTC G-3'

No.	Primer Name	Primer DNA Sequence
18	Tnl48-GSG-Sacl-rev	5'-GCG AGC TCG CCG CTG CCA TGC TCT GCC AGG TAG TTT TGC-3'
19	SphI-GSG-Tnl95	5'-ACA TGC ATG CTA GGC AGC GGC GAC CTG AGC CAG AAG CTG TTT G-3'
20	Tnl95-GSG-SphI-rev2	5'-ACA TGC ATG CTG CCG CTG CCG ACC TTG TGC TTG GAG CCC AGC-3'
21	SphI-GSGGG-Tnl95	5'-ACA TGC ATG CTA GGC GGC AGC GGC GGC GAC CTG AGC CAG AAG CTG TTT G-3'
22	Tnl95-GSGGG-Sph1rev2	5'-ACA TGC ATG CTG CCG CCG CTG CCG CCG ACC TTG TGC TTG GAG CCC AGC-3'
23	Sacl-Tnl48-0L	5'-GCG AGC TCT CTG ATG AAG AGA AAA AGC GTC G-3'
24	Tnl48-0L-Sacl-rev	5'-GCG AGC TCA TGC TCT GCC AGG TAG TTT TGC-3'
25	SphI-Tnl95-0L	5'-ACA TGC ATG CTA GAC CTG AGC CAG AAG CTG TTT G-3'
26	Tnl95-0L-SphI-rev2	5'-ACA TGC ATG CTG ACC TTG TGC TTG GAG CCC AGC-3'
27	SphI-Tnl116	5'-ACA CGC ATG CTC GCT GAT GCC ATG CTG CGT GCC CTG CTG GGC TCC AAG CAC AAG GTC AAC ATG GCG TCA ATG ACG GAC CAG CAG GCG-3'
28	SphI-Tnl116-GG	5'-ACA CGC ATG CTC GCT GAT GCC ATG CTG CGT GCC CTG CTG GGC TCC AAG CAC AAG GTC AAC GGC GGC GCG TCA ATG ACG GAC CAG CAG GCG-3'
29	SphI-Tnl116-L14	5'-ACA CGC ATG CTC GCT GAT GCC ATG CTG CGT GCC CTG CTG GGC TCC AAG CAC AAG GTC AAC CTC AGC GAG GAG ATG ATT GCT GAG-3'
30	SphI-Tnl-for	5'-ACA TGC ATG CTA ATG TCT GAT GAA GAG AAA AAG CG-3'
31	SphI-Tnl-rev	5'-ACA TGC ATG CTG GAC TCG CCG GCC TCA AAC ATC-3'
32	Sacl-Tnl-rev	5'-GCG AGC TCG GAC TCG CCG GCC TCA AAC ATC-3'
33	SphI-Tnl-GG-rev	5'-ACA TGC ATG CTG CCG CCG GAC TCG CCG GCC TCA AAC ATC-3'
34	Sacl-Tnl-GG-for	5'-GCG AGC TGC GCG GCA TGT CTG ATG AAG AGA AAA AGC-3'
35	Sacl-mDsRed	5'-GCG AGC TCA TGG CCT CCT CCG AGG ACG TC-3'
36	mDsRed-EcoRI	5'-CGG AAT TCT CAA GCT TCG AAT TCT TAG GCG CCG-3'
37	BamHI-Cop-fl-Kz	5'-CCC GGA TCC AGC CGC CAC CAT GGG CCC CGC CAT GAA GAT CGA GTG CCG-3'
38	Sph1-Cop-fl-rev	5'-ACA TGC ATG CGG GCG AAT GCG ATC GGG GTC-3'
39	BamHI-Cop-M3-Kz	5'-CCC GGA TCC AGC CGC CAC CAT GGA GAT CGA GTG CCG CAT CAC CGG C-3'
40	SphI-Cop-T216-rev	5'-ACA TGC ATG CGG GTC TTG AAG GCG TGC TGG TAC-3'
41	CopGreen-EcoRI	5'-CGG AAT TCT CAG GGC GAA TGC GAT CGG GGT C-3'
42	kzBamHI-Phi Yellow	5'-CCC GGA TCC AGC CGC CAC CAT GTC CAG CGG CGC CCT GCT GTT CC-3'
43	Sacl-Phi-fl	5'-GCG AGC TCA TGT CCA GCG GCG CCC TGC TGT TCC-3'
44	EcoR1-Phi-fl-rev	5'-CGG AAT TCT CAC AGG TAG GTC TTG CGG CAA TC-3'
45	SphI-TnC-EF2-G	5'-ACA TGC ATG CTA CAG AAC CCC ACC AAA GAG GAG-3'
46	SphI-TnC-EF2-GQ	5'-ACA TGC ATG CTA AAC CCC ACC AAA GAG GAG CTG-3'

No.	Primer Name	Primer DNA Sequence
47	SphI-TnC-EF2-GQN	5'-ACA TGC ATG CTA CCC ACC AAA GAG GAG CTG GAT G-3'
48	SphI-TnC-EF2-GQNP	5'-ACA TGC ATG CTA ACC AAA GAG GAG CTG GAT GCC-3'
49	SphI-TnC-EF4	5'-ACA TGC ATG CTA GGG GAG CAC GTC ATC GAG GAG G-3'
50	SphI-TnC-EF4-G	5'-ACA TGC ATG CTA GAG CAC GTC ATC GAG GAG GAC-3'
51	SphI-TnC-EF4-GE	5'-ACA TGC ATG CTA CAC GTC ATC GAG GAG GAC ATA G-3'
52	SphI-TnC-EF4-GEH	5'-ACA TGC ATG CTA GTC ATC GAG GAG GAC ATA GAA G-3'
53	SphI-TnC-EF4-GEHV	5'-ACA TGC ATG CTA ATC GAG GAG GAC ATA GAA GAC C-3'
54	KpnI-csTnC-EF2	5'-GGG GTA CCG GCC AGA ACC CCA CCA AAG AG-3'
55	KpnI-TnC-EF2-G	5'-GCG GTA CCC AGA ACC CCA CCA AAG AGG AG-3'
56	KpnI-TnC-EF2-GQ	5'-GCG GTA CCA ACC CCA CCA AAG AGG AGC TG-3'
57	KpnI-TnC-EF2-GQN	5'-GCG GTA CCC CCA CCA AAG AGG AGC TGG ATG-3'
58	KpnI-TnC-EF2-GQNP	5'-GCG GTA CCA CCA AAG AGG AGC TGG ATG CC-3'
59	KpnI-TnC-EF4	5'-GCG GTA CCG GGG AGC ACG TCA TCG AGG AGG-3'
60	KpnI-TnC-EF4-G	5'-GCG GTA CCG AGC ACG TCA TCG AGG AGG AC-3'
61	KpnI-TnC-EF4-GE	5'-GCG GTA CCC ACG TCA TCG AGG AGG ACA TAG-3'
62	KpnI-TnC-EF4-GEH	5'-GCG GTA CCG TCA TCG AGG AGG ACA TAG AAG-3'
63	KpnI-TnC-EF4-GEHV	5'-GCG GTA CCA TCG AGG AGG ACA TAG AAG ACC-3'
64	KpnI-TnC-EF4-rev	5'-GCG GTA CCC TGC ACA CCC TCC ATC ATC TTC-3'
65	KpnI-TnC-EF2-rev	5'-GCG GTA CCG GCG TCC TCT TTC ATC TGG CG-3'
66	BamH1-Not1-Kz-GFP	5'-CCC GGA TCC CGC GGC CGC CAC CAT GGT GAG CAA GGG CGA GGA G-3'
67	3'-EcoRI-RAS-GFP	5'-GCG AAT TCT TAG CTC AGC ACG CAC TTG CAG CTC ATG CAG CCG GGG CCG CTC TCG TCG GGG GGG TTC AGC TTG TAC AGC TCG TCC ATG CCG-3'

5. RESULTS

5.1 Construction of New Fluorescent Indicator proteins

5.1.1 On the Design of Troponin Linker Domains

The goal of this work was to find a suitable replacement for the calmodulin moiety employed in Cameleon-type calcium indicators, as the calmodulin domain or its binding partner M13 were suspected of being responsible for the indicators' poor performance in certain targeting experiments and transgenic organisms. Therefore, a new linker domain should ideally be a calcium binding protein that is not originally expressed in the cell cytosol, particularly not in neurons. As shown in the introductory part of this work, members of the muscle troponin C protein family seemed to be good candidates to fulfill these requirements since they are structurally related to calmodulin and undergo a significant conformational change on calcium binding. Furthermore, all troponin molecules are found only in complexed forms in muscle cells *in vivo*, thus interactions with cytosolic cellular regulatory mechanisms should be minimal.

Among the many known troponin isoforms, I chose troponin C variants from three different species for the following attempts to create new, functional fluorescent indicators based on troponin C proteins as calcium binding moieties: first, the 161 amino acid residue human cardiac muscle isoform of troponin C (humcTnC), second, chicken skeletal muscle troponin C (csTnC), 163 residues long, and third, isoform 1 of troponin C in the fruit fly *Drosophila melanogaster*. This *Drosophila* variant is 154 amino acids long and originates from the gene called TpnC41C or TnC41C. Since it is present only in fast-twitching adult fly muscles, it was assumed to have faster kinetic properties than the other two troponins.

Generally, the functionality of any newly designed indicator protein is almost impossible to predict since the fluorescent properties of such a large molecule depend on a countless variety of factors. FRET efficiency as well as a single chromophore fluorescence intensity are greatly influenced by structural features like chromophore orientation and distance, by sensitivity to the chemical environment like ionic strength and pH, and by resistance of the molecule to physical factors such as irradiation and temperature. Unfortunately, until now, no crystal structure of an established fluorescent indicator protein has been successfully solved, so clues as to what structural features make up a good

indicator are sparse. However, as discussed in the introduction, the abundant structural data available on troponin C and troponin I allows some insight into the form and location of their binding sites and surrounding elements. Of special importance are the EF-hand motifs of troponin C that are responsible for calcium binding, and the adjacent α -helical stretches stabilizing the EF-hand loop regions (see Figure 6 and Figure 8 of the introduction and Figure 9). Any functional calcium sensing indicator protein must comprise at least one of these EF-hand domains. Because of this, I decided to not only investigate the full length versions of each of the chosen troponin proteins in the following screen for new calcium indicator proteins, but also truncated versions containing structurally defined domains of the TnC in question.

CaM	-----MHDQLTEEQIAEFKEAFSLF	DKDGD-GTITTKEL	LGTVMRSLGQNPTAEEL	
csTnC	MASMTDQQAEARAFLSEEMIAEFKAAFDMF	DADGG-GDISTKEL	LGTVMRMLGQNPTKEEL	
chumTnC	--MDDIYKAAVEQLTEEQKNEFKAAFDIF	VLGAEDGCIISTKEL	LGVMMRMLGQNPTPEEL	
TPC1	-----MS---DELTKEQTALLRNAFNADFPE	KN-GYINTAMVGT	ILSMLGHQLDDATL	
TPC3	-----MSSVDEDLTPEQIAVLQKAFNSFDHQ	KT-GSIPTEMVAD	ILRLMQPFDKIL	
Consensus	L: E	:: AF. F	G I T .. :: :G: L	
CaM	QDMINEV	DADGNGTIYFPE	FLTMMARKMKDTD--SEEEIREAFRVF	DKDNGYISAAQL
csTnC	DAIIEEV	DEDGSGTIDFEE	FLVMMVRQMKEDAKGKSEELANCFRIF	DKNADGFIDIEEL
chumTnC	QEMIDEV	DEDGSGTVDFDE	FLVMMVRCMKDSDSKGKSEELSDLFRMF	DKNADGYIDLDEL
TPC1	ADIIAEV	DEDGSGQIEFEE	FTTLAARFLVEEDAEMMAELKEAFRLYD	KEGNGYITTVL
TPC3	EELIEEV	DEDKSGRLEFGE	FVQLAAKFIVEEDAEMQKELAEAFRLYD	KQNGFIPTCL
Consensus	:I EVD D .G : F EF	: .: : :	E: : FR::DK::G:I	L
CaM	RHVMTNLGEKLTDEEVDEMIREAD	DIDGDGQVNYEE	FVQMMTAK--	
csTnC	GEILRATGEHVIEEDIEDLMKDS	DKNNDGRIDFDE	FLKMMEGVQ-	
chumTnC	KIMLQATGETITEDDIEELMKDG	DKNNDGRIDYDE	FLEFMKGVE-	
TPC1	REILRELDLTKLTNDDLMMIEEI	DSDGSGTVDFDE	FMEVMTGGDD	
TPC3	KEILKELDDQLTEQELDIMIEEI	DSDGSGTVDFDE	FMEMMTGE--	
Consensus	::	:: : : : : : : : : D	:::G	:::EF::M .

Figure 9: Sequence alignment of calmodulin and the troponin C variants used in this work for calcium indicator construction. Red color indicates functional EF-hand loop regions, magenta indicates defunct EF-hand regions.

The TnC version that was most extensively investigated in this work is chicken skeletal muscle troponin C (csTnC). Apart from the full-length sequence, I cloned shorter domains of the protein, among them the amino acid stretch that makes up the N-terminal regulatory lobe and binds calcium with lower affinity (residues 1-90) (Strynadka et al., 1997). In addition, I designed constructs containing only single EF-hand loops together with parts of the stabilizing α -helices surrounding the loop region. A series of single amino acid residue deletions from the α -helices was conducted to see its effect on FRET

efficiency, as was an attempt to duplicate a single EF-hand multiple times in a row. Another approach was made in the csTnC construct that later became TN-L15. Here, the first 14 amino acid residues of the csTnC sequence were deleted. Since these residues make up the first N-terminal α -helix of the protein (see Figure 8 and Figure 9), the resulting protein bears more resemblance to the structure of calmodulin, which lacks this particular α -helix. Analogous deletions were executed in one chumTnC construct, named cardTN-L12, and one *Drosophila* construct, named TPC1-L5. In both cases, the α -helices preceding the first troponin EF-hand domain were eliminated, leaving a more calmodulin-like structure.

In another effort to copy the design of the Cameleon indicators, which are built from calmodulin and a peptide sequence that binds to calmodulin and thereby enhances the overall conformational change of the macromolecule, I created a series of csTnC binding peptides using the chicken skeletal muscle isoform of troponin I (csTnI). Since Troponin I is known to form a complex with csTnC *in vivo* and some of these interactions are modified by calcium, I selected some of the peptide sequences of csTnI considered to be responsible for binding to the N- and C-terminal csTnC domains according to the literature. These studies reported that the C-terminal part of TnI contains the inhibitory segment responsible for the interaction with TnC and actin-tropomyosin. It could be shown that a peptide comprising amino acids 96 through 148 (TnI₉₆₋₁₄₈) constituted the minimal sequence of TnI capable of mediating an inhibitory activity similar to that of the intact protein (Tripet et al., 1997). Another research group used amino acids 96-115 of the TnI inhibitory segment for binding studies with TnC and still observed an interaction of these two peptides (Mercier et al., 2000). In addition, crystal structures of TnC were solved that used N-terminal TnI amino acids 1 through 47 (TnI₁₋₄₇) for co-crystallization, showing that the entire TnI₁₋₄₇ peptide has multiple contacts with both TnC lobes and its C-end binds to the TnC C-lobe (Vassilyev et al., 1998). Considering these data, I created a set of peptides consisting of csTnI amino acid residues S₂-H₄₈, D₉₅-V₁₃₃, and R₁₁₆-M₁₃₅. These fragments could then be fused to the csTnC domains used as calcium binding linkers.

In addition to direct fusions, I equipped some of the TnI/TnC fusion constructs with short linker peptide sequences between the TnC and TnI fragments intended to add flexibility to the fusion protein and to facilitate any conformational changes. Various linkers have been described in the literature that usually comprise a peptide containing two or more glycine residues. Glycine, due to its small size, allows a rotation of the peptide

chain. However, it is advisable that longer linker peptides also contain some charged amino acid residues to ensure solubility (Whitlow et al., 1993). In this work, I designed small linker peptide sequences with alternating glycine and serine residues, namely the amino acid sequences Gly-Gly, Gly-Ser-Gly, and Gly-Gly-Ser-Gly-Gly.

Following the same considerations, I also created a series of full length and shortened domains of human cardiac TnC (humcTnC) and isoform 1 of *Drosophila melanogaster* troponin C analogously to the full length and truncated versions of csTnC described above.

5.1.2 Construction of CFP/YFP Constructs with csTnC, humTnC, and TPC1

As mentioned in the introduction, some of the earliest FRET indicators ever published used the calmodulin protein and a binding peptide sandwiched between the GFP variants CFP and YFP as fluorophores (Miyawaki et al., 1997). Since then, CFP together with its partner YFP have become the most popular and efficient FRET pair for fluorescent protein probe construction. However, with an ever increasing number of new fluorescent proteins being discovered or created through mutations, I also investigated other fluorescent proteins with improved physical and spectral properties as potential FRET pairs in this work which will be discussed in the next section.

The version of CFP used in most indicator constructs listed here was the ECFP variant; most YFP versions used here were based on the Citrine derivative that has enhanced pH and Cl⁻ stability (Griesbeck et al., 2001). The Citrine used in this work carries the additional mutation V163A designed to improve protein folding.

For the construction of troponin C domains as calcium binding moieties, I obtained full length and truncated troponin C domains by PCR from the cDNA of chicken skeletal muscle troponin C (csTnC) and *Drosophila* troponin C isoform 1 (TnC41C) using sense primers containing an SphI site at their 5' ends and reverse primers containing a SacI site at their 3' ends. Likewise, I obtained full length and truncated domains of human cardiac muscle troponin C (hcardTnC) from a cDNA sequence from which the intrinsic SacI site had to be removed first by site-directed mutagenesis, resulting in a silent mutation of the Glu135 codon from GAG to GAA. All troponin C DNA fragments were inserted between CFP and Citrine in the bacterial expression vector pRSETB carrying a CFP with an SphI

site at the 3' end and a Citrine with a SacI site at the 5' end. As explained above, all genes were inserted first in their full length versions, then shorter domains were engineered from csTnC and humcTnC in which only specific structural elements of the protein were used individually (Primer No. 1-14).

In addition to truncating domains, some of the csTnC linker domains were also fused to fragments of csTnI with different short linker residues inserted between the fusions. In particular, the csTnI fragments used here were amino acid residues S2-H48, D95-V133, and R116-M135. They were created by amplifying domains of chicken skeletal muscle TnI cDNA with sense and reverse primers containing both either an SphI site or a SacI site (Primer No. 15-34). The resulting csTnI DNA fragments carrying either a SphI site or a SacI site at both ends could then be cloned into the existing SphI or SacI sites in the troponin C indicator fusion constructs.

Proteins were expressed in BL21 bacteria using the T7 expression system in combination with a pRSETB plasmid carrying the fusion protein in question. Since the pRSETB plasmid also furnishes the fusion protein with an N-terminal polyhistidine tag, proteins could be purified from cleared cell lysates on nickel-chelate columns. Purified proteins could be subjected to a basic functional test by determining their fluorescence ratio change in Ca^{2+} -free and Ca^{2+} -saturated buffer systems (see Equation 1).

A selection of constructs that use the CFP/YFP FRET pair as fluorophores and show moderate to good responses to elevations in calcium concentration can be seen in Figure 10.

			% Ratio Change:
CFP	Troponin C	Citrine	30%
CFP	TnC-N90	Citrine	10%
CFP	TnC-EFn	Citrine	5-20%
CFP	TnI	Troponin C Citrine	30%
CFP	TnI	L Troponin C Citrine	L= GG: 35%
CFP	Troponin C	L TnI Citrine	L= GG: 30%
CFP	Troponin C	TnI ₂₋₄₈ Citrine	10%
CFP	Troponin C	L TnI ₂₋₄₈ Citrine	L= GSG/GGSGG: 20%
CFP	TnC-N90	TnI ₂₋₄₀ Citrine	30%
CFP	TnC-N90	L TnI ₂₋₄₈ Citrine	L= GSG: 30%; GGSGG: 35%
CFP	TnI ₉₅₋₁₃₃	Troponin C Citrine	20%
CFP	TnI ₉₅₋₁₃₃	L Troponin C Citrine	L= GSG: 45%; GGSGG: 60%
CFP	TnI ₉₅₋₁₃₃	TnC-N90 Citrine	40%
CFP	TnI ₉₅₋₁₃₃	L TnC-N90 Citrine	L=GSG: 40%; GGSGG: 35%
CFP	TnI ₁₁₆₋₁₃₅	Troponin C Citrine	70%
CFP	TnI ₁₁₆₋₁₃₅	L Troponin C Citrine	L=GG: 70%
CFP	TnI ₁₁₆₋₁₃₅	TN-L15 Citrine	60%
CFP	TN-L15	Citrine	140%
CFP	TN-L15-N90	Citrine	20%
CFP	TN-E17	Citrine	80%
CFP	TN-A21	Citrine	70%
CFP	cardTroponin C	Citrine	120%
CFP	cardTN ₁₋₁₃₅	Citrine	30%
CFP	cardTN-L12	Citrine	80%
CFP	TPC1	Citrine	150%
CFP	TPC1-L5	Citrine	160%

Figure 10: Summary of basic CFP/Citrine indicator constructs with an evaluation of their function.

Performance was evaluated as the maximal % change in the 527/476 nm emission ratio from zero calcium levels to calcium saturation. Troponin C, chicken skeletal muscle troponin C; TnC-N90, the N-terminal lobe of troponin C (amino acids 1-90); TnC-EFn, the individual EF-hands 1-4 of chicken skeletal muscle troponin C; TnI, chicken skeletal muscle troponin I; TnI 2-48, TnI 95-133, TnI 116-135, various short peptides derived from troponin I consisting of the indicated amino acid residues; TN-L15, truncated chicken skeletal muscle troponin C in which the N-terminal amino acid residues 1-14 are deleted, which makes the protein start at leucine 15; TN-L15-N90, N-terminal lobe of chicken skeletal muscle troponin C consisting of amino acid residues 15-90; TN-E17, TN-A21, truncated csTnC in which amino acids 1-16 and 1-20 are deleted; cardTroponinC, human cardiac muscle troponin C; cardTN1-135, human cardiac muscle troponin C lacking the last EF-hand domain; cardTN-L12, human cardiac muscle troponin C in which the N-terminal amino acid residues 1-11 are deleted, analogous to TN-L15; TPC1: *Drosophila* troponin C isoform 1; TPC1-L5: *Drosophila* troponin C isoform 1 in which amino acids 1-4 were deleted, analogous to TN-L15; L, linker peptides: either GG, GSG or GGSGG.

The best performing constructs of this series, that is the ones giving more than 100% maximal ratio change, were selected for further analysis. These constructs were named TN-humTnC for the indicator with human cardiac skeletal muscle troponin C (hcardTnC) as calcium binding moiety, TN-L15 for the indicator with chicken skeletal muscle troponin C (csTnC-L15) amino acids 15-163, and TN-TPC1-L5 for an indicator with *Drosophila* TnC isoform 1 (TnC41C). Interestingly, both csTnC and TPC1 worked best when the first N-terminal α -Helix was removed from the final protein (constructs TN-L15 and TN-TPC1-L5); this way their overall structure closely resembled calmodulin. The same deletion had no effect on human cardiac TnC, however; here, only the full length version of the protein showed a satisfying functional range.

Raw data of the basic calcium binding test used for evaluating all indicator constructs can be seen in Figure 11. Here, the emission spectra of the three best indicator constructs mentioned above (TN-L15, TN-humTnC, and TN-TPC1-L5) are shown at zero (dashed line, - Ca^{2+}) and saturating (solid line, + Ca^{2+}) calcium levels. The change of the emission ratio upon Ca^{2+} binding is 140% for TN-L15, 120% for TN-humTnC, and 160% for TN-TPC1-L5. As mentioned in the introduction, the C-terminal domain of TnC is known to have two high-affinity calcium binding sites that also bind magnesium, whereas the N-terminal lobe binds calcium specifically with a somewhat lower affinity. In agreement with this, addition of 1 mM magnesium to the binding assays reduced the maximal ratio change obtainable by addition of calcium of TN-L15 and TN-humTnC from 140 % to 100 % and 120 % to 70 %, respectively.

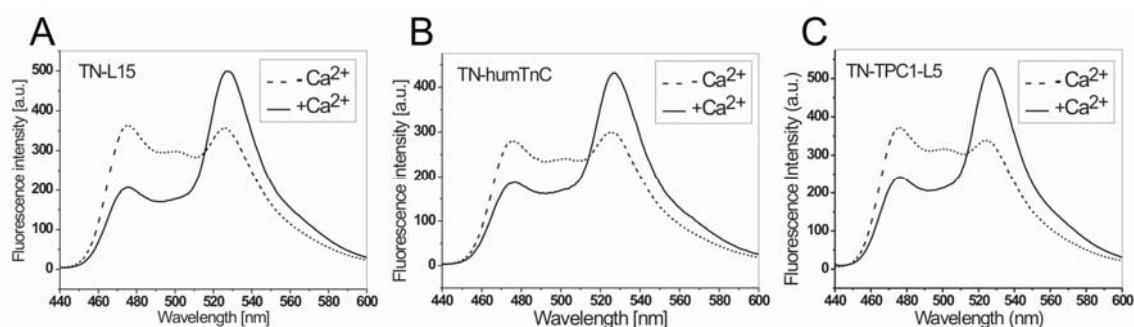


Figure 11: Effect of calcium binding on three CFP/Citrine indicator constructs. A, indicator protein TN-L15. B, indicator protein TN-humTnC. C, indicator protein TN-TPC1-L5. All constructs are excited at 432 nm and their emission spectra depicted at zero (dashed line, - Ca^{2+}) and saturating (solid line, + Ca^{2+}) calcium levels. The rise of the emission ratio upon Ca^{2+} binding is 140% for TN-L15, 120% for TN-humTnC, and 160% for TN-TPC1-L5.

In Figure 12, I investigated to what extent pH changes affected the emission ratios of TN-L15 obtained at zero calcium (50 μ M BAPTA, filled square, $-Ca^{2+}$) or calcium saturation (10 mM Ca^{2+} , filled circle, $+Ca^{2+}$). As expected, ratios were dependent on pH and began to drop from pH 6.8 downwards, reflecting the pH-sensitivities of Citrine and CFP. However, in the physiological range of cytosolic pH fluctuations between pH 6.8-7.3 the ratios were remarkably stable. This pH-resistance of my probes is an advantage over some recent non-ratiometric probes that use calmodulin and a single GFP as fluorophore, because these probes are intrinsically sensitive to minor pH changes and therefore artefact-prone when they are expressed in the cytosol (Nakai et al., 2001), (Nagai et al., 2001).

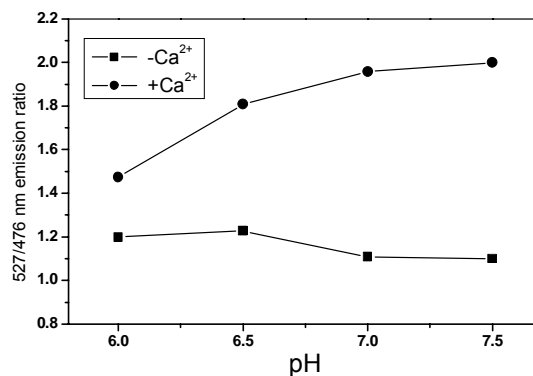


Figure 12: Stability of the emission ratio of indicator construct TN-L15 measured at varying pH-values and zero calcium (squares) or calcium saturation (circles).

5.1.3 Construction of Non-*Aequoria* Constructs

As mentioned before, most FRET indicators published so far were built with variants of CFP and YFP as fluorophores which makes this combination the most established FRET pair in the field. However, since both CFP and YFP have certain drawbacks such as a tendency to photoconvert easily (YFP) or emit at two different wavelengths (CFP), a replacement of these two fluorophores with other, physically more stable fluorescent proteins seemed a good way to attempt to improve FRET indicator performance. Furthermore, background fluorescence is often a problem when samples are illuminated in the CFP/YFP wavelength range, thus a red-shifted indicator requiring longer wavelengths for excitation and emission could help solve that problem. In the meantime, an ever increasing number of new fluorescent proteins with different spectral properties

has been discovered or created through mutations. These include for example the GFP variants "Sapphire", its improved version "T-Sapphire", and the circularly permuted version "cpSapphir"e which all display a large Stokes' shift (Cubitt et al., 1995), (Zapata-Hommer and Griesbeck, 2003). Additional proteins chosen from the large pool of non-*Aequoria* fluorescent proteins were "DsRed" in a tetrameric and a monomeric form (Matz et al., 1999), (Mizuno et al., 2001), (Campbell et al., 2002), and GFP homologues "Cop-Green" and "Phi-Yellow" (Shagin et al., 2004), (Verkhusha and Lukyanov, 2004), (Shaner et al., 2004). Here, I investigated new combinations of these fluorescent proteins with regard to their usefulness as FRET pairs, for example combinations of *Aequoria victoria*-GFP derivatives together with non-*Aequoria* proteins like Sapphire/DsRed-T4, cpSapphire/DsRed-T4, T-Sapphire/monomeric DsRed, and CFP/Phi-Yellow. Another new FRET pair combination contained the two non-*Aequoria* fluorescent proteins Cop-Green and Phi-Yellow.

I created calcium indicators out of these protein pairs by furnishing them with the troponin C linker proteins from the csTnC and humTnC series that worked best in the creation of CFP/YFP indicators (primer No. 35, 36). In particular, the TnC domains I chose as partners for the new fluorophores were TN-L15, full length csTnC, csTnC-N90, full length humcTnC, TPC1, and a few others. Figure 13 shows two indicator series containing the GFP-derivative Sapphire and the circularly permuted version cpSapphire in combination with a tetrameric form of DsRed (DsRed-T4), together with an evaluation of their maximal % change in the 590/507 nm emission ratio from zero calcium levels to calcium saturation. It is evident in the raw traces that the DsRed-T4 acceptor emission is much dimmer than the Sapphire donor emission. Unfortunately, this makes DsRed-T4 a rather unsuitable FRET partner for live tissue applications, even though the actual value of ratio change appears high in some of the constructs. I obtained similar results with combinations of Sapphire and a monomeric form of DsRed (Campbell et al., 2002); here, the DsRed emission intensity again turned out to be too weak for any useful applications in live cells (data not shown).

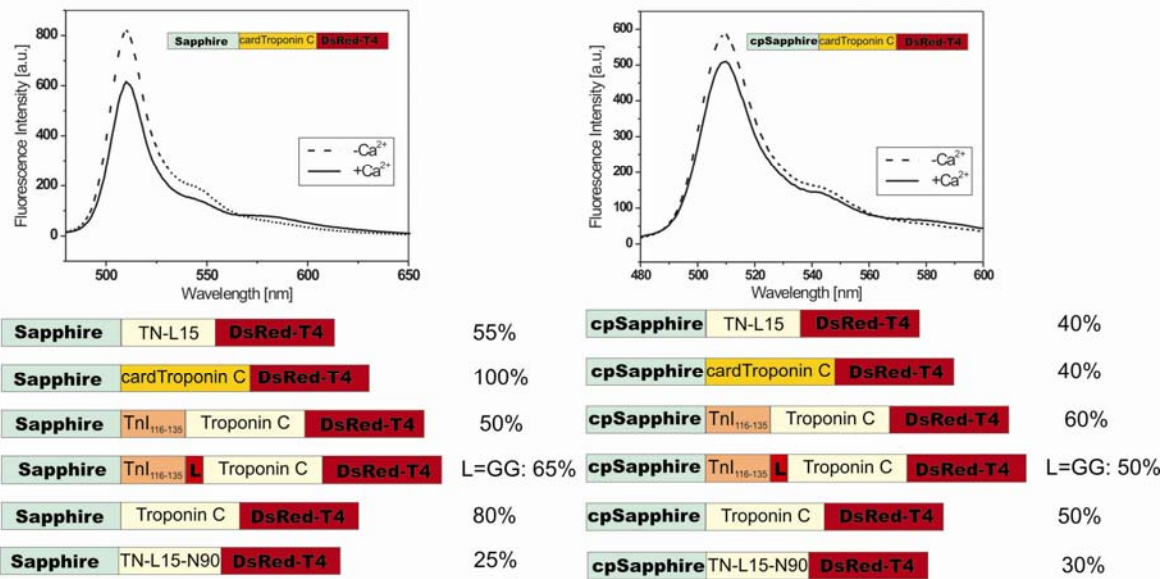


Figure 13: Indicator constructs using two Sapphire variants and DsRed-T4 as fluorophores and their rise in emission ratios in %. The upper part of the figure shows two examples of indicator fluorescence emission in Ca^{2+} free (dotted lines) and Ca^{2+} saturated (straight lines) conditions. Note the weak DsRed emission intensity at 590 nm. Troponin C, chicken skeletal muscle troponin C; TnI, chicken skeletal muscle troponin I; TN-L15, truncated chicken skeletal muscle troponin C in which the N-terminal amino acid residues 1-14 are deleted, which makes the protein start at leucin 15; TN-L15-N90, N-terminal lobe of chicken skeletal muscle troponin C consisting of amino acid residues 15-90; cardTroponinC, human cardiac muscle troponin C; L, linker peptide.

Other non-*Aequoria victoria* indicator constructs built during the course of this work contained combinations of the fluorescent proteins Cop-Green (the Copepoda-GFP ppluGFP2) and Phi-Yellow (Phialidium-YFP) (Shagin et al., 2004). Constructs were cloned by obtaining the DNA sequences of Cop-Green and Phi-Yellow through PCR from cDNA-containing plasmids (both Evrogen). The sense primer used for the amplification of the Cop-Green insert introduced a BamHI restriction site and the Kozak sequence GCC ACC ATG GCC at the 5' end of the Cop-Green sequence, thereby adding the new amino acids Met and Gly to the N-terminus of the polypeptide chain (primer No. 37). The antisense primer inserted a SphI restriction site at the 3' end of the Cop-Green sequence and deleted the original stop codon (primer No. 38). For the cloning of Phi-Yellow, an intrinsic SphI-site had to be removed first by a silent single point mutation that changed the codon of Cys84 from TGC to TGT. The Phi-Yellow insert was then amplified with a primer pair that introduced a SacI site at its 5' end and a EcoRI site at its 3' end (primer No. 43, 44). As in the creation of Sapphire/DsRed constructs, some of the troponin C fragments obtained in the cloning of CFP/YFP indicators (all of them with a SphI site at the 5' end and a SacI site at the 3' end) were ligated together with the Cop-Green and Phi-Yellow

inserts into the expression vector pRSETB. This resulted in fusion proteins containing the FRET donor Cop-Green at their N-terminus, a troponin C calcium binding domain in their middle, and Phi-Yellow as FRET acceptor at their C-terminus. Figure 14 shows a selection of calcium indicator proteins containing Cop-Green and Phi-Yellow as fluorophores and their response in % ratio change after addition of 10 mM CaCl_2 . During the experiments, the Cop-Green acceptor moiety was excited at 450 nm. The results show that Cop-Green and Phi-Yellow do not give satisfying ratio changes in their present configurations. The only exception was the combination CFP/Phi-Yellow which gave a moderate calcium response amounting to a 100% ratio change.

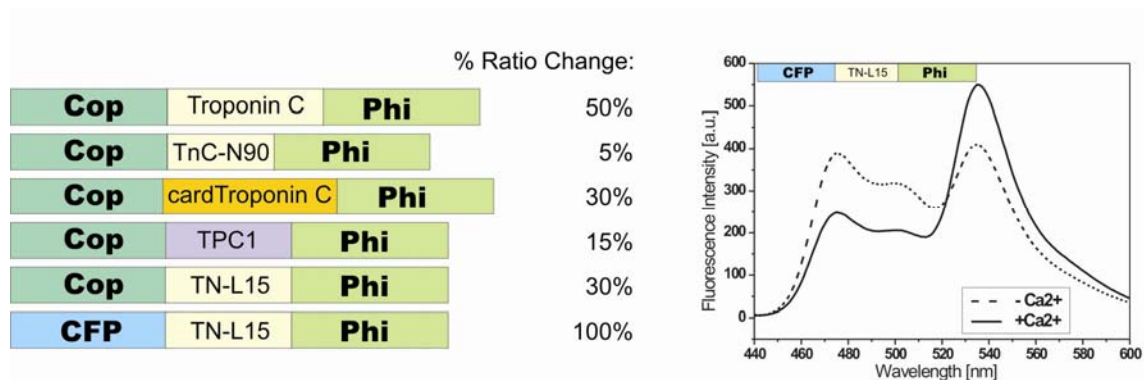


Figure 14: A selection of constructs containing the non-*Aegoria* fluorescent proteins Cop-Green and Phi-Yellow as fluorophores. Cop, Cop-Green; Phi, Phi-Yellow; Troponin C, chicken skeletal muscle troponin C; TnC-N90, the N-terminal lobe of troponin C (amino acids 1-90); TN-L15, truncated chicken skeletal muscle troponin C in which the N-terminal amino acid residues 1-14 are deleted, which makes the protein start at leucine 15; cardTroponinC, human cardiac muscle troponin C; TPC1: *Drosophila* troponin C isoform 1; The panel on the right shows the fluorescence emission of construct CFP-L15-Phi in Ca^{2+} free (dotted lines) and Ca^{2+} saturated (straight lines) conditions.

In order to test whether Phi-Yellow as an acceptor unit would be more resistant to bleaching processes than YFP, I transfected HeLa cells with two indicator proteins: TN-L15 containing Citrine as YFP-acceptor protein and the above mentioned CFP-L15-Phi construct. Cells expressing one of the two proteins were subjected to imaging experiments on the FRET setup under low calcium conditions. To maximize bleaching effects, no neutral density filters were used in the light source so that samples were illuminated with maximum intensity at 440 nm excitation wavelength during image acquisition. Acquisition rates alternated between 10 second intervals and continuous acquiring (700 ms/channel), and emission intensities as well as acceptor/donor ratios were monitored at their respective wavelengths. As can be seen in Figure 15B and D, emission intensities of all fluorescent proteins decreased irreversibly under the chosen maximum illumination conditions, which

indicates bleaching processes. The effect stopped when image acquisition rates were set back to 10 s intervals, but 535/485 nm ratios did not recover. In all experiments conducted ($n = 3$ for each construct) with TN-L15 containing CFP in combination with YFP, YFP emission intensity immediately dropped considerably faster than CFP emission intensity, thereby resulting in quickly falling ratio values during each bleaching period (Figure 15A and B). When the same experiments were performed with CFP and Phi-Yellow as acceptor, both CFP and Phi emissions declined at roughly the same rate during the first part of an experiment, so that the early ratio value of the CFP-L15-Phi probe was not affected (Figure 15C and D). During prolonged illumination however, Phi-Yellow emission began to decrease faster than CFP emission, and ratios dropped at rates similar to the TN-L15 probe. Judging by these observations, Phi-Yellow might indeed be a more stable acceptor protein than the YFP variants, at least under regular imaging conditions that generally require less intense illumination strengths.

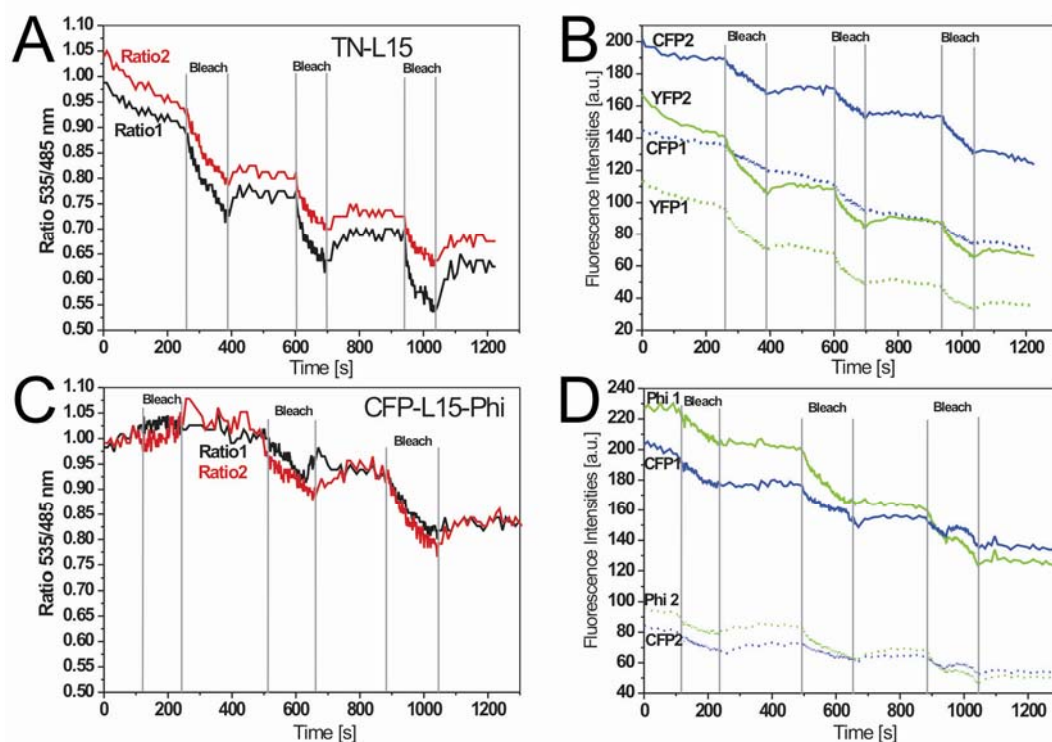


Figure 15: Bleaching experiments on TN-L15 and CFP-L15-Phi. Excitation was 440 nm, emissions monitored at 535 and 485 nm. Acquisition rates alternated between 10 s and 1.4 s (grey bars). A, B, Traces of TN-L15 showing a faster decrease in YFP emission resulting in declining ratios under bleaching conditions. C, D, Traces of CFP-L15-Phi whose emissions both drop at a similar rate during early imaging even though ratios decline in the later phase of the experiment, presumably due to higher bleaching rates of the acceptor protein.

5.1.4 Tuning Promising Constructs (I): Truncating and Multiplying the EF-hands of csTnC

One question that arose during the course of this work was whether the troponin C fragments employed as calcium binding domains could be reduced to a minimum length at which they kept their calcium binding abilities, but were altered enough to not be recognized by any protein binding machinery of the cell. To test this, the EF-hands No. II and IV of csTnC, together with their surrounding α -helical domains, were inserted between CFP and Citrine (primers No. 3, 4, 45-53). Additionally, I created truncated EF-hand linkers in which the first four amino acid residues of the sequence were removed progressively from the respective N-terminus, and each of the resulting constructs was tested for FRET efficiency (Figure 16). As it turned out, FRET was influenced by small alterations in the polypeptide chain such as a single amino acid deletion, emphasizing once again that distance as well as mutual orientation of the two fluorophores plays a significant role in the functionality of a FRET indicator. However, Figure 16 shows that the overall performance of all of these single EF-hand insertions was never quite satisfactory; it seems that the amount of conformational change resulting from such a short stretch of amino acids is too insufficient. Moreover, EF-hands contained in a protein are known to occur most often in pairs, which suggests they might only function properly in the form of a double-hand.



B

Name:	Amino acids:	% Ratio change:	Name:	Amino acids:	% Ratio change:
TN-EF2	Gly ⁵¹ -Ala ⁹¹	10%	TN-EF4	Gly ¹²⁷ -Gln ¹⁶³	5%
TN-EF2-G	Gln ⁵² -Ala ⁹¹	20%	TN-EF4-G	Gln ¹²⁸ -Gln ¹⁶³	0%
TN-EF2-GQ	Asn ⁵³ -Ala ⁹¹	20%	TN-EF4-GE	His ¹²⁹ -Gln ¹⁶³	0%
TN-EF2-GQN	Pro ⁵⁴ -Ala ⁹¹	10%	TN-EF4-GEH	Val ¹³⁰ -Gln ¹⁶³	25%
TN-EF2-GQNP	Thr ⁵⁵ -Ala ⁹¹	10%	TN-EF4-GEHV	Ile ¹³¹ -Gln ¹⁶³	20%

Figure 16: EF-hand derivatives of chicken skeletal muscle troponin C inserted between CFP and Citrine. A cartoon drawing of such a construct is shown in A. Panel B is a list of constructs carrying a truncated version of the linker moiety; the amino acid sequences of each linker are indicated in the middle. Ratio changes were calculated from measurements in zero and 10mM Ca²⁺ buffers.

To further investigate whether single EF-hand sequences could be converted to functional calcium binding linkers, I built a construct consisting of a single GFP analogous to a so-called Camgaroo indicator (Baird et al., 1999) in which the original calmodulin insert of the Camgaroo was exchanged for the same series of csTnC EF-hand II and IV truncated linkers used above (primers No. 54-65). I selected the four linker peptides that gave the largest fluorescence changes from the group and then doubled or tripled them by head-to-tail ligation of the insert. FRET efficiency and calcium binding properties again varied among the constructs, but no significant improvement in FRET signals could be achieved through the doubling and tripling of a single EF-hand (Figure 17).

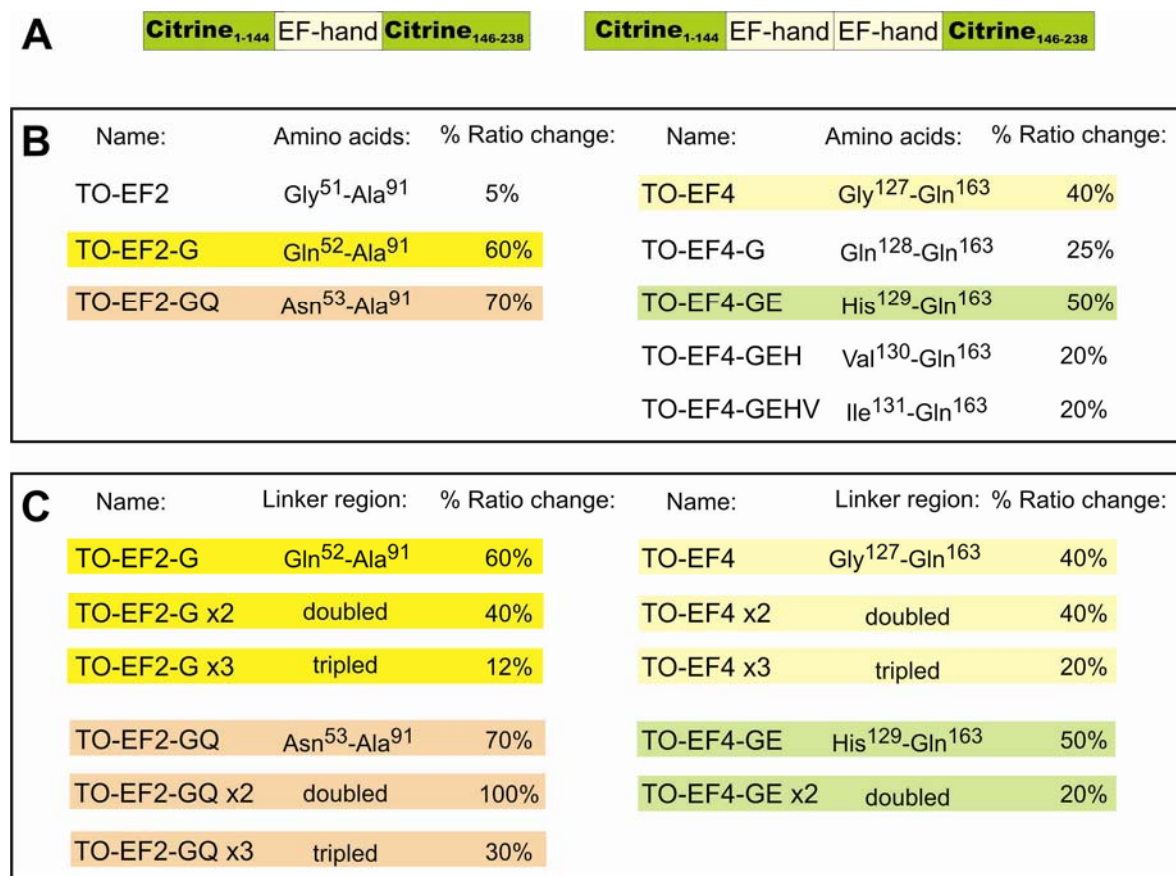


Figure 17: EF-hand derivatives of chicken skeletal muscle troponin C inserted in a single GFP indicator. A, cartoon drawing of two constructs with a single and a double insertion of an EF-hand. Panel B lists the constructs carrying truncated versions of the linker moiety; the amino acid sequences of each linker are indicated in the middle. Colors indicate the constructs that were chosen for doubling and tripling experiments. Panel C shows four constructs and the effect of doubling or tripling the respective EF-hand insert. All ratio changes were calculated from measurements in zero and 10mM Ca²⁺ buffers.

5.1.5 Tuning Promising Constructs (II): Mutating EF-hands of TN-L15

An abundance of structural data is available on the nature of calcium binding in an EF-hand, and site-directed mutagenesis of the six amino acid residues responsible for ion coordination has been used extensively to study changes in ligand binding properties and conformational behavior within troponin C (Davis et al., 2002), (Tikunova et al., 2002), (Tikunova and Davis, 2004). Of special interest were the effects of EF-hand mutations on two parameters: first, the affinity for magnesium, and second, the affinity for calcium, both quantified by their K_d values. It is obvious that any indicator of calcium dynamics in a physiological environment has to respond to calcium changes within the concentration ranges normally found in cell cytosols before and after a stimulus, that is a $[Ca^{2+}]$ -concentration of about 10^{-7} to 10^{-6} M (Tsien, 1999). Furthermore, it is desirable that the physiological amounts of magnesium present in any surrounding disturb calcium affinity as little as possible so as to not compromise the indicator's performance.

Therefore, in a first step, I established the K_d values for calcium and magnesium binding in the two indicator constructs TN-L15 and TN-humTC. In a second step, I inactivated systematically the individual EF-hands of chicken skeletal troponin C by removing the aspartate or glutamate residues at the X and -Z positions, that is the first and last amino acid of each loop region. In all four EF-hands of the TN-L15 indicator construct, Glu in position X was mutated to Gln, and analogously Asp in position -Z was changed to Ala. This resulted in a group of eight derivatives of TN-L15 named after the respective mutated amino acid residue: TN-L15 D31A, TN-L15 E42Q, TN-L15 D67A, TN-L15 E78Q, TN-L15 D107A, TN-L15 E118Q, TN-L15 D143A, and TN-L15 E154Q. In addition, some combinations of these single point mutations were done in the same molecule, leading to four more constructs called TN-L15 D31/67A, TN-L15 D31/67A, TN-L15 E42/78Q, TN-L15 D107/143A, TN-L15 E118/154Q. Amino acid residues were exchanged by introducing point mutations into codons of the csTnC gene sequence by site-directed mutagenesis with the primer extension method. Calcium dissociation constants were derived from titration assays by means of a calcium buffer systems to which magnesium was added when needed (Figure 18). Analogous titration assays were performed with varying magnesium concentrations and no calcium present to quantify the Mg^{2+} -sensitivity of the proteins.

Interestingly, a large number of mutated constructs completely lost their functionality and did not respond with a detectable ratio change to rising calcium

concentrations anymore. Some of the variants found to be still active included the constructs TN-L15 E78Q, TN-L15 D107A, TN-L15 E118Q, and TN-L15 E154Q, all of which had kept a ratio change of around 100% at full calcium saturation.

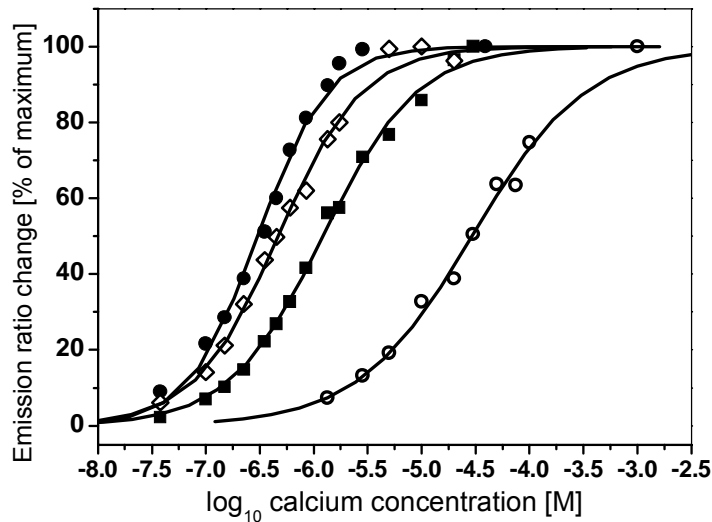


Figure 18: Calcium titration curves of TN-L15, TN-humTC, and two TN-L15-derivatives carrying mutated EF-hands. TN-L15 D31A/D67A (filled circles), TN-humTnC (open diamonds), TN-L15 (filled squares) and TN-L15 D107A (open circles). Emission ratio changes were normalized to the values at full calcium saturation.

Figure 18 shows the determination of calcium K_d values of four constructs by Ca^{2+} titrations in the presence of 1 mM free Mg^{2+} . Here, emission ratio changes were normalized to their values at full calcium saturation, and apparent Ca^{2+} dissociation constants derived from sigmoidal curve fits. The calcium K_d values that were found varied from 200 nM for TN-L15 D31/67A (filled circles), 470 nM for TN-humcTnC (open diamonds), 1.2 μM for TN-L15 (filled squares), to 27 μM for TN-L15 D107A (open circles). As expected, the mutation D107A by which the third C-terminal EF-hand of troponin C was inactivated resulted in an indicator with reduced calcium affinity. As a consequence, the corresponding calcium titration curve was significantly shifted to the right, as seen in Figure 18. Therefore this mutant appears to be more suitable for measuring larger changes in calcium, e.g. the ones encountered when indicators are targeted to synaptic sites or in close vicinity to channels. For comparison, inactivating both N-terminal sites by the double mutation E42Q/E78Q yielded a protein that left only the C-terminal high-affinity components intact, resulting in a K_d for calcium of only 300 nM (Figure 18, filled circles). A surprisingly high dissociation constant was found for the *Drosophila*

construct TN-TPC1-L5; its K_d in a Mg-free solution was 26 μM (data not shown). This value is very similar to the mutated form TN-L15 D107A, even though no EF-hands were altered in TN-TPC1-L5. Thus, TN-TPC1-L5 seemed not to be a good option for calcium imaging in cytosolic environments; but like TN-L15 D107A it might serve as an indicator for applications in which large changes in calcium concentration are expected.

Similar to the calcium K_d determinations, titration assays were undertaken to obtain magnesium dissociation constants of selected indicator constructs. A low magnesium dissociation constant indicates a high affinity of the protein for this ion, which consequently means that an indicator with a low magnesium K_d might be too sensitive to changes in $[\text{Mg}^{2+}]$ to be still reliable in the reporting of $[\text{Ca}^{2+}]$ changes. Hence, constructs with Mg^{2+} - K_d values close to the physiological concentration of 1 mM should be avoided. The Mg^{2+} dissociation constant found was 2.2 mM for TN-L15 and 0.5 mM for TN-humTnC, respectively. In all of the mutated TN-L15 derivatives presented here, alterations in the N-terminal, regulatory EF-hands No. I and II had no major effect on magnesium binding affinities. In contrast, when the third EF-hand was made defunct, Mg^{2+} affinity of the protein in question was lowered considerably. One example is TN-L15 D107A whose K_d value rose from the original 2 mM up to 5 mM. This again substantiates previous findings that suggest an involvement of the C-terminal, nonregulatory EF-hands of troponin C in magnesium binding (Tikunova et al., 2001), (Davis et al., 2002).

5.1.6 *In vitro* Kinetics

Only an indicator that allows a fast enough tracking of signals will be useful in time-lapse imaging experiments. The kinetic properties of a probe are determined by the on-rate k_{on} and the off-rate k_{off} of the ligand binding to the indicator macromolecule. The ratio $\frac{k_{off}}{k_{on}}$ is the K_d value of the macromolecule under consideration. Previous experiments conducted on Yellow Cameleon indicators indicated that the on-rates of calcium binding to these calcium probes were in the range of $10^6 \text{ M}^{-1} \text{ s}^{-1}$ and inverse off-rates amounting to a few hundred milliseconds (Miyawaki et al., 1997).

In the following set of experiments, I tested a selection of the new indicator constructs for their calcium dissociation rate constants. Since the calcium/indicator dissociation reaction should be of first order and therefore independent of the initial Ca^{2+}

concentration, I performed series of measurements in buffer solutions containing different initial calcium concentrations. In these experiments, indicator proteins were preincubated in calcium buffer solutions to ensure saturation of the protein. Thus, constructs with high Ca^{2+} Kd values such as TN-L15 D107A and TN-TPC1-L5 had to be subjected to higher initial free Ca^{2+} concentrations than high-affinity constructs with low Ca^{2+} Kd values. Example traces of individual dissociation experiments are shown in Figure 19. As expected for first order reaction kinetics, the off-rates determined in all of the experiments were independent of the chosen initial calcium concentration (data not shown). The τ values ($= 1/k_{\text{off}}$) obtained from the selected constructs in Figure 19 were 860 ms for TN-L15 (top left), 580 ms for TN-L15 D107A (top right), 560 ms for TN-humTnC (middle left), and 450 ms for the *Drosophila* variant TN-TPC1-L5 (middle right). Despite its origin from fast-twitching fly flight muscle, the *Drosophila* indicator did not perform considerably better than the rest. When compared to the troponin C indicator proteins under the same experimental conditions, Yellow Cameleon 2.3 (YC2.3) displayed a calcium dissociation rate constant of 870 ms (Figure 19, bottom).

By combining these findings and the Kd values derived from the titration experiments described in the previous section, calcium association rate constants (k_{on}) could be calculated through the relation $Kd = \frac{k_{\text{off}}}{k_{\text{on}}}$. It turned out that constructs with lower Kd values such as TN-L15 (Kd: 1.2 μM), TN-humTnC (Kd: 470 nM) and YC 2.3 (Kd: 4.3 μM) gave k_{on} values ranging from 1 - 3 $\times 10^6 \text{ M}^{-1} \text{ s}^{-1}$ which resembles the values originally published in Miyawaki (1997) for Yellow Cameleon 3.0 with a Kd of 5.4 μM and a k_{on} -rate of 2.4 $\times 10^6 \text{ M}^{-1} \text{ s}^{-1}$. Calculations of association rates of the constructs with higher Kd values such as TN-L15 D107A (27 μM) and TN-TPC1-L5 (26 μM) led to values between 60.000 to 90.000 $\text{M}^{-1} \text{ s}^{-1}$; these numbers reflect the relation $k_{\text{on}} = k_{\text{off}} / \text{Kd}$.

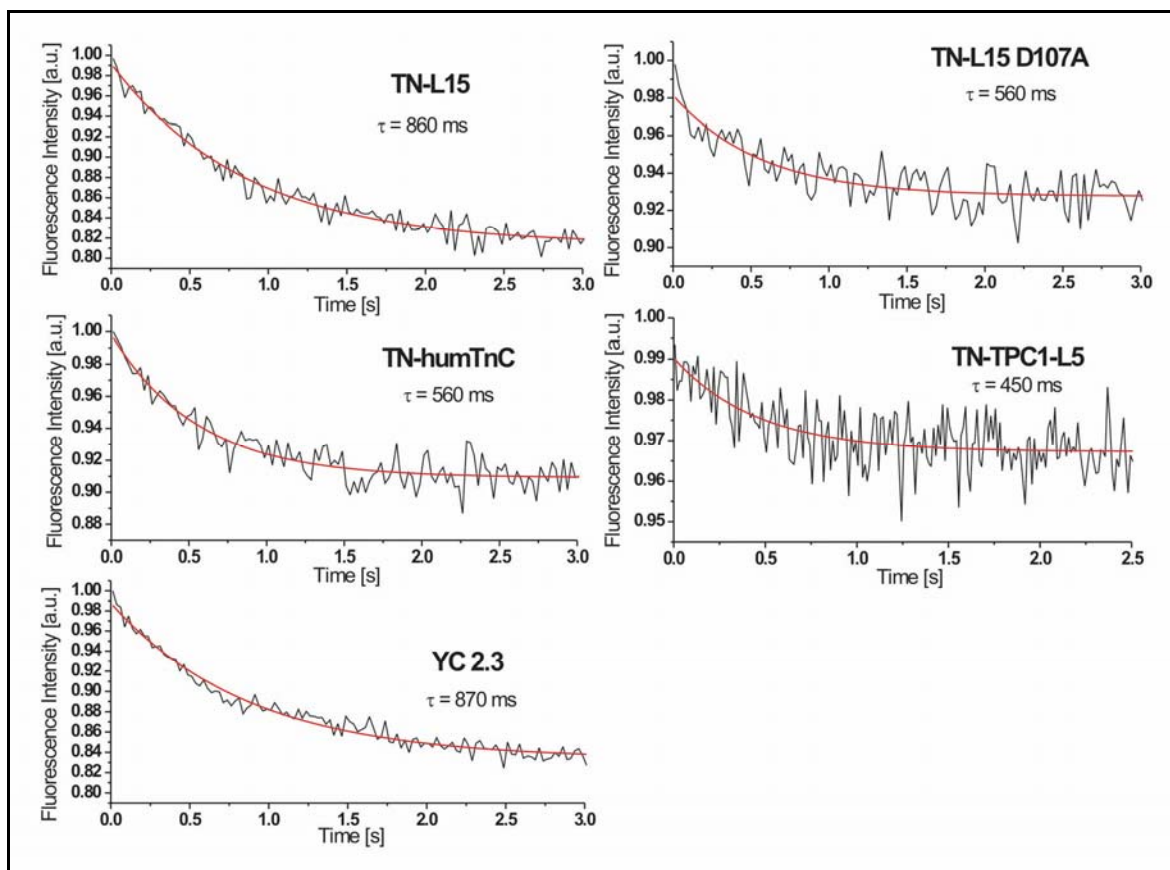


Figure 19: Dissociation kinetics of five indicator constructs. Samples were excited at 432 nm and Citrine emissions monitored at 528 nm. Data sets from at least five experiments were averaged and rate constants derived from monoexponential curve fittings.

5.2 Functionality of TnC-Indicators in Cell Culture: TN-L15, TN-humTC and their derivatives

5.2.1 Cytosolic Expression in HEK293

After completion of the *in vitro* tests, the next series of experiments dealt with the functionality of the newly constructed calcium indicators in living cells. I conducted first expression experiments in mammalian cells by transfecting different mammalian cell lines with pcDNA3 plasmids containing a CMV promoter for transient gene expression. Before the genes of interest could be cloned behind that promoter region, an optimized Kozak consensus sequence (GCC GCC ACC ATG G) had to be introduced by PCR at the 5' end of CFP to ensure sufficient gene transcription (primer No. 66). Similar to the cloning protocol used with the pRSETB vector, the indicator DNA sequences were cut by restriction with BamH1 and EcoR1 and ligated into the MCS region of the pcDNA3 plasmid. The resulting plasmid was used for transfections of cultured mammalian cells.

The cell line I eventually chose for the following experiments was the HEK293 line derived from human embryonic kidney cells, since it performed best in transfection assays. HEK293 cells were transfected by the Lipofectin transfection method and imaged 24 -72 hours later on a FRET setup.

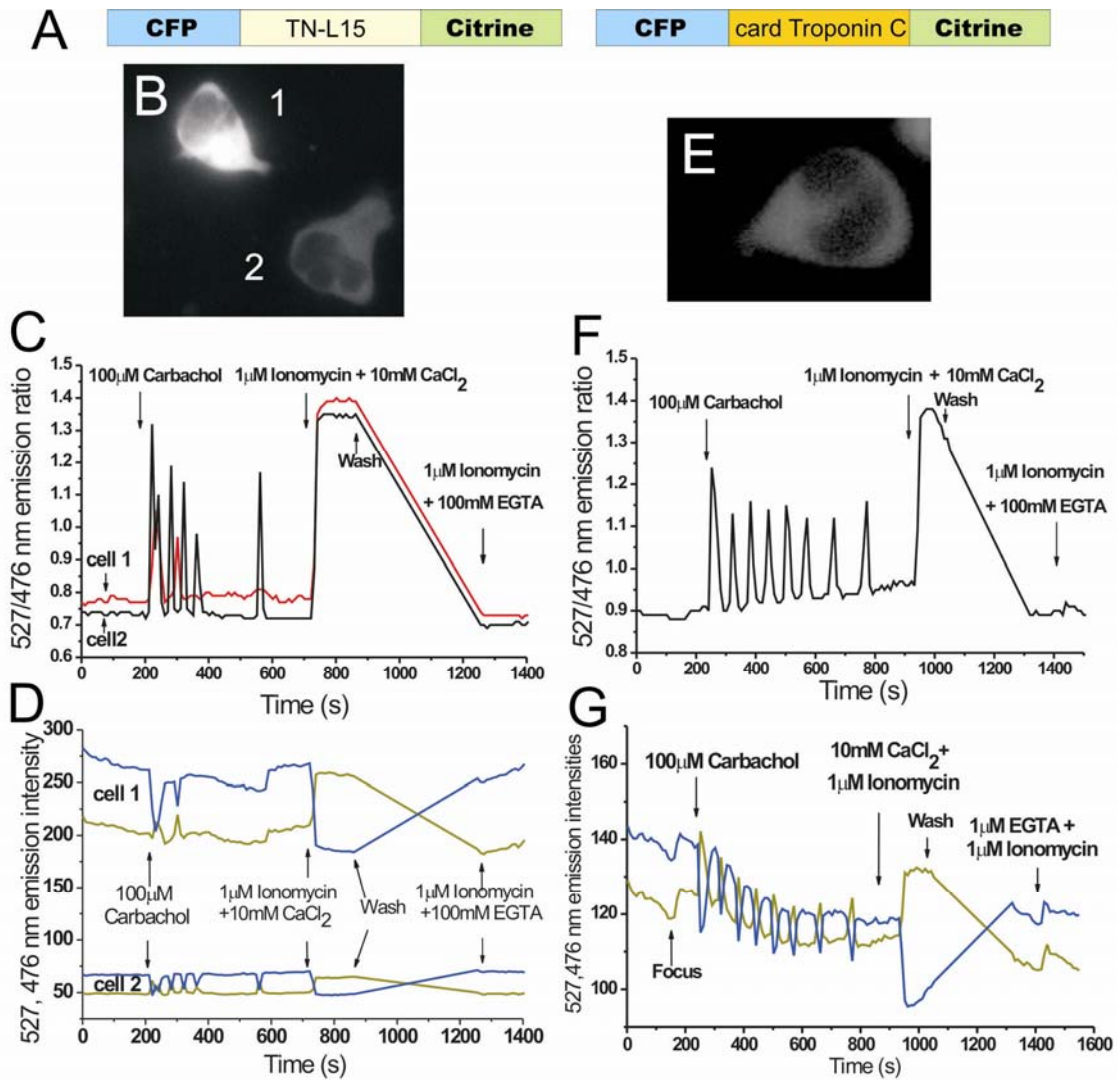


Figure 20: Functionality of TN-L15 and TN-humTnC in HEK293 cells. Cell images show the Citrine emission at 535/25 nm upon excitation at 440/20 nm. A, schematic drawing of the two constructs examined in this figure. B, HEK293 cells displaying cytosolic localization and different expression levels (cells 1 and 2) of TN-L15. C, ratio traces of the two cells depicted in B. Responses to stimulation with 100 μ M carbachol and treatment with 1 μ M ionomycin and 10 mM calcium to obtain the maximum ratio R_{max} , and with 100 μ M EGTA to obtain the base line ratio R_{min} are shown. D, corresponding intensity traces of CFP and Citrine emission for the ratios in C, showing individually the traces of the higher expressing cell 1 and the dimmer expressing cell 2. E, cytosolic expression of TN-humTnC in a HEK293 cell. F, imaging trace the cell in E showing the 527/476 nm emission ratio after stimulation with 100 μ M carbachol. G, corresponding intensity traces of CFP and Citrine emission for the ratios in F.

Figure 20B and E show the expression of TN-L15 and TN-humTnC in HEK293 cell culture. Since the troponin C that was integrated into the indicator fusion proteins originates from a part of the muscle troponin complex and is commonly not expressed as an isolated protein within the cytosol, it was satisfying to see that both indicator constructs showed good cytosolic expression. Fluorescence appeared evenly and homogeneously distributed within the cytosol of the cells with no signs of aggregation. The nucleus was excluded as expected for proteins with molecular weights of 69.7 and 72.5 kD, respectively for TN-L15 and TN-humTnC. In order to examine the functionality of the indicators inside live cells, we used the established carbachol response of HEK293 cells that can be stimulated via endogenous muscarinic receptors (Tong et al., 1999). Responses of HEK293 cells expressing TN-L15 and TN-humTnC after stimulation with 100 μ M carbachol can be seen in Figure 20C-G. Panel C shows the ratios and panel D the intensity changes of the individual emission wavelengths for two cells expressing different levels of TN-L15. Even though the overall expression level in one cell is considerably lower than in the other, the amplitude of the ratio signal in panel C is not affected, underscoring the advantage of ratiometric recordings. Generally, carbachol-induced oscillations of cellular free calcium that lead to repeated cycles of reciprocal intensity changes of CFP and Citrine could be readily imaged with both indicators. Imaging turned out to be dynamic and reproducible, and it was no problem to obtain R_{max} and R_{min} values. Maximal ratio changes within HEK293 cells were 100 % for TN-L15 and 70 % for TN-humTnC, which is in good accordance with the *in vitro* properties of these two probes. For comparison, the maximal ratio change obtainable with Yellow Cameleon 2.1 on our setup was 70 % (data not shown).

5.2.2 Cytosolic Expression in Dissociated Neurons

Apart from cell culture experiments in HEK293 cells, I also tested selected indicator constructs, above all TN-L15 and TN-humTnC, in primary cultures of dissociated rat hippocampal neurons. Two to six weeks after their preparation from rat embryos, cultured neurons were transfected by the calcium phosphate method and imaged two to four days later on the standard FRET setup. A rise in intracellular calcium was stimulated through application of glutamate or potassium to the medium in which the cells were imaged. Panel D of Figure 21 demonstrates that both TN-L15 and TN-humTnC responded

well to high potassium or glutamate stimulation. In some preparations, TN-L15 also succeeded in recording spontaneous activity of hippocampal neurons, demonstrating its usefulness for detecting endogenous activity patterns (Figure 21B).

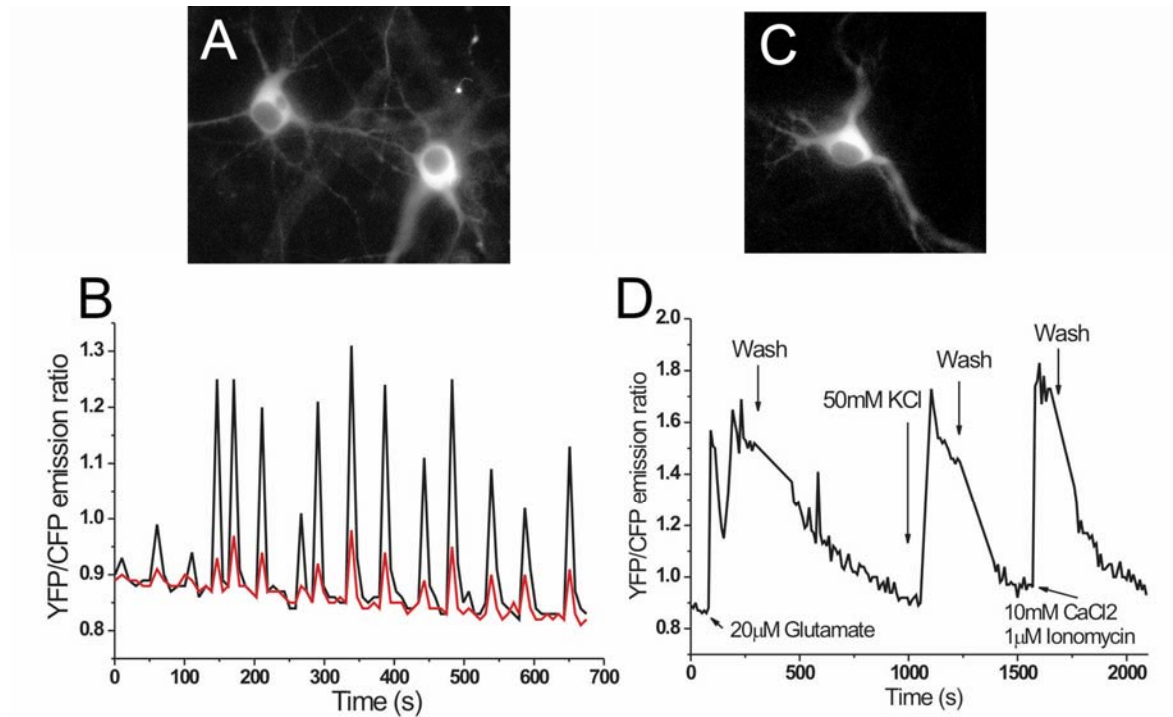


Figure 21: Dissociated rat hippocampal neurons three weeks in culture, all expressing TN-L15. B, imaging trace of the neurons in A, showing spontaneous calcium transients. **D,** imaging trace of the neuron in picture C, showing responses to glutamate, potassium and a forced calcium influx by means of ionomycin

5.2.3 Subcellular Targeting of TnC-based Indicators and Their Functionality in HEK293 Cells

The next task was to evaluate the properties of the new probes in targeting experiments by directing them to specific sites within cells. One aspect that makes genetically encoded probes so promising is the fact that they can be precisely localized in cellular organelles and microenvironments when they are fused to appropriate organellar targeting signals or localized host proteins. GFP-based indicators have reportedly been used for example in targeting experiments involving the nucleus, the ER, mitochondria, and the Golgi apparatus (Miyawaki et al., 1997), (Griesbeck et al., 2001), (Palmer et al., 2004). However, functional labelings of membranes, pre- or postsynaptic structures or

calcium channels have proven difficult so far when undertaken with GFP-based indicators. Especially conventional calmodulin-based indicators seemed to encounter problems with these types of targetings (see Figure 22B, D, G). Therefore, the obvious thing to do was to create a series of troponin-based indicators that carried different targeting sequences and to compare them to the analogous versions of targeted calmodulin-based cameleons.

One attractive cellular site appeared to be the plasma membrane, as submembrane calcium domains play a crucial role in a variety of biological phenomena ranging from secretion and ion channel modulation to signal transduction, yet are beyond the resolution of conventional light microscopy. Apart from the immediate membrane-targeting application, the same protein trafficking pathways are also frequently involved when other labelings are attempted, e.g. localizing an indicator to pre- or postsynaptic structures or fusing it to the pore of a calcium channel. Although membrane targeting experiments with calmodulin-containing indicators like ratiometric Perikam and Yellow Cameleons have been described before (Pinton et al., 2002), (Isshiki et al., 2002), our laboratory was not able to put them to use successfully. In our hands, regular Cameleons lost their calcium sensitivity when targeted to the membrane (Figure 22B, D, G) and the Perikams with their strong pH-sensitivity were not considered adequate for primary neurons, since these cells show substantial cytosolic pH-fluctuations after stimulation (Chesler and Kaila, 1992).

Figure 22 shows a comparison of membrane-targeting experiments using TN-L15 and Yellow Cameleons equipped with several membrane targeting sequences. All TN-L15 and Cameleon constructs were made in the identical manner and differed only in their calcium binding moiety. Figure 22A and B depict calcium responses of TN-L15 or YC2.1 to which the membrane targeting sequence of GAP43 was fused at the 5' end of the protein sequence. This targeting sequence consists of the 20 amino acid sequence MGCCMRRTKQVEKNDEDQKI that had been reported to comprise the membrane-anchoring signal of the GAP43 protein (Moriyoshi et al., 1996). The functionality of these constructs was then tested by expression in HEK293 cells.

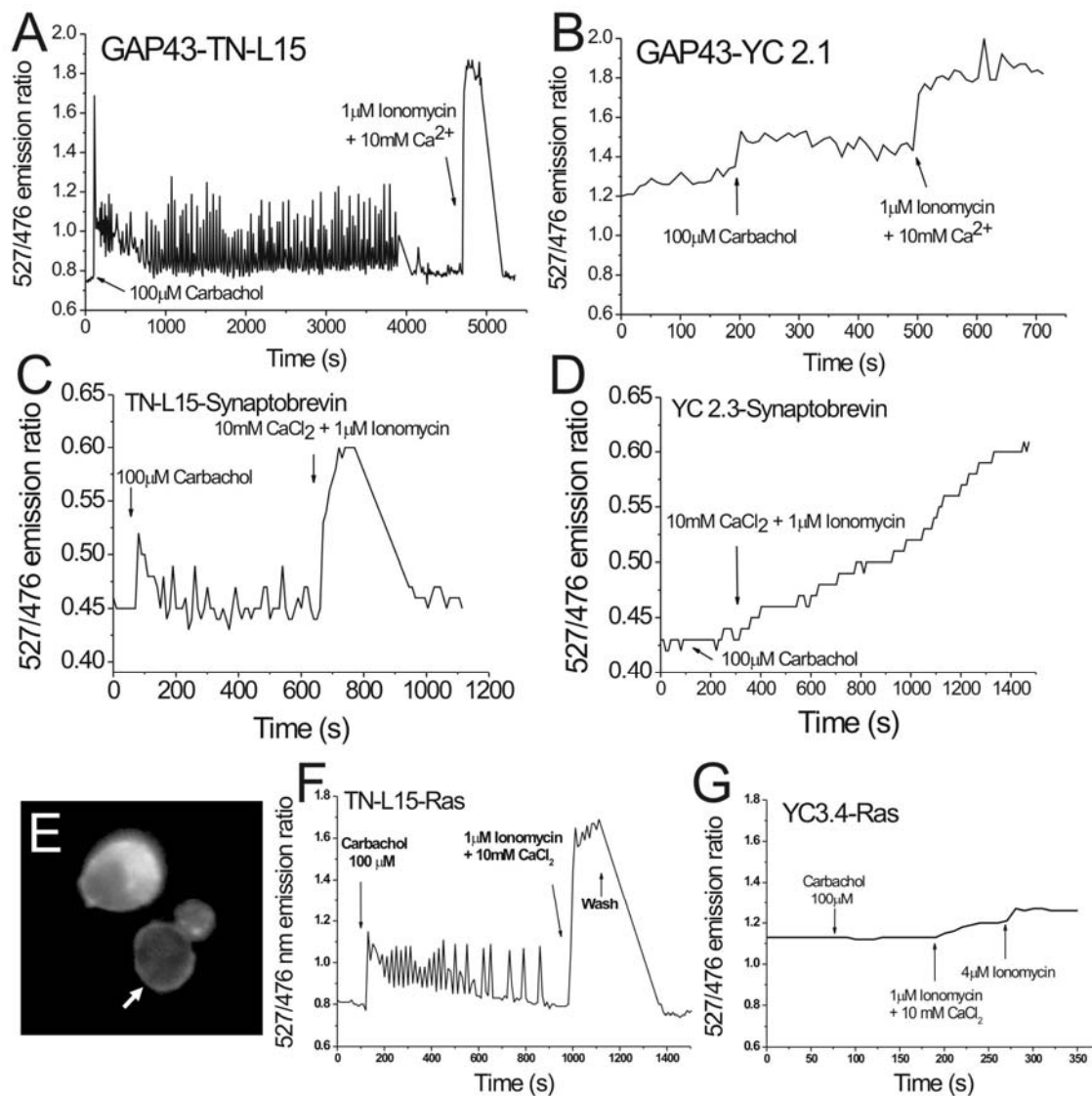


Figure 22: Comparison of membrane-targeting of TN-L15 and Yellow Cameleons using several membrane targeting sequences. A, Imaging trace with GAP43-TN-L15. Long lasting calcium oscillations after stimulation with carbachol are visible. In contrast, GAP43-YC2.1 performed poorly under identical conditions as seen in B. No oscillations were detectable, and also calibration with ionomycin indicated a reduced dynamic range. C, Imaging trace of TN-L15-Synaptobrevin. Good responses to stimulation with carbachol and ionomycin were readily detectable. D, Imaging trace of YC2.3-Synaptobrevin. The fusion construct has largely lost its calcium sensitivity and binding properties. No responses to carbachol stimulation were seen. E, monochrome picture of the HEK293 cell whose race is shown in F. Arrow, cell that was imaged. F and G, comparison of membrane targeting using the C-terminal targeting sequence of c-Ha-Ras. F, TN-L15Ras was fully functional under these conditions and had comparable properties to the indicator when localized in the cytosol. G, imaging trace using YC3.3Ras under identical conditions.

Imaging with GAP43-TN-L15 revealed long lasting calcium oscillations after stimulation with carbachol. As expected, the submembrane calcium oscillations in these cells were very similar to those seen with a cytosolic indicator. A final calibration with ionomycin/10 mM $CaCl_2$ and ionomycin/20 μ M EGTA to obtain the maximum and minimum ratios R_{max} and R_{min} verified that the indicator had its full dynamic range and

full functionality when targeted to the plasma membrane (Figure 22A). In contrast, GAP43-YC2.1 performed poorly under identical conditions (Figure 22B). No oscillations were detectable, and even the addition of ionomycin induced only a sluggish response, suggesting that the indicator had lost significant features of its calcium binding properties on the pathway to membrane insertion. The GAP43-YC2.1 trace shown here represents seven experiments, none of which gave a response.

I obtained similar results by fusing the indicators to the presynaptic protein Synaptobrevin (Elferink et al., 1989), (Nonet, 1999) and the C-terminal membrane targeting sequence of c-Ha-Ras (Moriyoshi et al., 1996). The fusions of TN-L15 or YC3.1 to Synaptobrevin were achieved through amplification of the Synaptobrevin gene by PCR in which a Kpn1-Site was introduced within a GGTGGS linker sequence at its 5'-end. Simultaneously, a Kpn1-site was introduced at the 3' end of TN-L15 or YC3.1, thereby deleting the original stop codons. The DNA fragments coding for the modified Synaptobrevin and TN-L15 or YC3.1 could be ligated together into an expression plasmid. Similarly, Ras-targeting was achieved by adding the membrane anchor sequence of c-Ha-Ras to the C-terminus of TN-L15 and Yellow Cameleon 3.3. For this, the indicator DNA sequences had to be extended with a sequence encoding the 20 amino acid sequence KLNPPDESGPGCMSCKCVLS of the c-Ha-Ras membrane-anchoring signal (Moriyoshi et al., 1996). The DNA sequences were fused by PCR to the 3' end of both indicator genes (primer No. 67).

An imaging trace of YC2.3-Synaptobrevin in HEK293 cells is shown in Figure 22D. As a fusion construct, YC2.3 had noticeably weaker calcium sensitivity and no responses to carbachol stimulation were detected. Ionomycin induced a slow rise of the ratio over several minutes that does not reflect the actual cytosolic rise in calcium levels after ionomycin treatment. The trace shown in Figure 22D is an example chosen from 9 different imaging experiments, none of which elicited a response of this probe. The same decrease of dynamic range that YC2.3-Synaptobrevin displayed in HEK293 cells was also found when this protein was expressed and purified from bacteria. This effect might therefore be attributed mainly to sterical problems within the indicator protein. In contrast, good responses to stimulation with carbachol and ionomycin were detectable with the analogous fusion construct TN-L15-Synaptobrevin (Figure 22C).

The last three panels of Figure 22 (E, F, and G) show imaging experiments using Ras-targeted versions of TN-L15 and Yellow Cameleon 3.3. A scheme of the construct

TN-L15-Ras is depicted in Figure 23. After expression of the Ras indicators in HEK293 cells, a ring-shaped labeling of the plasma membrane was evident (Figure 22E). For the evaluation of imaging experiments, I defined small regions following the brightly labelled contours of the membrane. Membrane-tagged TN-L15-Ras readily reported agonist-induced increases in cytosolic calcium and had the same dynamic range as in cytosolic expression (Figure 22F). YC3.3, on the other hand, was again defunct at the cell membrane. Interestingly, YC3.3-Ras was fully calcium sensitive this time when purified from bacteria and tested *in vitro*, suggesting that the addition of the targeting sequence did not cause a steric hindrance within this particular construct. YC3.3-Ras also appeared to fold and target correctly as it showed a similar membrane staining as TN-L15-Ras in HEK293 cells, and both CFP and Citrine emission were properly visible.

5.2.4 Subcellular Targeting in Neurons: TN-L15 D107A-Ras and Others

Since membrane targeting experiments with the new indicator TN-L15 had led to promising results in HEK293 cells, I undertook the next targeting studies with these constructs in dissociated neuronal cell cultures. Neurons, with their fast calcium dynamics during signal transduction and transmitter release, appeared to be ideal subjects to test live kinetic properties of the new indicator constructs. Furthermore, many research groups focus their studies on subcellular neuronal structures like pre- and postsynaptic sites or spines. The prospect of being able to specifically target calcium indicators to these sites has been exciting, and first publications reported successful attempts using for example the pH-sensitive GFP based probe synapto-pHluorin (Miesenbock et al., 1998), (Bozza et al., 2004).

I achieved labeling of the plasma membrane of hippocampal neurons by using once more the membrane anchor sequence of c-Ha-Ras already described in the previous section (Moriyoshi et al., 1996). When the targeted construct TN-L15-Ras (Figure 23A) was expressed in cultured hippocampal neurons, a clear and homogeneous membrane labelling was evident (Figure 23C). A small bright spot visible in most cells appeared to be associated with the Golgi.

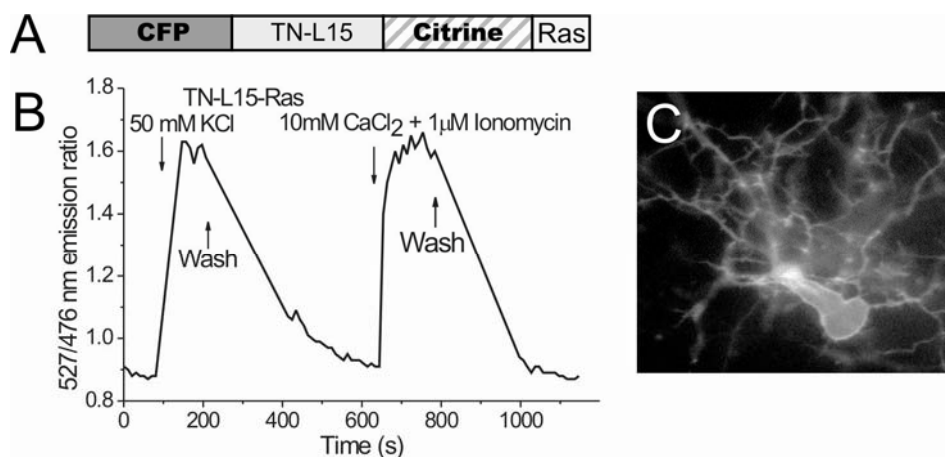


Figure 23: TN-L15-Ras in dissociated rat hippocampal neurons. A, schematic drawing of the construct with its C-terminal Ras targeting sequence. B, Imaging trace of the neuron depicted in C. After stimulation with 50 mM KCl, the indicator is already fully saturated and reaches the same maximum value that is achieved with CaCl₂/Ionomycin

Again, I defined small regions along the cell membrane for image evaluation. The TN-L15-Ras construct, however, soon proved to become saturated after stimulation with 50 mM potassium, which is probably due to the close vicinity to calcium channels in the plasma membrane (Figure 23B). Therefore, I switched to the analogous low calcium affinity version TN-L15 D107A-Ras that, with an *in vitro* K_d of 29 μM, appeared more suitable to quantify submembrane calcium rises in these cells. Stimulations of this probe with glutamate or high potassium elicited average ratio changes of about 19 % (n = 34) (Figure 24B and E). The TN-L15 D107A-Ras probe was not saturated under these conditions, and the application of ionomycin/10 mM calcium resulted in a further ratio increase up to an even higher maximum value. In some previous publications, the data produced in such a way with ratiometric indicators was used to calculate calcium concentrations by means of the Hill equation (Miyawaki et al., 1997), (Yu and Hinkle, 2000). In the case of TN-L15 D107A-Ras, such calculation attempts led to widely varying results, indicating a [Ca²⁺] between 5 and 30 μM. However, measurements using the cytosolic form of TN-L15 D107A did not differ from the ones employing the membrane-targeted version, leading to an identical average ratio change of 19 % (n = 12) and subsequent cytosolic [Ca²⁺] levels derived from the Hill equation of 6 to 20 μM. These somewhat implausible results might be explained by the fact that the calcium dissociation constant of TN-L15 D107A of 29 μM was determined only through *in vitro* measurements and assumes a different value in the cell cytosol. This effect could be even more pronounced in places close to the plasma membrane where protein movement is often

sterically hindered and ion diffusion rates are far from their values in aqueous environments. This finding is congruent with a recent report by Pologruto and coworkers (2004) who investigated a variety of GFP-based calcium indicators in cultured hippocampal brain slices. Their studies found distinct nonlinearities in calcium/indicator binding curves as well as discrepancies between *in vitro* and *in vivo* K_d values of GFP-based calcium indicators.

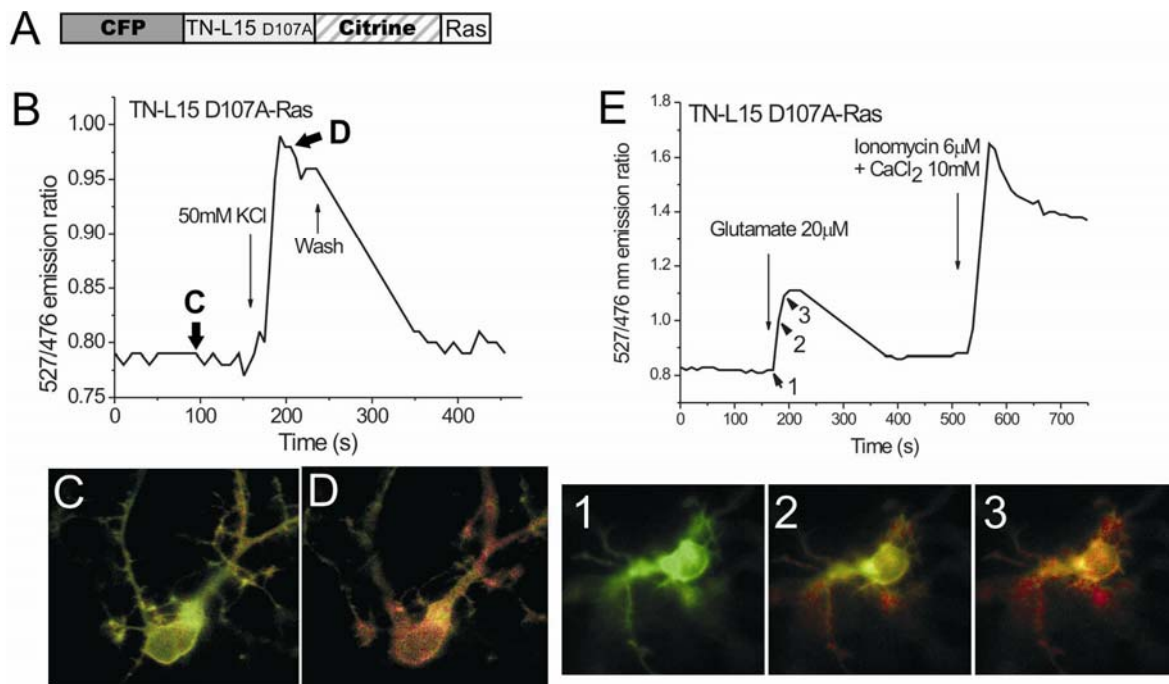


Figure 24: TN-L15 D107A-Ras in dissociated hippocampal neurons. A, schematic drawing of the construct with its C-terminal Ras targeting sequence. B, Imaging trace showing KCl stimulation of the neuron depicted in C and D. C and D, Ratio pictures of the cell at the time points indicated in B. E, Glutamate stimulation of the neuron shown in the ratio pictures taken at the time points 1-3. In contrast to TN-L15-Ras, the D107A variant is not fully saturated after stimulation and therefore better suited for imaging experiments at the plasma membrane.

Another question raised was whether the data obtained here support that long lasting submembrane calcium domains that are not in equilibrium with bulk cytosolic transients can exist in primary neurons. Such domains were found in the rat smooth muscle-derived cell line A7r5, in which long lasting global submembrane calcium domains were detected that reached peak values as high as 100 μ M (Marsault et al., 1997). Interestingly, submembrane calcium levels appeared to be elevated in these cells even under resting conditions. In order to examine this question, hippocampal neurons were co-transfected with the more sensitive membrane-targeted probe TN-L15-Ras and a nucleus-targeted version of Yellow Cameleon 2.3. In imaging experiments, the submembrane

calcium levels monitored with the more sensitive probe TN-L15-Ras (Figure 23B) could be compared to the rises in cytosolic calcium that were reflected in the responses of the nucleus-targeted YC2.3. Here, average cytosolic calcium transients appeared not significantly lower than submembrane levels in the cells under these conditions and on the time scale achievable with our imaging setup. However, measurements with improved temporal resolution will be necessary to obtain more detailed information about a possible permanent gradient in calcium concentration from the membrane towards the cytosol.

5.3 Transgenic Mice Expressing TN-L15 in the Cytosol of Neurons

5.3.1 Choosing an Adequate Promoter and Indicator Construct

Only few published studies so far managed to successfully image GFP-based indicator proteins in tissue of transgenic mice. Most of these indicators were non-ratiometric single GFP constructs, such as the probes synapto-pHluorin (Bozza et al., 2004), G-Camp (Ji et al., 2004), inverse pericam, and Camgaroo-2 (Hasan et al., 2004). Only two of those indicators worked in whole live animals, and none of them gave a response that exceeded the 20% range. The only ratiometric FRET indicator reported to have shown some functionality in transgenic mice was the Yellow Cameleon variant YC3.60. However, the maximum ratio signal obtained here amounted only to as little as 3% (Nagai et al., 2004).

In order to begin with the creation of transgenic mice expressing one of the new indicator constructs, a suitable promoter cassette had to be chosen. A promoter driving cytosolic expression mainly confined to neurons, preferably in a mosaic manner, seemed desirable. The construct of choice was therefore the Thy-1.2 expression cassette, which was first described by Caroni (Caroni, 1997), and later put to use successfully with fluorescent proteins by Feng and coworkers (Feng et al., 2000). According to Caroni, the Thy-1.2 expression cassette drives constitutive postnatal transgene expression in neurons, either in a generalized manner or in mosaic patterns, depending on the insertion site in the founder line. This agrees with the findings of Feng and coworkers who report a remarkable variability in the heritable patterns of expression among mice generated from the same construct, indicating the differences in integration site and/or copy number.

The indicator construct chosen for the creation of transgenic animals was the TN-L15 construct as it was the best characterized one of the group and displayed good functionality under conditions in which many other indicator proteins had previously failed. In the cloning procedure, the DNA sequence of the construct was equipped with an XhoI site at both ends to make it fit into the XhoI insertion site of the Thy-1.2 expression cassette plasmid as described by P. Caroni (Caroni, 1997). The expression cassette still contains untranslated 5'- and 3'-regions of the original Thy1.2 gene including untranslated exons together with their adjacent intron regions. This is an important feature because transgene constructs in mammals have been shown to express more efficiently when they contain 5' intron sequences that undergo a later RNA processing (Makrides, 1999). The TN-L15 sequence was inserted into the Thy-1.2 expression cassette plasmid, the promoter-transgene region linearized by enzyme restriction, and the resulting fragment used for oocyte injections in mice.

In addition to the original TN-L15 construct that I had used in the previous cell culture studies, I created a second TN-L15 variant in which the chromophores CFP and Citrine were exchanged for versions with improved spectral properties. The CFP donor was replaced by the Cerulean variant of CFP that has been reported to have a higher quantum yield and extinction coefficient than ordinary CFP and is said to appear brighter in tissue (Rizzo et al., 2004). The mutation S175G was added to the Citrine sequence in an attempt to enhance folding efficiency. The resulting "improved" construct named CER-L15 was again cloned into the Thy-1.2 expression cassette plasmid and used like its predecessor TN-L15 for a second round of mouse oocyte injections.



Figure 25: Schematic drawing of the Thy-1.2-TN-L15 expression cassette. Ia, Ib, II, IV are untranslated exon regions aiding in the efficiency of transgene expression. Modified from Caroni 1997.

5.3.2 Expression Patterns and Expression Levels

Founder animals carrying a transgene insertion were detected by tail tissue PCR using primer pairs sensitive for a region within the CFP and Citrine genes (see Materials and Methods section). A first round of DNA injections was performed with roughly 150 oocytes using the Thy1.2-TN-L15 DNA construct. Here, a total of 37 pups were born alive, and 5 individual animals out of this group could be identified as transgene positive by PCR. Likewise, 16 animals out of a pool of 196 pups from the later Thy1.2-CER-L15 oocyte injections gave a positive PCR signal. All of these founder animals were bred with wildtype mice, and fluorescence expression patterns and expression strength of animals of F1 and the following generations were analysed by examination of PFA-fixed brain slices as well as living, acute slices.

As it turned out, most of the early Thy1.2-TN-L15 lines displayed just a rather weak, global fluorescence expression distributed throughout the brain that could in most cases only be verified as GFP-derived by antibody staining techniques. One exception was a line named Thy1.2-TN-L15-B in which fluorescently labeled cell bodies could be reliably observed without further signal enhancements in PFA-stained and organotypic slices, even though the signal strength in this line was again far from ideal. Expression levels in TN-L15 homozygous animals were not significantly higher than in heterozygous animals.

Figure 26 shows fluorescence expression patterns of an heterozygous adult animal of the Thy1.2-TN-L15-B line in a PFA-fixed, anti-GFP stained, sagittal section of the brain lacking the cerebellum. Indicator expression was distributed over various regions of the brain including layers 4/5 of the cortex, the CA1 and CA3 regions of the hippocampus, and various thalamic nuclei.

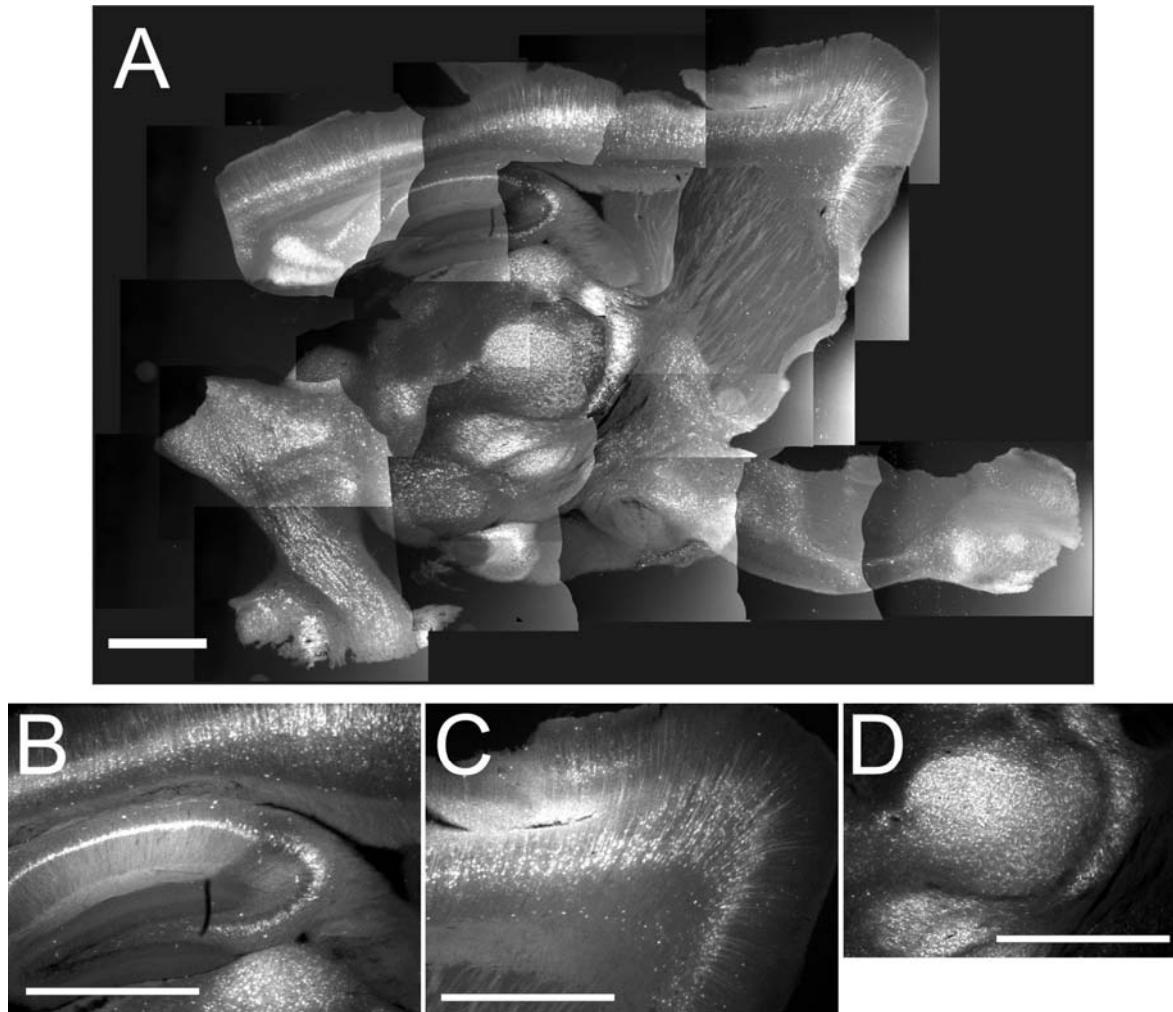


Figure 26: Expression patterns of Thy1.2-TN-L15 in mouse line B. Anti-GFP antibody stainings from an adult mouse (6 weeks). A, Sagittal image series of a the whole brain minus the cerebellum. B-D, Details from A showing expression patterns in the hippocampal CA1 and CA3 regions (B), cerebral cortex layers 4/5 (C), and thalamus (D). Scale bars: 1 mm.

In Figure 27, fluorescence patterns are visible in acute slices from the same mouse line Thy1.2-TN-L15-B. Brains from young, homozygous animals (P5 - P10) were cut into 200 μm thick slices which were kept in ACSF during image acquisition. The slices were illuminated at 515 nm to excite fluorescence of YFP, and exposure times varied between 2 and 10 seconds. Figure 27A shows a sagittal section of a cerebral hemisphere with expression patterns identical to the antibody staining in Figure 26. Figure 27 panels B through D show the expression in line Thy1.2-TN-L15-B in additional brain regions such as motor nuclei and the ventral respiratory group of the brain stem (Figure 27B), Purkinje cells of the cerebellar cortex and cells in the deep cerebellar nuclei (Figure 27C), and layers of mitral and tufted cells in the olfactory bulb (Figure 27D). Panels E and F of Figure 27 display enlarged views of neurons from the cerebral and cerebellar cortex of a

young Thy1.2-TN-L15-B mouse. The neuronal cell bodies are fluorescently labelled with the nuclei excluded, and no immediate evidence of any aggregation of the indicator protein is visible. However, dendritic and axonal processes are only faintly discernible in these preparations, suggesting that this mouse line might not be suitable for certain studies of these structures.

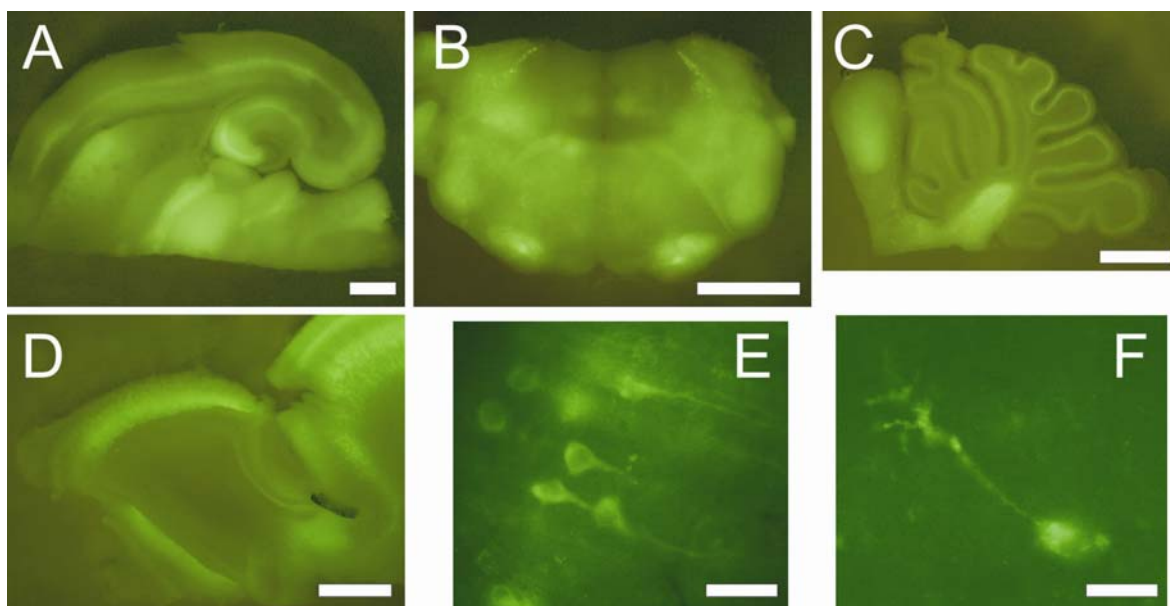


Figure 27: Fluorescence images of acute brain slices of mouse line Thy1.2-TN-L15-B. A, Horizontal section of a P10 TN-L15-B mouse showing widespread expression of the TN-L15 indicator protein. Excitation was at 515 nm, emission at 535 nm, exposure times varied between 2 and 10 s, slice thickness 200 - 230 μm . B, Brain stem section of the same mouse. C, Sagittal section of the cerebellum. D, Sagittal section of the olfactory bulb together with adjacent cortex areas. E, F, 40x magnification of single neurons expressing TN-L15 in the cerebral cortex (E) and cerebellar cortex (F). Scale bars: A-D: 1 mm; E, F: 10 μm .

The mouse lines derived from injections with the Thy1.2-CER-L15 transgene construct showed in most cases a typical Thy1.2-promotor transgene expression distribution similar to Line B of the Thy1.2-TN-L15 lines. General expression strength of the CER-L15 transgene tended to be a little higher, though, which might be due to higher DNA concentrations used in some of the mouse oocyte injections. Highest expression levels could be detected in a line called Thy1.2-CER-L15-C which gave clear and bright fluorescence signals even in unstained, PFA-fixed 50 μm thick brain slices, as can be seen in Figure 28. The expression patterns here resemble the previous mouse line Thy1.2-TN-L15-B with respect to cortical and hippocampal distribution. Similar to Line B, cortex layers 4/5 show a strong labeling as do hippocampal regions CA1 and CA3 (Figure 28A). In addition however, Line C also seems to express indicator protein in cortical layers 2/3

and the dentate gyrus of the hippocampus (Figure 28B and C). Very little expression could be detected in the cerebellar cortex and the olfactory bulb, and no separate motor nuclei were discernible in the brain stem (Figure 28A, Figure 29C and D).

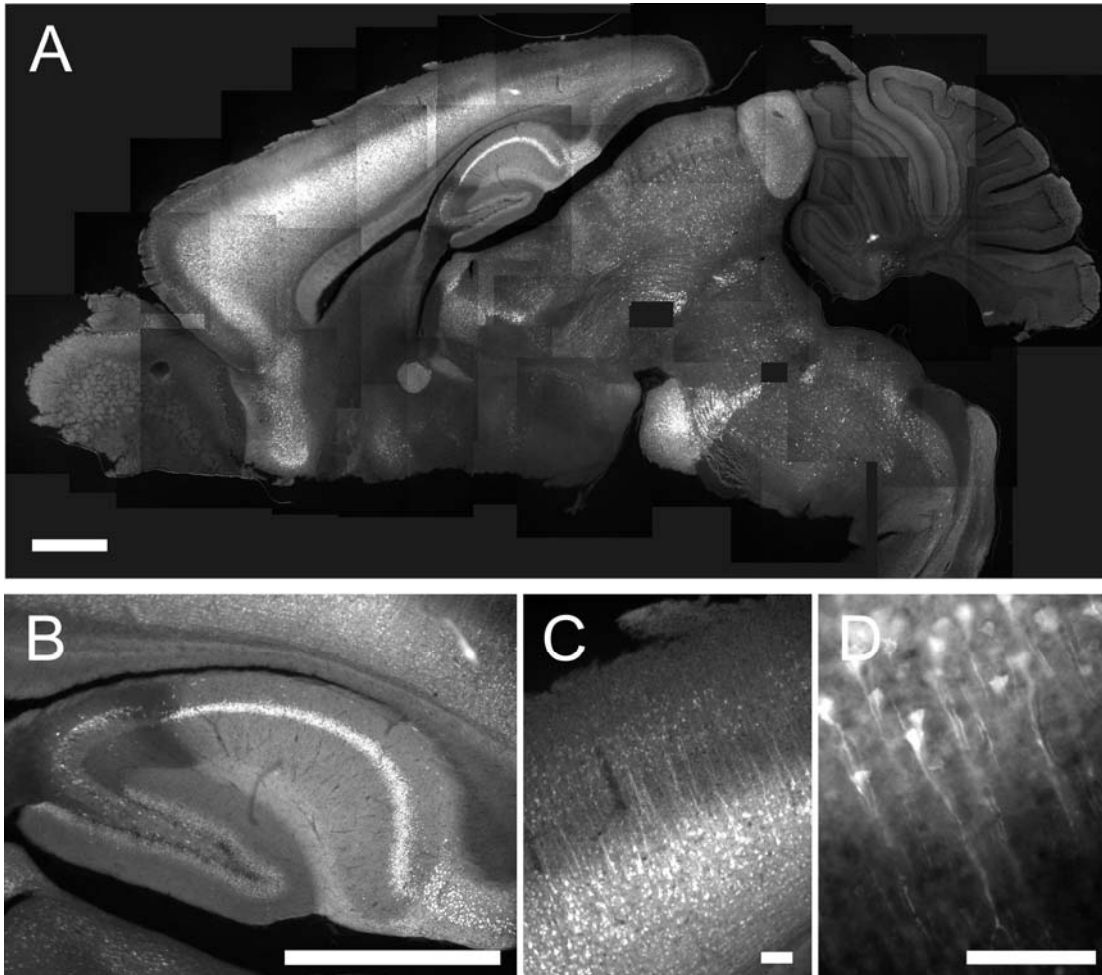


Figure 28: Expression patterns of mouse line Thy1.2-CER-L15-C. Unstained 50 μm sagittal sections from an adult mouse (8 weeks). A, Stitched image series of the whole brain. B-D, Details from A showing expression patterns in the hippocampal CA1, CA3 and DG regions (B), and cerebral cortex layers 2/3 and 4/5 (C and enlargement in D). Scale bars: A, B: 1 mm; C, D: 100 μm .

Acute 200 μm brain slices of the same mouse line Thy1.2-CER-L15-C can be seen in Figure 29. Since expression in mouse Line C was so much brighter than in the old Line B, exposure times for these images could be kept between 300 and 900 ms as opposed to the much longer exposure times that had to be used for Line B slices in Figure 27.

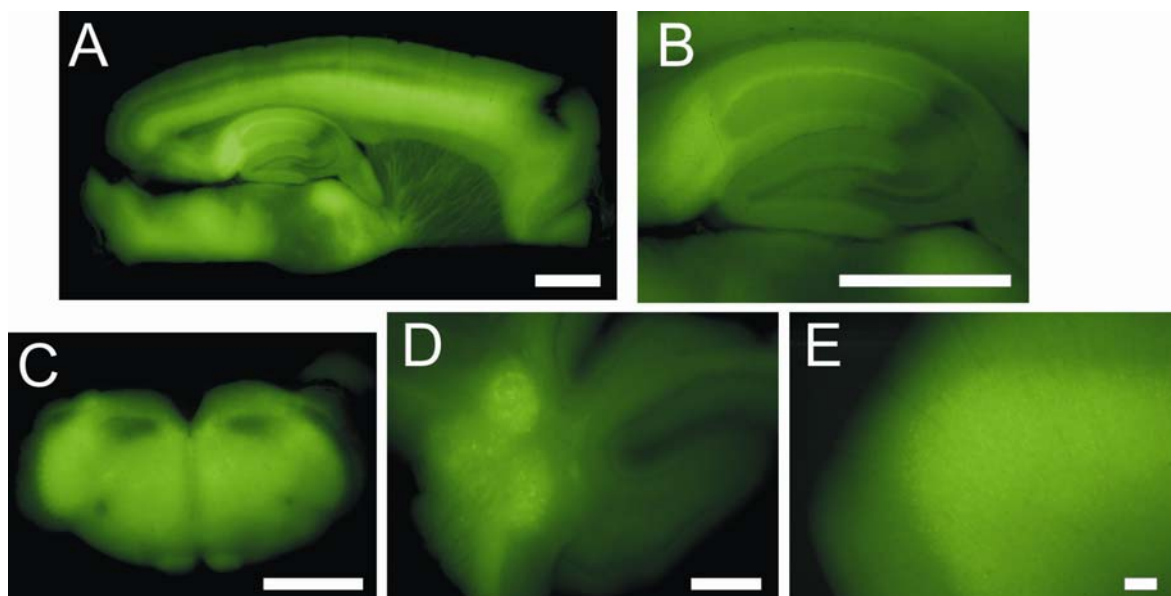


Figure 29: Fluorescence images of acute brain slices of mouse line Thy1.2-CER-L15-C. Excitation was at 515 nm, emission at 535 nm; exposure times varied between 300 and 900 ms. A, 400 μm sagittal section of a 8-week old CER-L15 Line C mouse showing widespread indicator distribution. B, Hippocampus of the same mouse. C, 200 μm section of the brainstem. D, Sagittal section of the cerebellum showing expression in the deep cerebellar nuclei. E, magnification of the cerebral cortex. Scale bars: A - D: 1 mm; E: 100 μm .

Another interesting question was whether expression levels of the fluorescent proteins would stay the same or go down with increasing age of the transgenic animals. To answer this, a western blot analysis of brain tissue was made in which cortical tissue of Thy1.2-TN-L15-B mouse brains at different ages was homogenized, separated on an acrylamide gel, and subjected to anti-GFP and anti- β -actin control antibody stainings. The resulting anti-GFP-staining in Figure 30 showed that the indicator expression levels seen in the bands at a molecular weight of 69 kD seemed to rise during the first two weeks after birth and remained constant during the following time, up to an age of almost a year. No protein bands of lower molecular weight indicating degradation products of the indicator construct could be detected by antibody stainings.

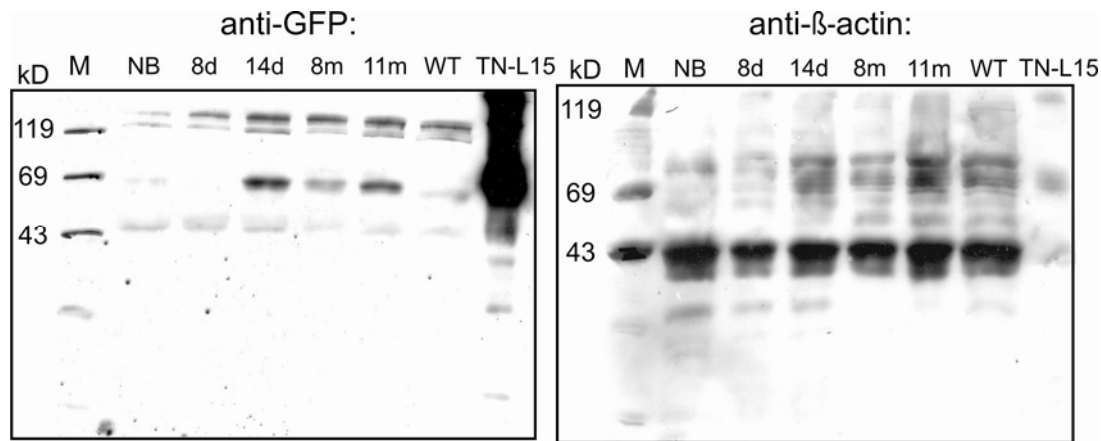


Figure 30: Western blots of Thy1.2-TN-L15-B mouse brains at different ages. Right side: anti-GFP staining showing the indicator band at roughly 69 kD; left side: anti- β -actin control staining depicting the protein load of each lane. M, molecular weight marker. NB, new born animal. 8d, 14d, 8-day and 14-day-old animals. 8m, 11m, 8 and 11-month old animals. WT, wild type control. TN-L15, raw preparation of indicator protein. Thanks to M. Friedrich for the help with this blot.

5.3.3 Imaging of Live Brain Tissue

The functionality of the indicator in live brain tissue was first tested in organotypic slice cultures prepared from young mice 3-5 days after birth. Slices were made after the protocol published by Stoppini and coworkers (Stoppini et al., 1991), then grown on a membrane for up to a week and used in fluorescence imaging experiments conducted on the standard fluorescence setup. One disadvantage here was the fact that since the setup possessed only an inverse microscope, the slices had to be laid upside down into the dish in order to allow direct fluorescence imaging. This way, the diffusion of pharmacological agents was probably delayed during experiments since before reaching visible sites of action, they had first to cross the membrane on which the slices were cultured. During imaging, slices were kept in HBSS and held in place at the bottom of the dish with the help of a platinum ring. Calcium responses were evoked by depolarizing the neurons with potassium; for this purpose, the KCl concentration of the HBSS solution was raised from 5 mM to 50 mM while images were taken at an interval of 5 s.

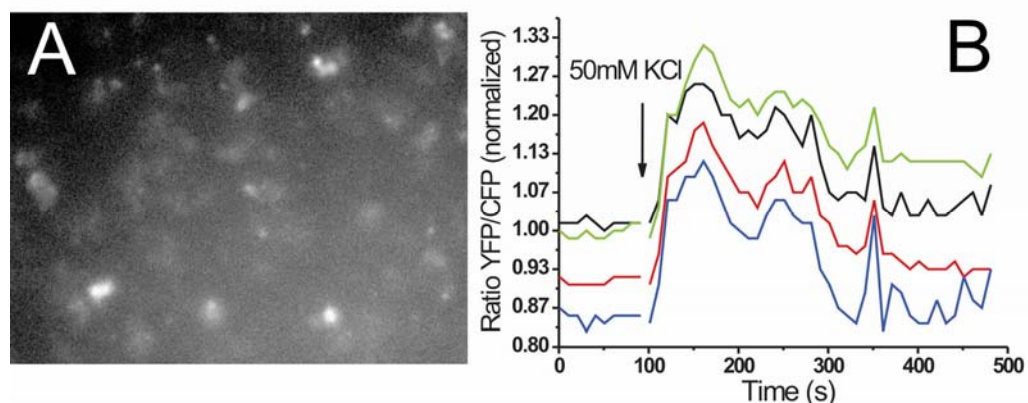


Figure 31: Calcium imaging trials in organotypic slice cultures. Slices were prepared from hippocampi of TN-L15-B-mice at age P4 and imaged after 2 weeks in culture. A, 535 nm fluorescence emission of a hippocampal slice preparation; cells are 40x magnified and excited at 432 nm. B, YFP/CFP ratio traces presumably reflecting the influx of calcium into the cells after the addition of 50 mM KCl to the slice preparation shown in A. A YFP/CFP ratio change of about 20% is visible after stimulation.

As can be seen in Figure 31, the image quality of labeled cells in a hippocampal slice after one week in culture was rather poor. Nonetheless, fluorescent dots were visible which presumably constituted cell bodies. After stimulation with 50 mM potassium chloride, I observed small but reproducible increases in YFP/CFP ratios of up to 20% and were assumed to originate from indicator protein signals. However, due to the unsatisfactory image quality no clear statements could be made as to whether the indicator was really functional in live brain slices. Therefore, more sophisticated imaging experiments using electrophysiology techniques in acute slices were necessary to substantiate these findings, some of which are mentioned in the following discussion section.

6. DISCUSSION

In this work, I developed novel types of ratiometric calcium indicators based on fluorescent proteins, and characterized them for their functionality in calcium imaging experiments *in vitro*, in cell culture and in live tissue.

6.1 *New Ratiometric Calcium Indicator Probes and Their Physical Properties*

6.1.1 **Generating New Functional Constructs**

Previously created calcium sensing probes use the protein calmodulin as a calcium binding linker, a protein that is considered problematic in live cell applications due to its importance in cell regulation processes. Such a highly regulated cytosolic protein has a strong probability of either interfering with cellular activities or being regulated itself. Therefore, the objective of the first part of this work was to incorporate into a FRET indicator a more specialized calcium binding protein that is not a natural cytosolic component. The choice fell on different forms of the muscle protein troponin C as this protein family has no other known function than regulating muscle contraction and thus could be expected to be minimally interfering with cellular biochemistry in non-muscle cells. After many optimization trials, combinations of troponin C variants could be established that displayed promising physical properties *in vitro* when fused between the two most widely used fluorophores CFP and YFP. Some of the best performing constructs were chosen for further analysis; these were the chicken skeletal muscle TnC probe called TN-L15, the human cardiac muscle TnC probe TN-humTnC, and the *Drosophila* troponin C isoform 1 probe TN-TPC1-L5. The calcium binding linker moiety in all of these three constructs consists of a single troponin C domain without any additional binding peptides like the calmodulin binding peptide M13 from myosin light chain kinase that is present in cameleons and other non-ratiometric indicators. This was considered fortuitous because any additional binding peptide has the potential to be interfered with when expressed in live cells.

When tested in zero and high calcium conditions, the three best troponin C constructs responded to high calcium with emission ratio changes in the range of 120 - 160%. However, when TN-L15 and TN-humTnC were subjected to more physiological

conditions such as the presence of 1 mM magnesium, it became evident that the troponin C calcium binding sites also competitively bound Mg^{2+} . This made the maximum ratio changes of TN-L15 and TN-humTnC drop to 100% and 70%, respectively, an effect that was also apparent in later cell culture experiments. Previous publications had already noted a sensitivity of the EF-hands of calmodulin and troponin C isoforms to magnesium along with calcium (Tikunova et al., 2001), (Davis et al., 2002). They found that by mutating certain amino acid residues involved in calcium complexing, the EF-hand sensitivity of calmodulin and troponin C to Mg^{2+} could be lowered. Such mutations offer the possibility to improve calcium specificity, and first trials in that direction have already been successfully undertaken (Mank M. et al., manuscript in preparation). Nonetheless, even under magnesium-free conditions, maximum ratios of the new indicators never exceeded a 150% ratio change. This is much lower than the best Cameleon type indicator (YC 3.60), that is reported to have *in vitro* ratio changes of up to 560% (Nagai et al., 2004).

There is, however, a general caveat against the current practice of evaluating the performance of a ratiometric indicator construct by ratio change values the way they are calculated in the literature (M. Mank, personal communication). Figure 32 exemplifies the correlation between changes in emission intensity values F_{max} and the resulting ratio change $\Delta R/R$ received through Equation 1. The y-axis of Figure 32A shows the differences in fluorescence emission values ($F_0 \pm \Delta F_{max}$) that a FRET donor like CFP and an acceptor like YFP need to decrease or increase from a starting point F_0 in order to obtain the ratio change values $\Delta R/R$ displayed on the x-axis. Assuming that the acceptor/donor ratio R_0 at point F_0 equals 1 in this example, $\Delta R/R$ can be transformed into:

$$\frac{\Delta R}{R} = \frac{F_0 + \Delta F_{max}}{F_0 - \Delta F_{max}} - 1 = \frac{2 \cdot \Delta F_{max}}{F_0 - \Delta F_{max}};$$

Consequently, as ΔF_{max} approaches F_0 , small variations in absolute emission intensities lead to overly large variations in ratio change $\Delta R/R$, which is demonstrated in Figure 32B. It appears that only for low values of ΔF_{max} do changes in the emission intensities result in near-linear rises in ratio change. Hence, a construct that has a reported ratio change of 560 % like the new Yellow Cameleon 3.60 indicator (Nagai et al., 2004) is actually only slightly more efficient than a construct reporting, for example, a 400 % ratio change like the one established by Mank and coworkers (Mank M. et al., manuscript in preparation). This discrepancy could also explain why ratiometric indicators with reported high *in vitro* ratio changes like YC 3.60 never reach the same high values in live cells, for

small signal attenuations in such a complex environment could lead to a supralinear decrease in ratio change.

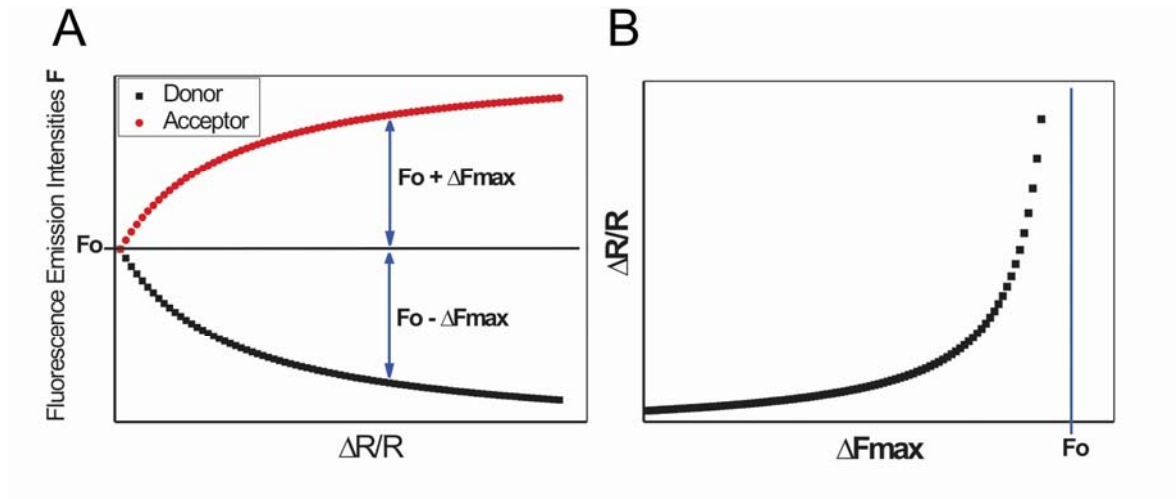


Figure 32: Correlation of donor and acceptor emission intensities F_{max} and ratio change $\Delta R/R$. A: Black squares show donor emission intensity values, red dots acceptor emission intensity values starting from a "zero calcium" value F_0 . B: Due to the nonlinearity of emission intensity curves, growing differences in emission intensities ΔF_{max} lead to increasingly large ratio changes and thus a "noisier" signal. Drawing courtesy of M. Mank.

Apart from the standard FRET pair combination CFP and YFP, I examined other fluorescent proteins in this work for their functionality in ratiometric calcium indicators. Most of them originate from other marine organisms than *Aequoria victoria*. The same troponin C domains that worked well as calcium binding inserts together with combinations of the fluorophores CFP and YFP were now inserted into the FRET pair combinations Sapphire/DsRed-T4, cpSapphire/DsRed-T4, T-Sapphire/mDsRed, and Cop-Green/Phi-Yellow. As it turned out, none of the tested troponin C domains gave satisfactory results with the new fluorophore pairs. This is unfortunate since the new FRET pairs were expected to suffer less from some of the drawbacks associated with CFP and YFP. A red shifted indicator containing a combination like Sapphire/DsRed could be more useful for imaging experiments in live tissue since it suffers less from the background autofluorescence that is commonly very high in the emission range of CFP and YFP. On the other hand, preliminary tests conducted with the new indicator construct CFP-L15-Phi indicated that a probe containing a substitute for YFP such as Phi-Yellow might suffer less from bleaching effects than the YFP variants, which would make them more robust acceptor proteins in long lasting imaging experiments.

Another approach to create new calcium binding insert types was undertaken by excising single EF-hand domains out of the full length troponin C protein and using these as calcium binding linkers. If the theories are correct that hold interactions of cell components with the calcium binding linker protein responsible for the known decrease in indicator performance, then cutting down the linker moiety to a minimum length might help solve that problem. Therefore, single EF-hands representing the smallest calcium binding unit of troponin C were generated in different lengths and alignments, and tested for their functionality. Unfortunately, none of these truncated calcium binding peptides resulted in a functional indicator protein, and neither did fusing two or three of them in a row. This indicates that maybe disrupting the natural order of EF-hand loop alignments together with their adjacent α -helical domains destroys their concerted action and range of conformational movement.

In conclusion, it is safe to say that the current rational approach of finding functional indicator constructs through selective cloning of each single DNA sequence constitutes a rather tedious and time-consuming process. A more random method using high throughput techniques would be desirable if one really wanted to exploit the manifold possibilities of combinations that a set of linker proteins like the troponin C family offer.

6.1.2 *In Vitro* Characterization of Selected Constructs

Another physical property that is important for judging the quality of a calcium probe is its K_d value for the ligand, in this case for calcium. A probe is considered to work efficient only in a concentration range of 0.1-10 times its K_d value (Molecular Probes, 2004). Since the present calcium indicators are meant to be used for reporting the calcium concentration inside cells, a K_d range from a few 100 nm to over 1 μ M calcium is necessary. Most of our probes displayed effective K_d values that would allow their use in physiological conditions, with the exception of the two constructs TN-L15 D107A and TN-TPC1-L5 whose K_d of $\sim 30 \mu$ M is too high for cytosolic applications. On the other hand, these two might be used in targeting experiments to the cell membrane and other places where the Ca^{2+} concentration is supposed to be higher.

It is important to keep in mind though that dissociation constants determined *in vitro* do not necessarily correspond faithfully to their values *in situ*, possibly because of the different biochemical environment in the cell cytoplasm. Studies comparing the K_d values of synthetic calcium indicator dyes *in vitro* and in cultured cells have reported that these

two sometimes differ considerably, and that values of K_d determined *in situ* within cells can be up to fivefold higher than values determined *in vitro* (Molecular Probes, 2004). This agrees with another study that looked more critically at the performance of genetically encoded indicators in live cells and also found that dissociation constants derived from *in vitro* fluorescence measurements should be treated with caution due to the discrepancies between measured and reported calcium K_d values (Pologruto et al., 2004). Nevertheless, one can assume that qualitative assessments can be made with *in vitro* K_d values indicating whether the use of an indicator in physiological applications appears possible. The values obtained from our probes seemed to allow their use in *in situ* experiments, which later proved correct.

Another important physical parameter of a calcium probe that should be looked into is its kinetic behavior since fast imaging will only be possible when binding and release of the ligand occur fast enough. The inverse k_{off} -rates measured *in vitro* with our indicators varied between 450 and 860 ms. The fastest off-rates were obtained from the two constructs TN-L15 D107A and TN-TPC1-L5, these two also have the highest K_d values for calcium. By using the relation of K_d to on- and off-rates that is given by $K_d = \frac{k_{\text{off}}}{k_{\text{on}}}$, on-rates k_{on} of the constructs could be approximated and appeared to be in the range of $1\text{-}3 \times 10^6 \text{ M}^{-1} \text{ s}^{-1}$ for our low- K_d constructs and $60.000\text{ - }90.000 \text{ M}^{-1} \text{ s}^{-1}$ for our high- K_d constructs. We refrained from confirming these association rates by experiments since knowledge of the exact ligand and indicator concentration is necessary for the determination of k_{on} ; these values are difficult to establish in *in vitro* assays and even more so in *in vivo* applications. Generally, the rather slow on- and off-rates seen here and in other protein probes like Cameleons (Miyawaki et al., 1997) are one major drawback that all ratiometric FRET indicators so far seem to suffer from. In contrast, the single GFP indicator GCaMP was reported to have faster off-rates of 200 ms (Nakai et al., 2001); however, this is also no match for most synthetic dyes and their off-rates of only a few milliseconds. Again, though, one should keep in mind that the *in vitro* values presented here need not necessarily correspond to the values *in situ* in living cells, where additional effects such as endogenous calcium buffers and differences in indicator concentration could influence the kinetic behavior of calcium-binding probes.

6.2 Tests in Live Cells

6.2.1 Cell Culture Experiments

From the *in vitro* data of a new indicator construct, only preliminary predictions can be made about the functionality of the probe under physiological conditions. Only *in situ* tests in cell culture and living animals will really divulge the true qualities of any construct for live imagings. First cytosolic expression studies with the new indicator constructs TN-L15 and TN-humTnC in cultured HEK293 cells and dissociated neurons showed that the probes were evenly distributed within the cytosol of the cells with no signs of aggregation. Such an expression pattern could not be taken for granted since the troponin C protein used as calcium binding linker in these constructs normally exists only as a bound form integrated into the muscle troponin complex. The fact that it could also be expressed as an isolated protein within the cytosol was therefore important. After stimulations that lead to a rise in intracellular calcium concentrations, the cytosolically expressed indicators gave reproducible signals, the amounts of which corresponded to the ratio change range obtained in *in vitro* experiments. In neuronal cell cultures, TN-L15 even managed to record spontaneous activities over a long period of time.

The next step involving cell culture experiments was to test the new constructs for their usefulness in protein targeting studies. Genetically encoded indicators have the great advantage that they can be targeted to sites of interest with the means of molecular biology, and numerous functional targetings of genetically encoded indicators had been reported before (Miyawaki et al., 1997), (Griesbeck et al., 2001), (Palmer et al., 2004). The indicator TN-L15 was furnished with different protein trafficking sequences that are known to direct and insert a protein into the plasma membrane of a cell. The targeting peptide sequences of GAP43 and c-Ha-Ras as well as protein fusions to the presynaptic protein synaptobrevin led to a successful membrane targeting in HEK293 cells, and the fusion construct TN-L15-Ras was also functional in cultures of dissociated neurons. Because TN-L15-Ras with its high affinity for calcium became instantly saturated after stimulus applications, the analogous low calcium affinity version TN-L15 D107A-Ras had to be used to study calcium dynamics at the cell membrane. Stimulations of TN-L15 D107A-Ras with glutamate or high potassium concentrations gave reproducible average ratio changes of about 19 % (n = 34). However, since the same ratio change value was also measured with the cytosolically expressed form of the indicator molecule,

attempts to use this data to calculate calcium concentrations by means of the Hill equation in the way some previous publications did (Miyawaki et al., 1999), (Yu and Hinkle, 2000), (Pologruto et al., 2004) seemed fruitless. Reasons for this might be that the calcium dissociation constant for TN-L15 D107A-Ras of 29 μM was only determined through *in vitro* measurements and that it assumes a different value in the different biochemical milieu of the cell. This effect could occur even stronger close to the plasma membrane where protein movement and ion diffusion rates are often impeded sterically and kinetically. As argued in the preceding paragraph, this finding seems congruent with the recent report by Pologruto and coworkers (Pologruto et al., 2004) who investigated the function of a variety of GFP-based calcium indicators in cultured hippocampal brain slices. Their studies found marked nonlinearities in calcium ion/indicator binding curves as well as discrepancies between *in vitro* and *in vivo* Kd values, which in their opinion make genetically encoded indicators problematic to use for quantitative Ca^{2+} imaging. In contrast to that, a recent study by Reiff et al. that compared fluorescence responses of various ratiometric and non-ratiometric indicators expressed in *Drosophila* larval neuromuscular junctions found a linear increase of indicator responses to rising electrical stimulus frequencies at non-saturating levels of calcium concentration (Reiff et al., 2005).

In our case it was possible to at least draw a qualitative conclusion from indicator signals that were simultaneously derived from the plasma membrane and the cytosol. When primary neurons were co-transfected with membrane-targeted TN-L15-Ras and nucleus-targeted YC2.3, no elevated calcium concentrations could be found at the plasma membrane when compared to bulk cytosolic transients. Such long lasting submembrane calcium domains that reached peak values as high as 100 μM had been found in the rat smooth muscle-derived cell line A7r5 (Marsault et al., 1997), and submembrane calcium levels appeared to be elevated in these cells even under resting conditions. On the time scale of our experiments, average cytosolic calcium transients were not significantly lower than submembrane domains, suggesting that no permanent gradient in calcium concentration from the membrane towards the cytosol is maintained in the neurons under these conditions. It will be interesting to further address these questions with improved temporal resolution.

Summarizing the experiments in which indicators were targeted to subcellular sites it can be said that in all cases tested so far, the new probe TN-L15 retained its activity while the corresponding targeted calmodulin-based probes were significantly modified in

their dynamic range. Little is known as to why the calcium sensitivity of the calmodulin moiety is restricted in many targetings. Possible reasons might be the occurrence of post-translational modifications such as phosphorylation on the pathway to membrane insertion, or interactions with calmodulin-binding proteins of distinct localization patterns within cells, or simply endogenous calmodulin binding which may be present at unusually high concentrations under the membrane and especially in the vicinity of channels and specialized areas such as synapses. The new troponin C-based indicators promise to have a higher success rate in obtaining certain functional targetings, though it remains to be seen whether these results can be reproduced *in situ* in complex environments like active zones of synapses and in transgenic animals.

6.2.2 TN-L15 in Transgenic Animals

Transgenic animals expressing genetically encoded calcium indicators are desired for many reasons. Imaging studies until now have almost always had to rely on synthetic calcium dyes, mostly AM ester derivatives based on the calcium buffer BAPTA, like the Fura and Fluo dye series. Loading mammalian brain slices with AM esters poses certain problems concerning the efficiency and site of indicator loading, and it becomes increasingly difficult in animals over a certain age (Yuste, 2000). In contrast, the vast variety of gene promoter constructs available nowadays allows the expression of transgenes in very specialized cell types, and fusions of probes to protein trafficking signals even make specific subcellular localizations possible.

Many of the genetically encoded calcium indicators on the market have been used for expression studies in transgenic mice, but only a few of them showed responses that could be used for any functional imaging (Ji et al., 2004), (Hasan et al., 2004), (Nagai et al., 2004), (Hara et al., 2004). In all cases examined so far, the dynamic range of transgenically expressed indicators decreased drastically in comparison to *in vitro* and cell culture data. The reasons for this loss of function are not known, and there have been numerous speculations about its cause. Some attribute it to genetic occurrences like gene silencing or a formation of protein precipitates in inclusion bodies (Hasan et al., 2004). Many theories blame the calmodulin unit that is used in most constructs and might interact with regulatory mechanisms of the cell which normally manage the signalling function of calmodulin. If the latter is correct, then one could assume that the new troponin C containing constructs ought to work better in transgenic applications, since TnC is not a

natural component of neurons and therefore not as regulated. Recent data from imaging experiments in the neuromuscular junction of *Drosophila* flies, however, did not substantiate these postulations (Reiff et al., 2005). This comparative study of a number of genetically encoded indicators showed that TN-L15 performed just as well as calmodulin-based variants when compared in electrophysiological stimulations at the fly neuromuscular junction (Figure 33). The dynamic range of all tested ratiometric probes decreased when compared to the *in vitro* ratio change level, down to 8-12 % depending on the experimental parameters.

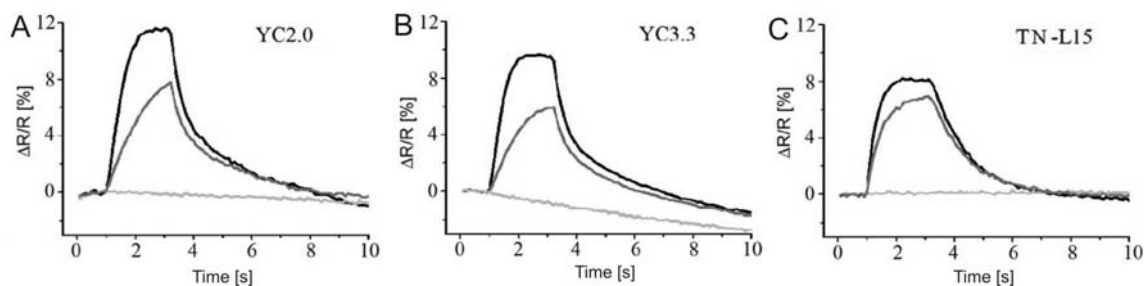


Figure 33: Comparing the performance of three ratiometric calcium indicators at *drosophila* larval neuromuscular junction presynaptic boutons using different stimulus intensities. A, Yellow Cameleon 2.0; B, Yellow Cameleon 3.3; C, TN-L15. Boutons were stimulated at 80 Hz (black), 40 Hz (grey), and 0 Hz (light grey). Modified from Reiff et al. (2005)

Better signal quality seems to be achievable though with confocal imaging techniques like two-photon imaging which allows optical sectioning, thereby greatly reducing background signals. Here, ratio changes of up to 40 % were obtained in fly neuromuscular junction electrode stimulations (T. Hendel, unpublished results), a value already approaching the maximum one could expect under these experimental circumstances based on the influences of rather high indicator K_d values and the *in-vivo* calcium concentration range.

For the creation of transgenic mice expressing one of the new troponin indicator constructs, the expression cassette Thy-1.2 published by Caroni and coworkers was chosen as transgene promoter (Caroni, 1997). This gene construct promised transgene expression in neurons of the CNS in either a general or, more preferable, a mosaic pattern. The animals that were obtained in this work after oocyte injections with Thy-1.2-TN-L15 displayed general expression patterns indeed, labelling whole sections of the brain with densely colored cell bodies. Expression was strongest in the bodies of labelled cells and faded out in the cell protrusions, allowing imaging experiments only on cell bodies. Preliminary tests of the functionality of the indicator in live brain slices were conducted by

preparing organotypic brain slices and stimulating them with 50 mM KCl on a standard FRET setup. Even though the image quality was not ideal, a response of 10-20 % ratio change could be reproducibly detected, hinting towards a functional calcium indicator. Further electrophysiological tests of the indicator response properties in transgenic animals are currently in progress by means of patch clamping in acute brain slices (M. Parkis, unpublished results). First data from electrical stimulations of whole-cell patched neurons indicate a promising responsiveness of TN-L15 in neocortical brain slices. In the experiment shown in Figure 34, current injections into a patched neocortical layer 5 neuron from a mouse expressing TN-L15 led to fluorescence responses of the indicator protein amounting to up to 8 % ratio change after background subtraction and correction for bleach decline of the ratio (Figure 34A). Even higher responses of up to 25% were seen during spontaneous trains of action potentials. This compares very favorably to published results using cameleon-based indicators in CCD-camera imaging experiments. Generally, it can be expected that even better responses would be measured using a confocal imaging technique.

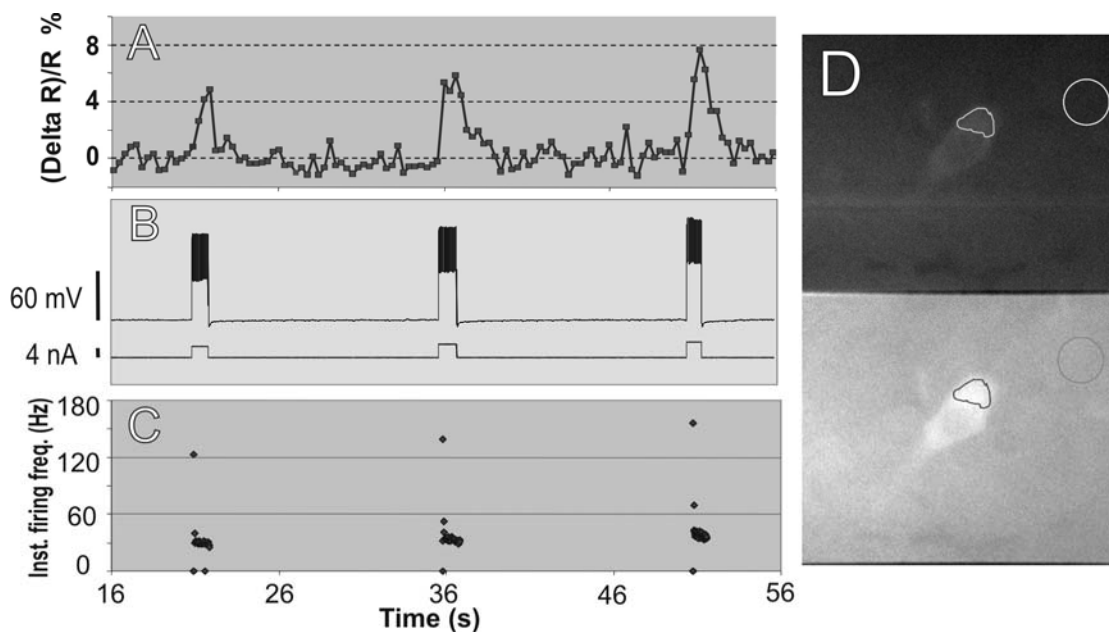


Figure 34: Indicator responses to calcium influx in patched neurons of neocortical layer 5 in acute brain slices of mouse line Thy1.2-TN-L15-B. A, Ratio changes of indicator response to rises in calcium after stimulation shown in B. B, Current injections into the cell and resulting trains of action potentials. C, Firing frequency of the action potentials shown in B. D, Picture of the cortical neuron used in this experiment; regions of interest were drawn on the cell body in both the YFP and the CFP channel from which ratio changes could be calculated. Circles depict areas used for the background subtraction of the signal. Pictures courtesy of M. Parkis.

Since expression strength of the indicator proteins in the TN-L15 lines was weaker than desired, new mouse lines were produced with the enhanced indicator variant CER-L15. Fluorescence expression level analysis of a number of new mouse lines expressing CER-L15 showed distinctively brighter fluorescence patterns when compared to previous TN-L15 mouse lines. This raises hopes that image quality in future experiments using acute brain slices will improve, and that even *in vivo* imaging in the brains of living animals will become possible with the new mouse lines.

6.3 Further Outlook

Even though some promising results could be achieved with the new troponin C-based calcium indicators presented here, there still remains the need for stronger and more stable signals especially *in vivo*. One way of improving indicator performance could be to further engineer the TnC linker proteins toward less magnesium sensitivity, lower calcium dissociation constants, and faster kinetic properties. Another approach to enhance indicator properties could be the exchange of present fluorophores by new fluorescent proteins with better spectral and physical properties. A systematic screening method allowing to speed up the cloning and testing process of new linker domain and fluorophore combinations would be extremely helpful for that purpose.

Besides the established applications in live cell imaging and transgenic animals, fluorescent indicators containing troponin C could also prove useful in the field of pharmaceutical screening tests. Human cardiac troponin C is a well-known drug target for calcium sensitizing agents that modulate the calcium binding behaviour of cardiac TnC and strengthen the contraction of the human heart (Pollesello et al., 1994). A fluorescent indicator containing human troponin C like TN-humTnC may therefore be put to use in simple *in vitro* assays to identify small chemical compounds or polypeptides of clinical interest that act as calcium-sensitizing agents, in particular for certain clinical settings such as congenital heart failure.

7. REFERENCES

- Amsterdam A, Lin S, Hopkins N** (1995) *The Aequorea victoria green fluorescent protein can be used as a reporter in live zebrafish embryos*. Dev Biol **171**: 123-129.
- Baird GS, Zacharias DA, Tsien RY** (1999) *Circular permutation and receptor insertion within green fluorescent proteins*. PNAS **96**: 11241-11246.
- Berchtold MW, Brinkmeier H, Muntener M** (2000) *Calcium ion in skeletal muscle: Its crucial role for muscle function, plasticity, and disease*. Physiol Rev **80**: 1215-1265.
- Berridge MJ, Lipp P, Bootman MD** (2000) *The versatility and universality of calcium signalling*. Nat Rev Mol Cell Biol **1**: 11-21.
- Bozza T, McGann JP, Mombaerts P, Wachowiak M** (2004) *In vivo imaging of neuronal activity by targeted expression of a genetically encoded probe in the mouse*. Neuron **42**: 9-21.
- Campbell RE, Tour O, Palmer AE, Steinbach PA, Baird GS, Zacharias DA, Tsien RY** (2002) *A monomeric red fluorescent protein*. PNAS **99**: 7877-7882.
- Caroni P** (1997) *Overexpression of growth-associated proteins in the neurons of adult transgenic mice*. J Neurosci Methods **71**: 3-9.
- Chalfie M, Tu Y, Euskirchen G, Ward WW, Prasher DC** (1994) *Green fluorescent protein as a marker for gene expression*. Science **263**: 802-805.
- Chesler M, Kaila K** (1992) *Modulation of pH by neuronal activity*. Trends Neurosci **15**: 396-402.
- Cody CW, Prasher DC, Westler WM, Prendergast FG, Ward WW** (1993) *Chemical structure of the hexapeptide chromophore of the Aequorea green-fluorescent protein*. Biochemistry **32**: 1212-1218.
- Cubitt AB, Heim R, Adams SR, Boyd AE, Gross LA, Tsien RY** (1995) *Understanding, improving and using green fluorescent proteins*. Trends Biochem Sci **20**: 448-455.

- Davis JP, Rall JA, Reiser PJ, Smillie LB, Tikunova SB** (2002) *Engineering competitive magnesium binding into the first EF-hand of skeletal troponin C*. *J Biol Chem* **277**: 49716-49726.
- Elferink LA, Trimble WS, Scheller RH** (1989) *Two vesicle-associated membrane protein genes are differentially expressed in the rat central nervous system*. *J Biol Chem* **264**: 11061-11064.
- Erickson MG, Alseikhan BA, Peterson BZ, Yue DT** (2001) *Preassociation of calmodulin with voltage-gated Ca(2+) channels revealed by FRET in single living cells*. *Neuron* **31**: 973-985.
- Farah CS, Reinach FC** (1995) *The troponin complex and regulation of muscle contraction*. *FASEB J* **9**: 755-767.
- Feng G, Mellor RH, Bernstein M, Keller-Peck C, Nguyen QT, Wallace M, Nerbonne JM, Lichtman JW, Sanes JR** (2000) *Imaging neuronal subsets in transgenic mice expressing multiple spectral variants of GFP*. *Neuron* **28**: 41-51.
- Fiala A, Spall T, Diegelmann S, Eisermann B, Sachse S, Devaud JM, Buchner E, Galizia CG** (2002) *Genetically expressed cameleon in Drosophila melanogaster is used to visualize olfactory information in projection neurons*. *Curr Biol* **12**: 1877-1884.
- Gordon AM, Homsher E, Regnier M** (2000) *Regulation of contraction in striated muscle*. *Physiol Rev* **80**: 853-924.
- Griesbeck O, Baird GS, Campbell RE, Zacharias DA, Tsien RY** (2001) *Reducing the environmental sensitivity of yellow fluorescent protein. Mechanism and applications*. *J Biol Chem* **276**: 29188-29194.
- Griesbeck O** (2004) *Fluorescent proteins as sensors for cellular functions*. *Curr Opin Neurobiol* **14**: 636-641.
- Hara M, Bindokas V, Lopez JP, Kaihara K, Landa LR, Jr., Harbeck M, Roe MW** (2004) *Imaging endoplasmic reticulum calcium with a fluorescent biosensor in transgenic mice*. *Am J Physiol Cell Physiol* **287**: C932-C938.

-
- Hasan MT, Friedrich RW, Euler T, Larkum ME, Giese G, Both M, Duebel J, Waters J, Bujard H, Griesbeck O, Tsien RY, Nagai T, Miyawaki A, Denk W (2004)** *Functional fluorescent Ca²⁺ indicator proteins in transgenic mice under TET control.* *PLoS Biol* **2**: 763-775.
- Heim R, Tsien RY (1996)** *Engineering green fluorescent protein for improved brightness, longer wavelengths and fluorescence resonance energy transfer.* *Curr Biol* **6**: 178-182.
- Helmchen F (2000)** Calibration of fluorescent calcium indicators. In: *Imaging Neurons: A Laboratory Manual* (Yuste R, Lanni F, Konnerth A, eds), pp 32.1-32.9. Cold Spring Harbor: CSHL Press.
- Herranz R, Diaz-Castillo C, Nguyen TP, Lovato TL, Cripps RM, Marco R (2004)** *Expression patterns of the whole Troponin C gene repertoire during Drosophila development.* *Gene Expr Patterns* **4**: 183-190.
- Higashijima Si, Masino MA, Mandel G, Fetcho JR (2003)** *Imaging neuronal activity during zebrafish behavior with a genetically encoded calcium indicator.* *J Neurophysiol* **90**: 3986-3997.
- Hirose K, Kadowaki S, Tanabe M, Takeshima H, Iino M (1999)** *Spatiotemporal dynamics of inositol 1,4,5-trisphosphate that underlies complex Ca²⁺ mobilization patterns.* *Science* **284**: 1527-1530.
- Honda A, Adams SR, Sawyer CL, Lev-Ram V, Tsien RY, Dostmann WRG (2001)** *Spatiotemporal dynamics of guanosine 3',5'-cyclic monophosphate revealed by a genetically encoded, fluorescent indicator.* *PNAS* **98**: 2437-2442.
- Houdusse A, Love ML, Dominguez R, Grabarek Z, Cohen C (1997)** *Structures of four Ca²⁺-bound troponin C at 2.0 Angstrom resolution - further insights into the Ca²⁺-switch in the calmodulin superfamily.* *Structure* **5**: 1695-1711.
- Isshiki M, Ying Ys, Fujita T, Anderson RGW (2002)** *A molecular sensor detects signal transduction from caveolae in living cells.* *J Biol Chem* **277**: 43389-43398.

- Itoh RE, Kurokawa K, Ohba Y, Yoshizaki H, Mochizuki N, Matsuda M** (2002) *Activation of Rac and Cdc42 video imaged by fluorescent resonance energy transfer-based single-molecule probes in the membrane of living cells.* Mol Cell Biol **22**: 6582-6591.
- Jain RK, Ranganathan R** (2004) *Local complexity of amino acid interactions in a protein core.* PNAS **101**: 111-116.
- Ji G, Feldman ME, Deng KY, Greene KS, Wilson J, Lee JC, Johnston RC, Rishniw M, Tallini Y, Zhang J, Wier WG, Blaustein MP, Xin HB, Nakai J, Kotlikoff MI** (2004) *Ca²⁺-sensing transgenic mice: postsynaptic signaling in smooth muscle.* J Biol Chem **279**: 21461-21468.
- Johnson JD, Nakkula RJ, Vasulka C, Smillie LB** (1994) *Modulation of Ca²⁺ exchange with the Ca(2+)-specific regulatory sites of troponin C.* J Biol Chem **269**: 8919-8923.
- Jurado LA, Chockalingam PS, Jarrett HW** (1999) *Apocalmodulin.* Physiol Rev **79**: 661-682.
- Kawasaki H, Nakayama S, Kretsinger RH** (1998) *Classification and evolution of EF-hand proteins.* BioMetals **11**: 277-295.
- Kerr R, Lev-Ram V, Baird G, Vincent P, Tsien RY, Schafer WR** (2000) *Optical imaging of calcium transients in neurons and pharyngeal muscle of C. elegans.* Neuron **26**: 583-594.
- Kunkel MT, Ni Q, Tsien RY, Zhang J, Newton AC** (2005) *Spatio-temporal dynamics of protein kinase B/Akt signaling revealed by a genetically encoded fluorescent reporter.* J Biol Chem **280**: 5581-5587.
- Lewit-Bentley A, Rety S** (2000) *EF-hand calcium-binding proteins.* Curr Opin Struct Biol **10**: 637-643.
- Lippincott-Schwartz J, Patterson GH** (2003) *Development and use of fluorescent protein markers in living cells.* Science **300**: 87-91.

-
- Makrides SC** (1999) *Components of vectors for gene transfer and expression in mammalian cells*. *Prot Expr Purif* **17**: 183-202.
- Marsault R, Murgia M, Pozzan T, Rizzuto R** (1997) *Domains of high Ca²⁺ beneath the plasma membrane of living A7r5 cells*. *EMBO J* **16**: 1575-1581.
- Matz MV, Fradkov AF, Labas YA, Savitsky AP, Zaraisky AG, Markelov ML, Lukyanov SA** (1999) *Fluorescent proteins from nonbioluminescent Anthozoa species*. *Nat Biotechnol* **17**: 969-973.
- Mercier P, Li MX, Sykes BD** (2000) *Role of the structural domain of troponin C in muscle regulation: NMR studies of Ca²⁺ binding and subsequent interactions with regions 1-40 and 96-115 of troponin I*. *Biochemistry* **39**: 2902-2911.
- Mercier P, Spyropoulos L, Sykes BD** (2001) *Structure, dynamics, and thermodynamics of the structural domain of troponin C in complex with the regulatory peptide 1-40 of troponin I*. *Biochemistry* **40**: 10063-10077.
- Miesenbock G, De Angelis DA, Rothman JE** (1998) *Visualizing secretion and synaptic transmission with pH-sensitive green fluorescent proteins*. *Nature* **394**: 192-195.
- Miyawaki A, Griesbeck O, Heim R, Tsien RY** (1999) *Dynamic and quantitative Ca²⁺ measurements using improved cameleons*. *PNAS* **96**: 2135-2140.
- Miyawaki A, Llopis J, Heim R, McCaffery JM, Adams JA, Ikura M, Tsien RY** (1997) *Fluorescent indicators for Ca²⁺ based on green fluorescent proteins and calmodulin*. *Nature* **388**: 882-887.
- Mizuno H, Sawano A, Eli P, Hama H, Miyawaki A** (2001) *Red fluorescent protein from *Discosoma* as a fusion tag and a partner for fluorescence resonance energy transfer*. *Biochemistry* **40**: 2502-2510.
- Molecular Probes** (2004) Technical focus: Loading and calibration of intracellular ion indicators. In: *The Handbook - A Guide to Fluorescent Probes and Labeling Technologies* www.probes.com.

- Moriyoshi K, Richards LJ, Akazawa C, O'Leary DDM, Nakanishi S** (1996) *Labeling neural cells using adenoviral gene transfer of membrane-targeted GFP*. *Neuron* **16**: 255-260.
- Nagai T, Sawano A, Park ES, Miyawaki A** (2001) *Circularly permuted green fluorescent proteins engineered to sense Ca²⁺*. *PNAS* **98**: 3197-3202.
- Nagai T, Yamada S, Tominaga T, Ichikawa M, Miyawaki A** (2004) *Expanded dynamic range of fluorescent indicators for Ca²⁺ by circularly permuted yellow fluorescent proteins*. *PNAS* **101**: 10554-10559.
- Nagy A, Gertsenstein M, Vintersten K, Behringer R** (2003) Production of transgenic mice. In: *Manipulating the Mouse Embryo: A Laboratory Manual* (Nagy A, Gertsenstein M, Vintersten K, Behringer R, eds), pp 291-351. Cold Spring Harbor: CSHL Press.
- Nakai J, Ohkura M, Imoto K** (2001) *A high signal-to-noise Ca²⁺ probe composed of a single green fluorescent protein*. *Nat Biotechnol* **19**: 137-141.
- Nonet ML** (1999) *Visualization of synaptic specializations in live C. elegans with synaptic vesicle protein-GFP fusions*. *J Neurosci Methods* **89**: 33-40.
- Ormo M, Cubitt AB, Kallio K, Gross LA, Tsien RY, Remington SJ** (1996) *Crystal structure of the Aequorea victoria green fluorescent protein*. *Science* **273**: 1392-1395.
- Palmer AE, Jin C, Reed JC, Tsien RY** (2004) *Bcl-2-mediated alterations in endoplasmic reticulum Ca²⁺ analyzed with an improved genetically encoded fluorescent sensor*. *PNAS* **101**: 17404-17409.
- Pinton P, Tsuboi T, Ainscow EK, Pozzan T, Rizzuto R, Rutter GA** (2002) *Dynamics of glucose-induced membrane recruitment of protein kinase C beta II in living pancreatic islet beta -cells*. *J Biol Chem* **277**: 37702-37710.
- Pollesello P, Ovaska M, Kaivola J, Tilgmann C, Lundstrom K, Kalkkinen N, Ulmanen I, Nissinen E, Taskinen J** (1994) *Binding of a new Ca²⁺ sensitizer, levosimendan, to recombinant human cardiac troponin C. A molecular modelling,*

-
- fluorescence probe, and proton nuclear magnetic resonance study.* J Biol Chem **269**: 28584-28590.
- Pologruto TA, Yasuda R, Svoboda K** (2004) *Monitoring neural activity and [Ca²⁺] with genetically encoded Ca²⁺ indicators.* J Neurosci **24**: 9572-9579.
- Prasher DC** (1995) *Using GFP to see the light.* Trends Genet **11**: 320-323.
- Reid BG, Flynn GC** (1997) *Chromophore formation in green fluorescent protein.* Biochemistry **36**: 6786-6791.
- Reiff DF, Thiel PR, Schuster CM** (2002) *Differential regulation of active zone density during long-term strengthening of Drosophila neuromuscular junctions.* J Neurosci **22**: 9399-9409.
- Reiff DF, Ihring A, Guerrero G, Isacoff EY, Joesch M, Nakai J, Borst A** (2005) *In vivo performance of genetically encoded indicators of neural activity in flies.* J Neurosci **25**: 4766-4778.
- Rizzo MA, Springer GH, Granada B, Piston DW** (2004) *An improved cyan fluorescent protein variant useful for FRET.* Nature Biotechnology **22**: 445-449.
- Romoser VA, Hinkle PM, Persechini A** (1997) *Detection in living cells of Ca²⁺-dependent changes in the fluorescence emission of an indicator composed of two green fluorescent protein variants linked by a calmodulin-binding sequence - a new class of fluorescent indicators.* J Biol Chem **272**: 13270-13274.
- Rudolf R, Mongillo M, Rizzuto R, Pozzan T** (2003) *Looking forward to seeing calcium.* Nat Rev Mol Cell Biol **4**: 579-586.
- Sambrook J, Russell D** (2001a) Gel electrophoresis of DNA and pulsed-field agarose gel electrophoresis. In: Molecular Cloning: A Laboratory Manual (Sambrook J, Russell D, eds), pp 5.1-5.86. Cold Spring Harbor: CSHL Press.
- Sambrook J, Russell D** (2001b) Preparation and analysis of eukaryotic genomic DNA. In: Molecular Cloning: A Laboratory Manual (Sambrook J, Russell D, eds), pp 6.1-6.64. Cold Spring Harbor: CSHL Press.

- Seth A, Otomo T, Yin HL, Rosen MK** (2003) *Rational design of genetically encoded fluorescence resonance energy transfer-based sensors of cellular Cdc42 signaling*. *Biochemistry* **42**: 3997-4008.
- Shagin DA, Barsova EV, Yanushevich YG, Fradkov AF, Lukyanov KA, Labas YA, Semenova TN, Ugalde JA, Meyers A, Nunez JM, Widder EA, Lukyanov SA, Matz MV** (2004) *GFP-like proteins as ubiquitous metazoan superfamily: evolution of functional features and structural complexity*. *Mol Biol Evol* **21**: 841-850.
- Shaner NC, Campbell RE, Steinbach PA, Giepmans BNG, Palmer AE, Tsien RY** (2004) *Improved monomeric red, orange and yellow fluorescent proteins derived from *Discosoma* sp. red fluorescent protein*. *Nat Biotechnol* **22**: 1567-1572.
- Shimomura O, Johnson FH, Saiga Y** (1962) *Extraction, purification and properties of aequorin, a bioluminescent protein from the luminous hydromedusan, Aequorea*. *J Cell Comp Physiol* **59**: 223-239.
- Spyracopoulos L, Gagne SM, Li MX, Sykes BD** (1998) *Dynamics and thermodynamics of the regulatory domain of human cardiac troponin C in the apo- and calcium-saturated states*. *Biochemistry* **37**: 18032-18044.
- Stoppini L, Buchs PA, Muller D** (1991) *A simple method for organotypic cultures of nervous tissue*. *J Neurosci Methods* **37**: 173-182.
- Strynadka NC, Cherney M, Sielecki AR, Li MX, Smillie LB, James MN** (1997) *Structural details of a calcium-induced molecular switch: X-ray crystallographic analysis of the calcium-saturated N-terminal domain of troponin C at 1.75 Å resolution*. *J Mol Biol* **273**: 238-255.
- Sundaralingam M, Bergstrom R, Strasburg G, Rao ST, Roychowdhury P, Greaser M, Wang BC** (1985) *Molecular structure of troponin C from chicken skeletal muscle at 3-angstrom resolution*. *Science* **227**: 945-948.
- Szczesna D, Guzman G, Miller T, Zhao J, Farokhi K, Ellemberger H, Potter JD** (1996) *The role of the four Ca²⁺ binding sites of troponin C in the regulation of skeletal muscle contraction*. *J Biol Chem* **271**: 8381-8386.

-
- Takeda S, Yamashita A, Maeda K, Maeda Y** (2003) *Structure of the core domain of human cardiac troponin in the Ca²⁺-saturated form*. *Nature* **424**: 35-41.
- Taketo M, Schroeder AC, Mobraaten LE, Gunning KB, Hanten G, Fox RR, Roderick TH, Stewart CL, Lilly F, Hansen CT** (1991) *FVB/N: an inbred mouse strain preferable for transgenic analyses*. *PNAS* **88**: 2065-2069.
- Tikunova SB, Black DJ, Johnson JD, Davis JP** (2001) *Modifying Mg²⁺ binding and exchange with the N-terminal of calmodulin*. *Biochemistry* **40**: 3348-3353.
- Tikunova SB, Rall JA, Davis JP** (2002) *Effect of hydrophobic residue substitutions with glutamine on Ca²⁺ binding and exchange with the N-domain of troponin C*. *Biochemistry* **41**: 6697-6705.
- Tikunova SB, Davis JP** (2004) *Designing calcium-sensitizing mutations in the regulatory domain of cardiac troponin C*. *J Biol Chem* **279**: 35341-35352.
- Tong J, Du GG, Chen SR, MacLennan DH** (1999) *HEK-293 cells possess a carbachol- and thapsigargin-sensitive intracellular Ca²⁺ store that is responsive to stop-flow medium changes and insensitive to caffeine and ryanodine*. *Biochem J* **343**: 39-44.
- Tripet B, Van Eyk JE, Hodges RS** (1997) *Mapping of a second actin-tropomyosin and a second troponin C binding site within the C terminus of troponin I, and their importance in the Ca²⁺-dependent regulation of muscle contraction*. *J Mol Biol* **271**: 728-750.
- Tsien RY** (1998) *The green fluorescent protein*. *Annu Rev Biochem* **67**: 509-544.
- Tsien RY** (1999) *Monitoring cell calcium*. In: *Calcium as a Cellular Regulator* (Carafoli E, Klee C, eds), pp 28-54. New York: Oxford University Press.
- Vassilyev DG, Takeda S, Wakatsuki S, Maeda K, Maeda Y** (1998) *Crystal structure of troponin C in complex with troponin I fragment at 2.3-Angstrom resolution*. *PNAS* **95**: 4847-4852.
- Verkhusha VV, Lukyanov KA** (2004) *The molecular properties and applications of Anthozoa fluorescent proteins and chromoproteins*. *Nat Biotechnol* **22**: 289-296.

- Violin JD, Zhang J, Tsien RY, Newton AC** (2003) *A genetically encoded fluorescent reporter reveals oscillatory phosphorylation by protein kinase C*. *J Cell Biol* **161**: 899-909.
- Whitlow M, Bell BA, Feng SL, Filpula D, Hardman KD, Hubert SL, Rollence ML, Wood JF, Schott ME, Milenic DE** (1993) *An improved linker for single-chain Fv with reduced aggregation and enhanced proteolytic stability*. *Protein Eng* **6**: 989-995.
- Yang F, Moss LG, Phillips GN** (1996) *The molecular structure of green fluorescent protein*. *Nat Biotech* **14**: 1246-1251.
- Yeh E, Gustafson K, Boulianne GL** (1995) *Green fluorescent protein as a vital marker and reporter of gene expression in drosophila*. *PNAS* **92**: 7036-7040.
- Yu R, Hinkle PM** (2000) *Rapid turnover of calcium in the endoplasmic reticulum during signaling. Studies with cameleon calcium indicators*. *J Biol Chem* **275**: 23648-23653.
- Yuste R** (2000) *Loading brain slices with AM esters of calcium indicators*. In: *Imaging Neurons: A Laboratory Manual* (Yuste R, Lanni F, Konnerth A, eds), pp 34.1-34.9. Cold Spring Harbor: CSHL Press.
- Zaccolo M, De Giorgi F, Cho CY, Feng LX, Knapp T, Negulescu PA, Taylor SS, Tsien RY, Pozzan T** (2000) *A genetically encoded, fluorescent indicator for cyclic AMP in living cells*. *Nat Cell Biol* **2**: 25-29.
- Zaccolo M** (2004) *Use of chimeric fluorescent proteins and fluorescence resonance energy transfer to monitor cellular responses*. *Circ Res* **94**: 866-873.
- Zapata-Hommer O, Griesbeck O** (2003) *Efficiently folding and circularly permuted variants of the Sapphire mutant of GFP*. *BMC Biotechnol* **3**: 5.
- Zhang J, Ma YL, Taylor SS, Tsien RY** (2001) *Genetically encoded reporters of protein kinase A activity reveal impact of substrate tethering*. *PNAS* **98**: 14997-15002.

Zhang J, Campbell RE, Ting AY, Tsien RY (2002) *Creating new fluorescent probes for cell biology.* Nat Rev Mol Cell Biol **3**: 906-918.

THANKS AND ACKNOWLEDGEMENTS

First I want to thank our department head Prof. Alexander "Axel" Borst for running our little "Department of Systems and Recreational Neurobiology" in such an easygoing and sweet-tempered way. He always tried hard to make everyone feel at home here. My thanks and admiration also go out to his friend and loyal sidekick Jürgen "Bulle" Haag who has proven time and again that a severe regimen of coffee breaks and the publication of high-ranking papers in Nature and Co. are not mutually exclusive tasks. Way to go, Bulle!

Next and above all, I have to express my gratitude to my supervisor Oliver "OJ" Griesbeck for graciously taking me on as his first PhD student ever. Not only has he always furnished us all with a constant stream of the most creative project ideas, he also proved to rarely lose his stubborn sense of humor and genial optimism, not even under the fiercest onslaughts of doubt and criticism his heretical followers put him through (and goodness knows we've strived hard!). To Oliver I dedicate the poet's words: "Good nature and good sense must ever join / to err is human, to forgive, divine."

I'm also much indebted to all my fellow PhD students with whom I have had the honor of sharing a wonderful three years in and out of the lab. They have been an immense help and a great moral support when times got rough. When shadows of fear and doubt ever happen to cloud over your projects, there is nothing more soothing and reassuring to the troubled mind than to see your fellow-comrades doing even worse. Thank you so much for all the fun we had, fellas!

Special thanks go to the members of the Griesbeck lab at this point, that is Anja, trustworthy provider of invaluable technical help and the latest gossip; Michi, creator of outstanding Western blots and garlic-drenched noodles, and Margie and Stephan, my cheerful partners during the dark and dismal days deep down in the dungeon named "Tierstall". Last but not least I have to mention Marco here, who has always been a great buddy possessed by an incredibly persistent eagerness to penetrate down to the very bottom of The Truth, only to find that, alas, the truth is often not a very pleasant sight. I will sorely miss all of you guys.

Last, I owe a lot to Alex Milbradt and his merry gang of "Moroder-Jungs" who have always set a such a wonderful example of how to master life's numerous obstacles with lovable cynicism and delightful disrespectfulness. Science truly deserves more dauntless and steadfast men of their kind!

CURRICULUM VITAE

Education:

since April 02: PhD thesis at the Max-Planck-Institut of Neurobiology, Martinsried, Germany under supervision of Dr. Oliver Griesbeck and Prof. Dr. Alexander Borst: "Genetically Encoded Calcium Indicators Based on Troponin C and Fluorescent Proteins".

April 01 - Dec. 01: Diploma thesis at Roche Diagnostics, Penzberg, Germany and Prof. Dr. Robert Huber, Max-Planck-Institut for Biochemistry Martinsried, Germany: "Entwurf, Herstellung und Untersuchung von Kristallisationskonstrukten der Aurora-Proteinkinasen Aurora-A und IPL1".

April 99 - Feb. 00: Ten-months internship at the Max-Planck-Institut of Biochemistry, Martinsried, Germany. Lab rotations in the research groups Holak, Jentsch, Bornkamm, Neupert and Moroder

April 96 - April 01: Undergraduate studies in Biochemistry at the University of Tübingen, Germany.

July 95: Graduation from High School: Luisengymnasium, Munich, Germany.

Publications:

Mank M, Reiff DF, Heim N, Friedrich M, Borst A, Griesbeck O (2005) A FRET-based calcium biosensor with fast signal kinetics and high fluorescence change. Manuscript submitted.

Heim N, Griesbeck O (2004) *Genetically encoded indicators of cellular calcium dynamics based on troponin C and green fluorescent protein*. J Biol Chem **279**: 14280-14286.

Griesbeck Oliver, Heim Nicola. *Genetically encoded bioindicators of calcium-ions*. European Patent No. 1505073

Renner C, Behrendt R, Heim N, Moroder L (2002) *Photomodulation of conformational states. III. Water-soluble bis-cysteinyl-peptides with (4-aminomethyl) phenylazobenzoic acid as backbone constituent*. Biopolymers **63**: 382-393.